

DISS. ETH NO. 14658

Analysis of Flow Patterns

The influence of soil compaction and soil structure on the infiltration pathways of dye tracer solutions and the quantitative evaluation of flow patterns.

Beatrice Kulli Honauer

2002

DISS. ETH NO. 14658

Analysis of Flow Patterns

The influence of soil compaction and soil structure on the infiltration pathways of dye tracer solutions and the quantitative evaluation of flow patterns.

A dissertation submitted to the
SWISS FEDERAL INSTITUTE OF TECHNOLOGY
for the degree of Doctor of Natural Sciences

presented by
BEATRICE KULLI HONAUER
Dipl. Sci. Nat. ETHZ

born April 2. 1970
citizen of Olten and Solothurn

accepted on the recommendation of

Prof. Hannes Flühler, examiner
Prof. Rainer Schulin, co-examiner
Prof. Philippe Baveye, co-examiner

Zürich, 2002

*To my mother Trudi,
my husband Philipp,
and Benjamin, our little son.*

Summary

Infiltration patterns visualized by means of dye tracers provide information about the flow regime in a given soil under given boundary and initial conditions. The tracer distribution in the soil is affected by the soil structure and in particular the sequence of soil horizons. Soil compaction may remarkably change soil structure and the continuity of the pore network.

The goal of this thesis was (i) to find out how soil compaction affects water infiltration patterns, (ii) to link soil properties, in particular its layering structure, with types of flow patterns, and (iii) to develop a method for a quantitative analysis and comparison of flow patterns.

Compaction modifies the pore system, often by reducing the pore volume or by destroying the structure. As a consequence, not only pre-consolidation load, bulk density or porosity are changed, but also the transport properties of the soil. The effects of heavy vehicle traffic on the infiltration patterns of dye tracer solutions were studied at different sites under vehicles equipped with caterpillar tracks and vehicles on wheels. The influences of soil compaction made visible by the tracer infiltration images were then compared with effects found by laboratory measurements (bulk density, porosity and pre-consolidation load).

The results show that in most of the cases there is a good agreement between effects found on the basis of soil mechanical measurements and flow patterns. The pre-consolidation load was found to be a good indicator to predict soil stability and the bulk density was sensitive for detecting compaction effects.

The experiment showed that soil mechanical measurements may provide information about how compaction propagates with depth whereas infiltration patterns showed the changes of the water infiltration pathways caused by soil compaction. At one site, which was trafficked with a sugarbeet harvester, soil compaction led to an increased preferential flow regime. After compaction, the fine pore structures in the topsoil were locked up and no longer available for water infiltration. The water was ponding on the surface and preferentially entering open worm burrows, bypassing the main root zone.

Most of the tracer experiments were conducted with Brilliant Blue as a tracer and by comparing the flow patterns of trafficked with non-trafficked plots. However, the spatially variable soil structure makes it difficult to compare the flow patterns of neighbouring plots quantitatively. Comparing the flow patterns before and after compaction at one and the same plot overcomes this basic experimental difficulty of discriminating treatment effects from between-plot variability. Therefore, an experiment was carried out with two fluorescent tracers applied onto the same plot, one before and the other after controlled compaction with a heavy vehicle. The distributions of the two dyes in the excavated soil profiles were photographed separately using a digital camera and a light source, both equipped with tracer-specific filters. The superposition of the two flow patterns shows the effect of the compaction treatment directly. This method is more sensitive than experiments using a single tracer and the quantification of the differences is easier, because the flow patterns can be compared one-to-one.

However, it is technically less demanding and less costly to use the single tracer technique. This technique requires the analysis of numerous images of patchy stained profiles. To compare such images objectively is one major focus of this thesis. Therefore, we wanted to develop a quantitative method to analyze the spatial distribution of the stained areas in vertical profiles and to link the characteristics of these patterns with soil properties, in particular its structure. Since soil layers strongly affect the infiltration patterns we first divided the flow patterns into layers of similar patterns. All layers found at several sites were then partitioned into groups of similar layers by hierarchical clustering. This classification reliably distinguishes between a homogeneous infiltration and preferential flow regime, but also between zones of pronounced preferential flow and zones of lateral spreading, e.g. sand or gravel lenses. The dye coverage and the mean width of the stained structures were the most indicative characteristics for the different clusters. We found good agreement between the sequences of layers found in the flow patterns and the soil horizons.

Zusammenfassung

Infiltrationsmuster von Farbtracern in vertikalen oder horizontalen Bodenprofilen geben Aufschluss über das Transport Regime im Boden bei bestimmten Anfangs- und Rahmenbedingungen. Die Tracerverteilung im Boden wird durch die Bodenstruktur beeinflusst, insbesondere durch die Abfolge der Bodenhorizonte. Bodenverdichtung verändert die Struktur und Kontinuität des Porensystems. Das Ziel dieses Doktorats war (i) den Einfluss von Bodenverdichtung auf die Infiltrationsmuster von Farbtracern zu untersuchen, (ii) den Einfluss der Bodenstruktur auf die Fliessmuster zu untersuchen und einen Zusammenhang zwischen bestimmten Bodenhorizonten und Fliessmustertypen herzustellen und (iii) eine quantitative Methode zur Analyse und zum Vergleich von Fliessmustern zu entwickeln.

Bodenverdichtung verändert das Porensystem häufig durch eine Reduktion des Porenraums oder durch eine Zerstörung der Struktur. Dadurch werden nicht nur bodenmechanische Parameter wie Lagerungsdichte, Vorbelastung oder Porosität verändert, sondern auch die Transporteigenschaften des Bodens. Der Effekt von Befahrungen auf die Infiltrationsmuster der Tracerlösung im Boden wurde an verschiedenen Standorten unter Raupen- und Radfahrzeugen untersucht. Verdichtungseffekte, die anhand der Tracerbilder festgestellt wurden, wurden dann mit bodenmechanischen Messungen verglichen.

Die Resultate zeigen in den meisten Fällen eine gute Übereinstimmung zwischen den beiden Methoden. Die Vorbelastungsmessungen gaben Aufschluss über die Verdichtungsempfindlichkeit eines Bodens geben und , wie die Lagerungsdichte, sensitiv den Effekt einer Befahrung zeigt. Die bodenmechanischen Messungen gaben Aufschluss über die Tiefenwirkung der Verdichtung, während die Infiltrationsmuster die durch die Bodenverdichtung verursachten Veränderungen der Fliesswege zeigten. Ein Befahrungsversuch mit einem Zuckerrübensvollernter führte zu einer Zunahme des präferenziellen Transportes im Boden. Nach der Verdichtung war das feine Porennetzwerk im Oberboden nicht mehr am Transport beteiligt. Das Wasser staute sich auf der Bodenoberfläche und floss durch einige vertikale Wurmgänge schnell in grosse Tiefe, wobei der Hauptwurzelraum umflossen wurde.

Die meisten Farbtracerexperimente dieser Studie wurden mit dem Farbstoff 'Brilliant Blue' durchgeführt, wobei die Fliessmuster in befahrenen und unbefahrenen Versuchsflächen miteinander verglichen wurden. Das Vergleichen von Fliessmusterbildern verschiedener Plots wird jedoch durch die räumliche Variabilität der Bodenstruktur und damit der Fliessmuster erschwert. Der Vergleich von Fliessmustern vor und nach der Befahrung auf derselben Fläche wäre wesentlich einfacher. Deshalb wurde ein weiteres, methodologisch orientiertes Experiment durchgeführt, bei dem zwei Fluoreszenztracer auf dieselbe Versuchsfläche appliziert wurden, einer vor und einer nach der Befahrung. Die Verteilungen der beiden Farbstoffe konnte mit Hilfe einer digitalen Kamera und tracerspezifischer Filterung des Lichtes unabhängig voneinander aufgenommen werden. Die Überlagerung der beiden Fliessmuster zeigte den Effekt der Verdichtung direkt. Diese Methode ist empfindlicher als der Vergleich von Fliessmustern aus verschiedenen Versuchsfläche, da die Muster eins-zu-eins verglichen werden können und der Effekt nicht durch die räumliche Variabilität der Muster gestört wird.

Für Routineversuche ist die Applikation von einem Farbtracer und der Vergleich von Fliessmustern verschiedener Flächen jedoch einfacher und weniger kostspielig. Das Ergebnis sind zahlreiche Infiltrationsmuster, entweder von ein und derselben Versuchsfläche, von verschiedenen Plots oder von verschiedenen Standorten. Solche Muster objektiv zu vergleichen ist ein weiteres Ziel dieser Arbeit.

Wir wollten eine quantitative Methode zur Analyse der räumlichen Verteilung der gefärbten Bereiche in den vertikalen Bodenprofilen entwickeln und anschliessend die Eigenschaften dieser Muster mit der Bodenstruktur verknüpfen. Da die Fliessmuster stark von der Schichtung des Bodens beeinflusst werden, wurden sie zuerst in Schichten eingeteilt. Alle Schichten der Fliessmuster von 25 Versuchsflächen an 8 Standorten wurden dann mit Hilfe hierarchischer Clusterbildung in Gruppen ähnlicher Schichten eingeteilt. Die Gruppen unterschieden zuverlässig zwischen Horizonten mit homogener Infiltration und Horizonten mit präferenziellen Fliesswegen, aber auch zwischen Zonen mit ausgeprägtem präferenziellem Fluss und Zonen mit lateraler Ausbreitung des Tracers, wie zum Beispiel Sand- oder Kieslinsen. Der Farbbedeckungsgrad und die mittlere Breite der der gefärbten Strukturen waren

die Faktoren, die die Cluster am stärksten unterschieden. Wir fanden eine gute Übereinstimmung zwischen der Schichtabfolge der Fließmustern und derjenigen der Bodenhorizonte.

Acknowledgements

I am grateful to all the people supporting my studies during the last years. Especially: Markus Berli and Michael Gysi for their great collaboration and stimulating discussions on soil compaction; Jörg Leuenberger for the help in planning and conducting the field experiments; Markus Jauslin for planning and conducting the experiments at the site of Buttisholz; Hannes Wydler for imaging and evaluating the tracer infiltration patterns at the site of Buttisholz; Christian Stamm for his introduction to dye tracer experiments and for his contribution during the development of the method for the analysis of the flow patterns; Andreas Papritz for discussing and explaining statistical issues; Irène Forrer for introducing me to image analysis and providing me her IDL programs; Maxime Jaquillard for his fieldwork and the evaluation of the results on the site of Frauenfeld; Frank Richter, Hanspeter Läser, Werner Attinger, Maya Bundt and Stephan Sennrich for their help in the field; Hans Ulrich Hoppler and Stephan Sennrich for developing ideas for the description and comparison of patterns; Peter Lehmann for patiently listening to my worries and sharing successful moments, for discussing scientific problems and for having a good time in the office; Prof. Hannes Flühler and Prof. Rainer Schulin for the opportunity to work on this project; Prof. Philippe Baveye for discussing my ideas on several occasions and for being my co-examiner; and to all the other members of the Soil Physics Group for having a good collaboration.

Special thanks to the Research and Development fund of the Swiss Gas Industry (FOGA) for the Financial support of the project: ‘Assessment and Prediction of the Mechanical Impact on the Subsoil by the Installation of Gas Pipelines in Agricultural Soils’

I also thank the Swiss Federal Research Station for Agricultural Economics and Engineering (FAT), for supporting this collaboration at the Frauenfeld site.

Table of contents

CHAPTER 1

INTRODUCTION	1
1.1 VISUALIZING SOIL COMPACTION WITH DYE TRACERS	1
1.2 TRACER INFILTRATION EXPERIMENTS	2
1.3 QUANTITATIVE COMPARISON OF TRACER DISTRIBUTIONS	3
1.4 SCOPE OF THE THESIS	4
1.5 REFERENCES	5

CHAPTER 2

VISUALIZING SOIL COMPACTION BASED ON FLOW PATTERN ANALYSIS	7
2.1 INTRODUCTION	8
2.2 MATERIAL AND METHODS	9
<i>Field experiment</i>	9
<i>Laboratory measurements</i>	11
<i>Dye infiltration experiment</i>	11
<i>Image processing</i>	12
2.3 RESULTS AND DISCUSSION	12
<i>Soil physical properties</i>	12
<i>Flow patterns</i>	15
<i>Discussion</i>	20
2.4 CONCLUSIONS	20
2.5 ACKNOWLEDGEMENTS	21
2.6 REFERENCES	22

CHAPTER 3

A MULTI-TRACING METHOD FOR DETECTING SOIL COMPACTION IMPACTS	25
3.1 INTRODUCTION	26
3.2 MATERIALS AND METHODS	27
<i>Test site</i>	27

<i>Field experiment</i>	28
<i>Dye tracer infiltration</i>	29
<i>Fluorescent tracers</i>	31
<i>Detection of the tracer distribution</i>	31
<i>Digital image processing</i>	32
<i>Qualitative and quantitative analysis of the results</i>	33
3.3 RESULTS	35
<i>Qualitative results</i>	35
<i>Quantitative results</i>	37
3.4 DISCUSSION AND CONCLUSIONS	39
3.5 ACKNOWLEDGEMENTS	40
3.6 REFERENCES	41

CHAPTER 4

COMPACTION OF AGRICULTURAL AND FOREST SUBSOILS BY TRACKED HEAVY CONSTRUCTION MACHINERY43

4.1 INTRODUCTION	44
4.2 MATERIAL AND METHODS	47
4.3 RESULTS	55
4.4 DISCUSSION AND CONCLUSIONS	62
4.5 ACKNOWLEDGEMENT	67
4.6 REFERENCES	68

CHAPTER 5

COMPARING INFILTRATION PATTERNS IN SOILS73

5.1 INTRODUCTION	74
5.2 MATERIAL AND METHODS	76
<i>Field experiments</i>	77
<i>Image processing</i>	77
<i>Defining and discriminating of layers</i>	78
<i>Cluster analysis</i>	84
5.3 RESULTS AND INTERPRETATION	85
<i>Layer detection</i>	85
<i>Cluster analysis</i>	87

<i>Comparison of the layers found in the patterns and the soil horizons</i>	<i>88</i>
<i>Analysis of the characteristics of the flow patterns</i>	<i>91</i>
5.4 DISCUSSION AND CONCLUSIONS	94
5.5 ACKNOWLEDGEMENTS	95
5.6 REFERENCES	96

CHAPTER 6

SYNTHESIS	99
------------------------	-----------

LIST OF FIGURES.....	103
-----------------------------	------------

LIST OF TABLES.....	107
----------------------------	------------

CURRICULUM VITAE	109
-------------------------------	------------

Chapter 1

Introduction

1.1 Visualizing soil compaction with dye tracers

Soil compaction is usually a pore volume reduction caused by a load applied onto the surface of a given soil compartment. In addition to a reduced pore space, the soil structure may collapse and/or pores that were interconnected prior to compaction might be sheared off. Infiltration may be impeded and the availability of water and air to plants and microorganisms cut down, which adversely affects soil quality (Horton et al., 1994; Craul, 1994; Alakukku, 1996).

Soil compaction can be measured by soil mechanical and soil physical measurements, as for instance pre-consolidation load, bulk density or porosity (Gysi et al., 2000). These indicators give some information about the compaction status of a soil and can be used to demonstrate the compaction effects of heavy vehicle traffic at various depths. However, it is difficult to predict the effect of soil compaction on water transport or plant growth based solely on soil mechanical measurements.

One possibility of visualizing soil compaction effects on the water transport are dye tracer infiltration experiments. Von Albertini et al. (1995) found that comparing the spatial distribution of a dye tracer in vertical profiles was a sensitive method to investigate the structural recovery of compacted arable land. The comparison of the tracer distributions observed in vertical or horizontal profiles of trafficked and non-trafficked plots shows the effect of a compaction event on the infiltration pathways of water. Since the spatial distribution of the stained flow paths depend not only on the pore volume, but also on the connectedness of the pore system this method should be sensitive for the detection of soil compaction or shearing.

1.2 Tracer infiltration experiments

The flow regime and typical infiltration pathways of water into a soil are strongly affected by soil structure and the sequence of soil horizons. This can be visualized by staining the pathways that are actively conducting the infiltrating water (Ghodrati and Jury, 1990; Gjetterman et al., 1997; Zehe and Flühler, 2001). The flow patterns observed in vertical or horizontal profiles are characteristic for a given soil (Flury et al., 1994), but also depend on the experimental conditions. Infiltration rate, soil moisture prior to infiltration, but also the chemical properties and concentration of the dye tracer play a major role for the outcome of the experiment (Weiler and Naef, 2001).

Taking pictures with a suitable camera and proper illumination and digitizing of these pictures allow an efficient analysis of the tracer distribution by digital image processing. The evaluation of the pictures taken in the field can be carried out in different ways. Samples taken in the profiles or calibration samples attached to the profile while taking the pictures allow us to determine the tracer concentration based on the grey or colour values of the digital image (Ewing and Horton, 1999; Forrer et al., 2000; Aeby et al., 2001). The result is a 'concentration map' of the tracer. Another possibility is to distinguish between stained and unstained soil and to evaluate the spatial characteristics of the resulting 'flow pattern' (Flury et al., 1994; Baveye et al., 1998).

Dye tracer experiments can be carried out to study diverse subjects. The flow regimes at different sites can be compared, or the flow regime at one site can be studied under different infiltration conditions (Flury et al., 1994; Zehe and Flühler, 2001). The behaviour of tracers with different chemical properties can be examined under field conditions using them as measurable or at least observable surrogate compounds that behave similarly to certain pollutants (Aeby et al., 2001). In the field, the infiltration pattern of the dye on the profile wall can be used to take soil samples of flow paths and matrix separately (Bundt et al., 2000; Sinaj et al. 2002). Or, as in the case of my thesis, tracer infiltration patterns can be used to examine the effect of soil compaction on soil structure and water infiltration (Von Albertini et al, 1995).

In many if not most cases, the tracer distribution in the soil profile needs to be quantified, either in order to study transport properties of soil or tracer or to compare the resulting infiltration patterns of different treatments.

1.3 Quantitative comparison of tracer distributions

It depends on the objective of a study whether concentration maps or flow patterns are better suited. Concentration maps allow us to calculate the statistics of the horizontal and vertical distributions of the tracer mass or to measure overall or local concentration gradients of tracer concentrations in different regions of the image (Forrer et al., 2000). However, the spatial structure of the infiltration pattern contains more information than the distributional characteristics just mentioned.

Flow patterns, showing the dye covered area, cannot be used to evaluate tracer mass nor concentrations, but allow us to evaluate the spatial distribution of the infiltration pathways. There are many possibilities of quantifying and comparing flow patterns, for instance based on fractal geometry (Baveye et al., 1998), on the vertical or horizontal distribution of dye coverage (Zehe and Flühler, 2001) or on the mean width or length of the stained areas (Weiler and Naef, 2001). Each of these methods considerably condenses and simplifies the original information by extracting one special property of the pattern and making it accessible for further analysis. This simplification is necessary, because flow patterns cannot be compared on a one-to-one basis. Whether a stained worm burrow is on the left or on the right hand side of a profile does not matter, as long as it is continuous and reaches a certain depth. In addition it is not possible to compare objects directly because the features of the flow patterns (e.g., stained worm burrows or cracks) do not always look alike (as for instance letters) and are, in addition, spatially interconnected. Furthermore, flow patterns are 2-dimensional cuts through the 3-dimensional network of pathways. This creates additional differences between flow pattern, depending on how certain features are oriented with respect to the exposed and visible profile wall.

In this study we develop a method for a quantitative comparison of flow patterns which sensitively and reliably discriminates dissimilar patterns and groups similar patterns.

1.4 Scope of the thesis

The first aim of my thesis was to study the effect of soil compaction on the infiltration patterns of dye tracers and to compare the effects observed in the patterns with soil mechanical and soil physical measurements. I was interested to find out whether both methods lead us to the same conclusions in terms of the assessment of soil compaction and of the extent to which the information gained by these methods is complementary.

The second aim was to link flow patterns found in dye tracer experiments to the underlying soil structure and soil properties. The idea was that if we would know the relation between a pattern type and type of soil or soil layer, we might be able to estimate the type of flow pattern on the basis of a given soil.

For both goals it was necessary to develop a method to quantitatively analyse flow patterns. This is the third aim of my thesis. The main focus in this context was on developing a method to quantify flow patterns which allows an objective comparison of infiltration patterns observed at different sites or under different treatments.

1.5 References

- Aeby, P., U. Schultze, D. Braichotte, M. Bundt, F. Moser-Boroumand, H. Wydler and H. Flühler (2001). "Fluorescence Imaging of Tacer Distributions in Soil Profiles." *Environmental Science and Technology*. 35(4): 753-760.
- Alakukku, L., 1996. Persistence of soil compaction due to high axle load traffic. II. Long-term effects on properties of fine-textured and organic soils. *Soil & Tillage Research*. 37: 223-238.
- Baveye P., C.W. Boast, S. Ogawa, J.Y. Parlange, and T. Steenhuis, 1998. Influence of image resolution and thresholding on the apparent mass fractal characteristics of preferential flow patterns in field soils. *Water Resources Research*, 34 (11): 2783-2796.
- Bundt M., Albrecht A., Froidevaux P., Blaser P., Fluhler H., 2000. Impact of preferential flow on radionuclide distribution in soil. *Environmental Science & Technology* 34 (18): 3895-3899
- Craul, P. J., 1994. Soil compaction on heavily used sites. *Journal of Arboriculture*. 20(2): 69-74.
- Ewing, R. P., and R. Horton, 1999. Discriminating dyes in soil with color image analysis. *Soil Science Society of America Journal*. 63: 18-24.
- Flury, M., H. Flühler, W. A. Jury, and J. Leuenberger, 1994. Susceptibility of soils to preferential flow of water: A field study. *Water Resources Research* 30(7):1945-1954.
- Forrer, I. N., and R. Kasteel, 1999. Longitudinal and lateral dispersion in an unsaturated field soil. *Water Resources Research*. 35(10): 3049-3060.
- Forrer, I. N., A. Papritz, R. Kasteel, H. Flühler, and D. Luca, 2000. Quantifying dye tracer in soil profiles by image processing. *European Journal of Soil Science*. 51: 313-322.
- Ghodrati M., and W. A. Jury, 1990. A field study using dyes to characterize preferential flow of water. *Soil Science Society of America Journal*. 54: 1558-1563

- Gjettermann B., K. L. Nielsen, C. T. Petersen, H. E. Jensen, S. Hansen, 1997. Preferential flow in sandy loam soils as affected by irrigation intensity. *Soil Technology*. 11: 139-152.
- Gysi M., G. Klubertanz, and L. Vulliet, 2000. Soil compaction due to heavy wheel traffic. Field data and modelling. *Soil and Tillage Research*. 56(3-4):117-129.
- Horton, R., M. D. Ankeny, and R. R. Allmaras, 1994. Effects of compaction on soil hydraulic properties. In: B. D. Soane, and C. van Ouwerkerk (Editors), *Soil Compaction in Crop Production*. Elsevier Science B. V. pp. 141-165.
- Sinaj S., Ch. Stamm, G.S. Toor, L.M. Condon, T. Hendry, H.J. Di. K.C. Cameron, and E. Frossard, 2002. Phosphorus exchangeability and leaching losses from two grassland soils. *J. Environ. Qual.*, 31: 319-330.
- Von Albertini, N., J. Leuenberger, H. P. Läser, and H. Flühler, 1995. Regeneration der Bodenstruktur eines verdichteten Ackerbodens unter Kunstwiese. *Bodenkundliche Gesellschaft der Schweiz Dokument* 7: 10-16. Juris Druck und Verlag Dietikon.
- Weiler M., and F. Naef, 2001. Effects of macropore flow on runoff generation. *Journal of Hydrological Processes* (in press).
- Zehe E., and H. Flühler, 2001. Slope scale variation of flow patterns in soil profiles. *Journal of Hydrology* 247:116-132.

Chapter 2

Visualizing soil compaction based on flow pattern analysis

B. Kulli, M. Gysi, and H. Flühler

Accepted for publication in 'Soil & Tillage Research'

Abstract

Soil compaction modifies the pore system, often in the sense of degrading or destroying the soil structure. As a consequence, not only the soil mechanical parameters like the pre-consolidation load or bulk density are being changed, but also the transport properties of the pore system. Compaction induced changes of water infiltrability and availability of water and air to plants and microorganisms may hamper the functioning of the soil environment.

We studied the effects of the mechanical impact applied by a sugar beet harvester on soil porosity, bulk density and on the water infiltration regime under field conditions on a sandy loam in Switzerland. Three treatments were compared: multiple vehicle passage, single passage and control (no traffic). Bulk density, total porosity and macroporosity were determined in the laboratory. In the field, a dye tracer solution was homogeneously applied onto the plots of the three treatments. Vertical profiles were prepared and color slide pictures taken with a normal photographic camera. The images were processed by digital image analysis in order to analyze the spatial distribution of the stained areas.

An obvious effect of the mechanical impact was an increase of preferential flow. The water was ponding on the soil surface of the trafficked plots and funneled into preferential flow ports, mainly worm burrows. Wetting of the main root

zone decreased because a significant fraction of the infiltrating solution bypassed the matrix. The effect was more pronounced in the multiple passage plot than in the single passage plot.

These results agree well with the laboratory measurements. In the single passage plot, a significant effect was observed down to a depth of 15 cm. The plot with the multiple passage showed a stronger effect down to greater depth.

The laboratory measurements indicate subsoil compaction, which can not be concluded from the results of the tracer experiments. The flow patterns, on the other hand, visualize the compaction effects and yield qualitative information about compaction induced changes of the infiltration regime of the soil.

2.1 Introduction

Soil compaction is usually a pore volume reduction caused by a load applied onto the surface of a given soil compartment. In addition to a reduced pore space the soil structure may collapse. Infiltration might be impeded and the water and air availability to plants and microorganisms cut down which adversely affects the soil quality (Horton et al., 1994; Craul, 1994; Alakukku, 1996).

The role of soil structure for water infiltration can be assessed by using dye staining techniques to trace the infiltration pathways e.g. in compacted and non-compacted soils. Various studies showed that flow patterns are a sensitive indicator to characterize different infiltration regimes (Ghodrati and Jury, 1990; Flury et al., 1994; Gjetterman et al., 1997; Zehe and Flühler 2001; Weiler and Naef, 2001). Von Albertini et al. (1995) found that comparing the spatial distribution of a dye tracer in vertical profiles was a sensitive method to investigate the structural recovery of compacted arable land. Forrer et al. (2000) as well as Ewing and Horton (1999) developed methods to process images of flow patterns digitally in order to obtain the dye coverage as well as the concentration distribution of the dye tracer.

In our field experiments, we investigated the effects of a sugar beet harvester on the flow paths of water in a unploughed eutric cambisol in Switzerland. The tracer solution was applied onto two plots subjected to single passage and

multiple passage respectively and on a control plot (untrafficked). We compared the stained flow patterns observed on several vertical profiles of each treatment. In addition, samples were taken to assess soil compaction effects in terms of bulk density and porosity in the laboratory.

As the bulk density and the porosity are fairly well investigated parameters for quantifying soil compaction, we focussed on the effects of the compaction on water and solute flow and compared it with laboratory determined compaction indicators referred to above and on the question whether such processes could be judged on the basis of laboratory determined compaction indicators.

2.2 Material and methods

Field experiment

The experiment was performed on a skeleton-free eutric cambisol near Frauenfeld in Switzerland (Swiss national coordinates: 270 000/707 950, topographical map sheet 1053: Frauenfeld). The site is located in a wide valley bottom at a distance of 400 m from the river Thur. At the same site we conducted field experiments that focussed on the mechanics of compaction by such machinery (Gysi et al., 2000). For the readers convenience we summarize the main features of these experiments and site. The topsoil is a sandy loam. Layers of coarser material are found in the subsoil. The bulk density is 1.4 kg L^{-1} and the pre-consolidation load 80 kPa. The organic C content varies between 0.5 to $5 \times 10^{-3} \text{ kg kg}^{-1}$. One year prior to the field experiment, winter wheat was grown at the experimental site and harvested with a plot-combined harvester. During the past 10 years, the farmer practiced a soil preserving cultivation method without ploughing. No obvious plough pan was detected with the penetrometer.

We investigated the effects of a single vs. multiple passage. Therefore we compared three treatments, a reference plot, a plot where the vehicle passed once, and a plot where it passed four times. The machine was a self-propelled six-row sugar beet harvester, model Kleine SF10 (Fig. 2.1). Driving speed was 1 m s^{-1} . The lifting units of the combine harvester were in the raised position.

Detailed information about the tyres are shown in Table 2.1. The total weight of the sugar beet harvester was 285.2 kN. The load was unevenly distributed onto the wheels. The highest load was applied to the right front wheel, where the contact pressure (ratio between wheel load and contact area) was 151 kPa.



Figure 2.1 Sugar beet harvester used in the experiment.

Table 2.1 Detailed information about the tyres.

	right front wheel	right back wheel
specification	Radial tyre (Goodyear)	Radial tyre (Goodyear)
dimension	710/70R38	700/50-26.5
inflation pressure [kPa]	220	190
load [kg]	10`765	5`000
contact area [m ²]	0.71	0.30
calculated contact pressure [kPa]	151	165

The three plots were at all times exposed to natural precipitation. At the time of the compaction experiment, the top soil was near the actual field capacity. The matric potentials measured with a set of tensiometers installed at depths of 0.1,

0.2, 0.3, 0.4, 0.5, and 0.6 m close to the control plot showed -26, -25, -50, -45, -37, -27 hPa, respectively.

Laboratory measurements

One day after the passages, undisturbed soil samples were taken underneath the tyre track at the center of the right front wheel at depths of 0.10 - 0.20, 0.20 - 0.30, 0.30 - 0.40, 0.40 - 0.50 and 0.50 - 0.60 m. Eight samples were taken at each depth. Total porosity, macroporosity and bulk density were measured by the gravimetric method as described by Gysi et al (2000). The macroporosity is defined by draining to a matric potential of -30 hPa (SSSA, 1997).

Dye infiltration experiment

A solution of the dye Brilliant Blue FCF at a concentration of 4 gL^{-1} was used to stain the flow paths. The general toxicity of Brilliant Blue was found to be low and the dye can be considered as a suitable and environmentally acceptable tracer for studying solute transport in soil (Flury and Flühler, 1994). Being neutral or anionic, Brilliant Blue is not strongly adsorbed by negatively charged soil constituents. However, considerable adsorption of Brilliant Blue may occur, which diminishes its suitability for tracing the travel time of water itself (Flury and Flühler, 1994; Ketelsen and Mayer-Windel, 1997; Allaire-Leung et al., 1999). Especially for comparing flow patterns of different soils the soil specific adsorption of the dye tracer should be accounted for. In our case the non-ideality of Brilliant Blue is not relevant because we use it for tracing the flow paths and not for travel time or water infiltration depth. In addition, we used this dye tracer in a relative sense for discriminating the flow patterns in different treatments at one single site.

The tracer was applied at a constant rate of 5 mm h^{-1} for 8 h, using the sprinkling apparatus described by Flury et al. (1994). The top 0.1 m of the soil were removed before sprinkling to exclude the effect of pores being blocked by shearing and smearing due to the wheel action close to the surface.

The next day, a soil pit was excavated and vertical profiles prepared. The stained flow patterns were photographed on 6 to 10 profiles within a square of 1 m^2 . These replicated vertical profiles were prepared with a separation distance of 0.1

m. Using the method by Forrer et al. (2000), a Kodak color- and grayscale as well as a frame were attached to the profile to be used in the course of image processing.

Image processing

The color slides were developed and digitized onto a photo CD by a commercial laboratory. The images were then processed using digital image analysis. First, the images were geometrically corrected to standardize the resolution and coordinate system of the individual pictures. The result was a digital image, where one pixel represents 1 mm² of a soilprofile. Inhomogeneous illumination was corrected in each individual picture using the gray values on the frame. The color values on the grayscale were used to correct systematic variations in color between the pictures, as they may be caused by changes in light during the day or by differences of the film material. These image processing steps were conducted as described by Forrer et al. (2000).

According to their color values, the pixels were then classified as stained or unstained using a supervised classification based on the maximum-likelihood criterion (Using PCI Software, 1994). The resulting binary image shows the flow paths of the tracer solution in the soil. The distribution of the dye coverage with depth was calculated for each image, by horizontally counting the pixels indicating stained soil for every pixel row of the image.

2.3 Results and discussion

Soil physical properties

In Figure 2.2 we report the measurements of bulk density, macroporosity and the ratio of total porosity and macroporosity for the three treatments. In the single passage plot all parameters show a significant treatment effect at depth of 0.15 m (Wilcoxon test, $P < 0.05$). The macroporosity and the ratio of macroporosity and total porosity show a significant change at a depth of 0.35 m, opposite to the bulk density.

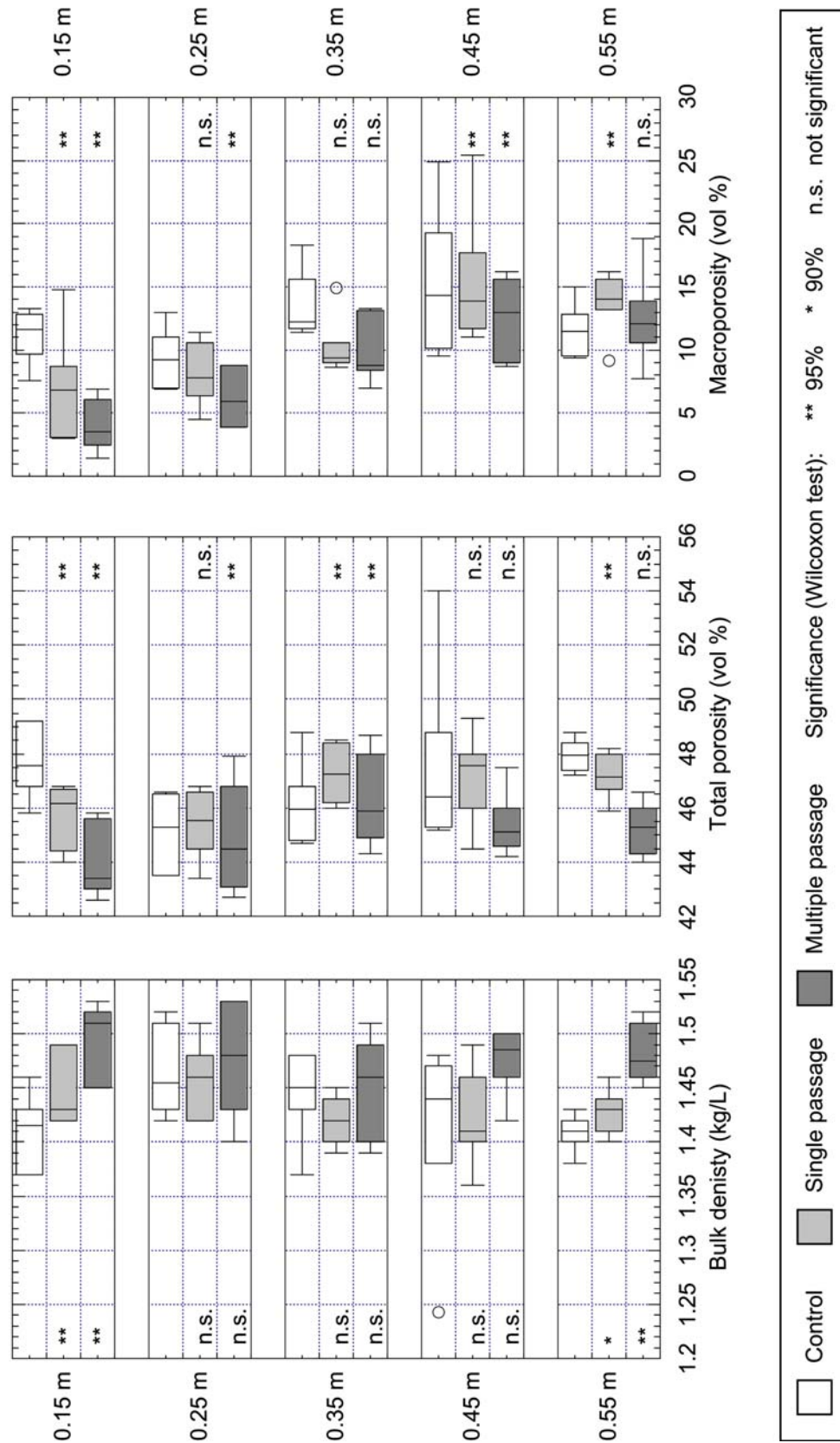


Figure 2.2 Bulk density, total porosity and macroporosity with depth in the three treatments.

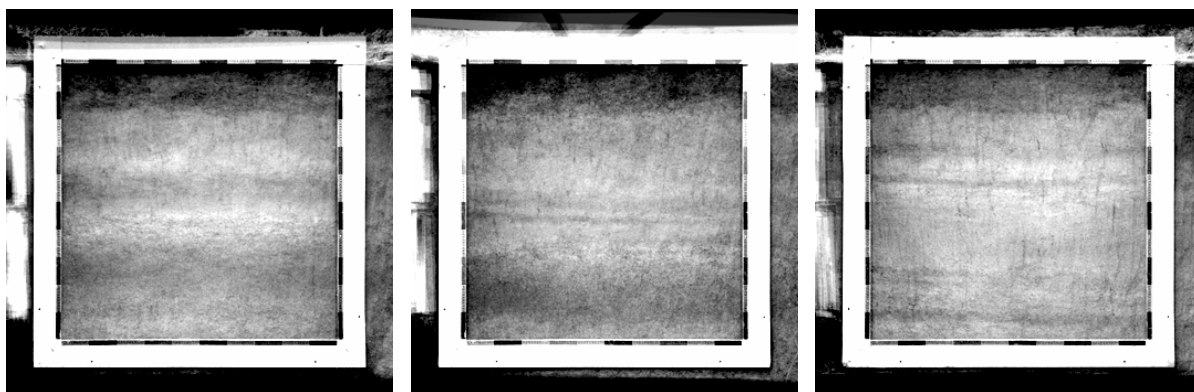


Figure 2.3 Superimposed blue channels of the flow pattern pictures for each treatment. The blue channel shows the background of the soil profiles without the dye tracer. The little squares show the sampling depths at 0.15 m, 0.25 m, 0.35 m, 0.45 m, and 0.55 m.

The multiple passage plot shows strong effects at depth of 0.15 m. At 0.25 m and 0.35 m, only the bulk density does not show any significant difference. At 0.45 m depth, none of the parameters is significantly different from those of the control plot. At 0.55 m depth, the bulk density shows a significant difference between the multiple passage plot and the control. Although no obvious plough pan was found with the penetrometer prior to the experiment, the laboratory measurements indicate the existence of a compacted layer at a depth of 0.25 m. Since the field site was not ploughed for the preceding 10 years, this denser layer is probably an old plough pan. In the single passage plot, only the topsoil above this plough pan was slightly, and in the multiple passage plot strongly compacted. In the latter case the effect was less pronounced at a depth of 0.25 m to 0.35 m.

At 0.55 m depth bulk density shows a significant effect in the multiple passage plot which suggests a compaction down to 0.55 m. At 0.45 m depth, the difference between the treatment was measurable, though minor and statistically not significant. It is conceivable that a previously already compact layer was not affected but transmitted the load to the underlying softer layer at 0.55 m depth leading to the observed compaction.

In Figure 2.3 the blue channel images of all flow patterns pictures taken in a plot are superimposed. The blue channel can be used to view the background image of a soil profile, because the spectral signature of the dye is only visible in the red and green channel. These images show that the layers are increasingly

heterogeneous with increasing depth below 0.4 m. Therefore, we cannot exclude the possibility that the differences measured at depths of 0.45 and 0.55 m are treatment effects or simply caused by a differing texture of the sampled layers.

Flow patterns

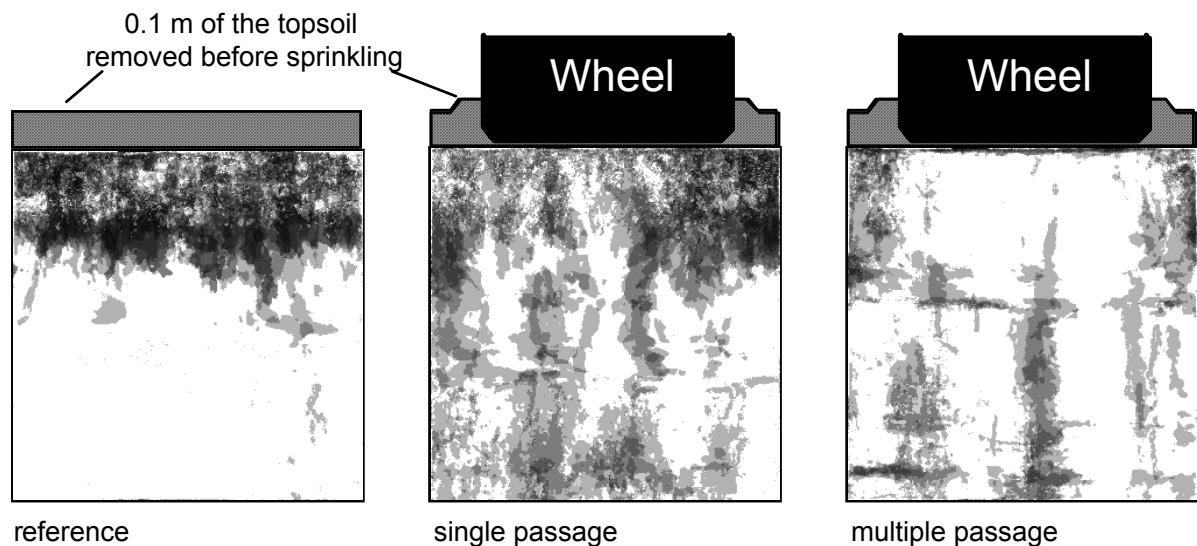


Figure 2.4 Superimposed images of all flow patterns observed in the individual treatments. The intensity of shading of a given areal unit (pixel) stands for the fraction of the pictures being stained at this particular coordinate.

The 6 to 8 flow pattern images per treatment exhibit systematic compaction effects very likely induced by the passage of the sugar beet harvester. In the compacted plots a larger area of the subsoil was stained than in the control plot. In Figure 2.4 all replicated flow patterns of the individual treatments are superimposed. The 0.1 m of topsoil, removed before sprinkling, and the wheel of the sugar beet harvester are schematically shown above the observed flow pattern. While the tracer solution directly infiltrated the soil in the control plot, it was ponding on the surface of the other two plots at the same sprinkling rate. The infiltration was apparently impeded due to top soil compaction. As the flow patterns show, the pore network accessible for infiltrating the solution into the top soil of the control plot is fine and more homogeneously distributed than in the compacted plots, while in the affected plots only very few flow paths pass the top soil right underneath the area of the passage of the wheel. On the left and the right of the profile, beneath the area not covered by the wheel, the flow patterns of the two trafficked plots look systematically similar to the patterns of

the control. Therefore we interpret the differences in pattern as compaction induced and not as being the result of a spatial trend (larger scale variability) in this particular field.

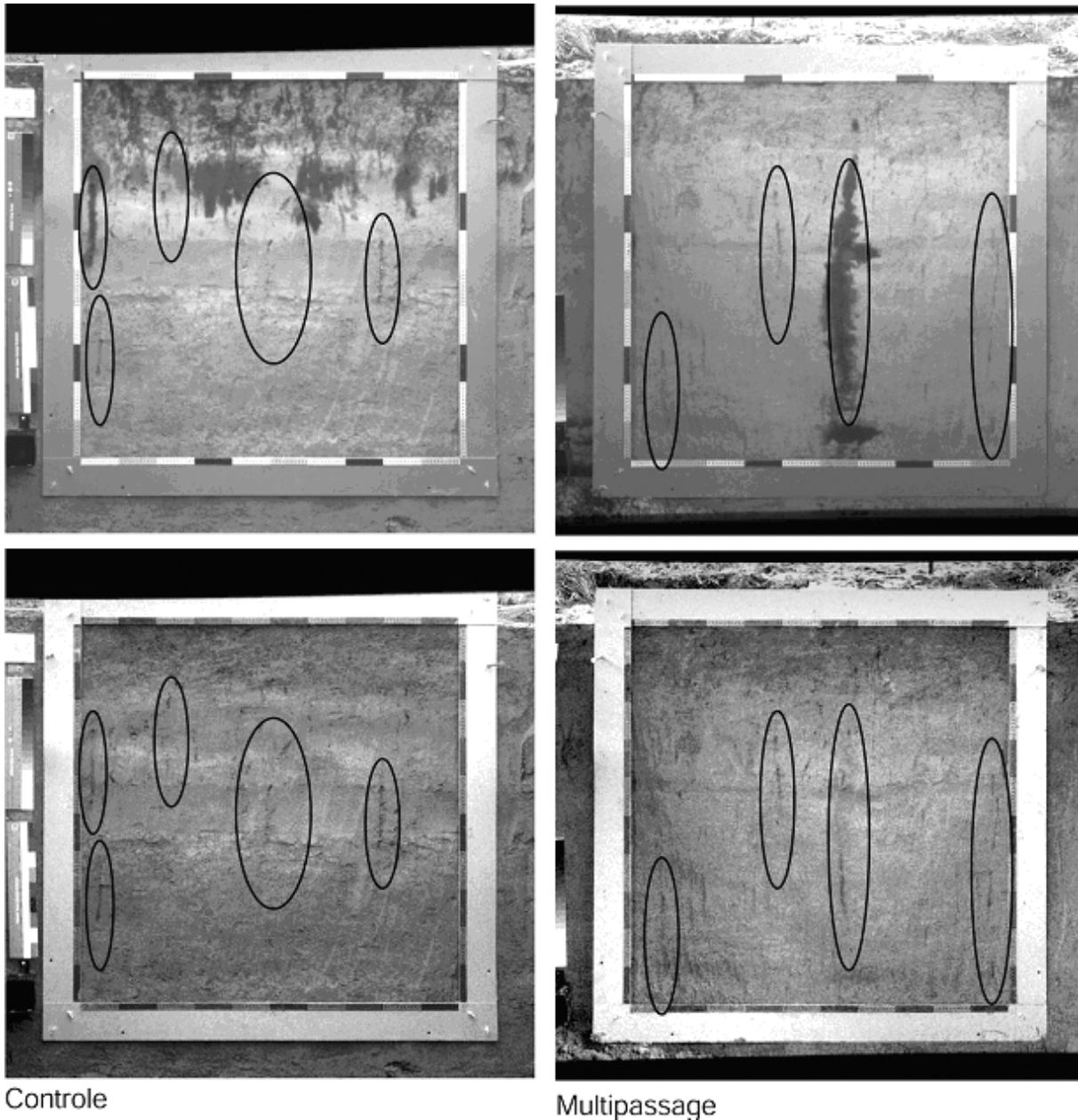


Figure 2.5 Example plot for the multiple passage plot and the control showing the role of worm burrows for the transport of the dye tracer. Above: red channel showing the flow pattern. Below: blue channel showing the soil structure without the flow pattern.

More vertically oriented worm burrows were stained under the two trafficked plots. Due to ponding, the water was probably funneled into these preferential flow ports. Figure 2.5 shows an example image for the control and the multiple

passage plot. In the upper part, the red channel image of the two pictures is shown, where the stained areas are clearly visible. The lower part shows the blue channel image. Here, the spectral signature of the dye is filtered and the soil structure without the flow pattern is visualized. Obvious earthworm channels are marked by ellipses. In both profiles one of the earthworm channels is stained. In the profile of the control plot, the earthworm channel only covers a small part of the stained pattern, while in the compacted profile, it is the mayor transport pathway.

Figure 2.6 shows the dye covered area horizontally aggregated per pixel depth increment, expressed as a function of depth for the profiles of each plot. The range between the first and the third quartile is given for each treatment. The depth profiles of the control plot can be clearly distinguished from those of the multiple passage plot. In the top 0.3 m, the dye coverage in the control profiles is much larger than in the multiple passage plot. Between 0.3 m and 0.6 m depth, the ranges are overlapping, while below 0.6 m there is definitely some dye tracer detected in the profiles of the multiple passage plot and almost nothing in the profiles of the control plots. The front of the dye solution probably reached greater depth in the trafficked plots due to compaction induced preferential flow. The flow patterns of the single passage profiles can not be distinguished from those of the other two treatments. Patterns resembling those of the control profiles were found as well as the ones similar to those of the multiple passage plot.

Figure 2.7 shows box plots indicating the variability of the averaged dye coverage in depth increments of 0.1 m for all profiles and each plot. On the right side the significance of the difference between the two treatments and the control are shown (Wilcoxon Rank sum Test) considering all the data, also the points marked as outliers in the plot. The multiple passage plot differs significantly (0.95%) from the control down to a depth of 0.35 m. The single passage plot differs significantly only for the two depths 0.25 and 0.95 m. When the outliers marked in the plot are not considered for the rank sum test, we find an at least 90% significance at all depths for the difference between the control and the multiple passage plot, and at depths of 0.25, 0.65, 0.85 and 0.95 m for the single passage plot.

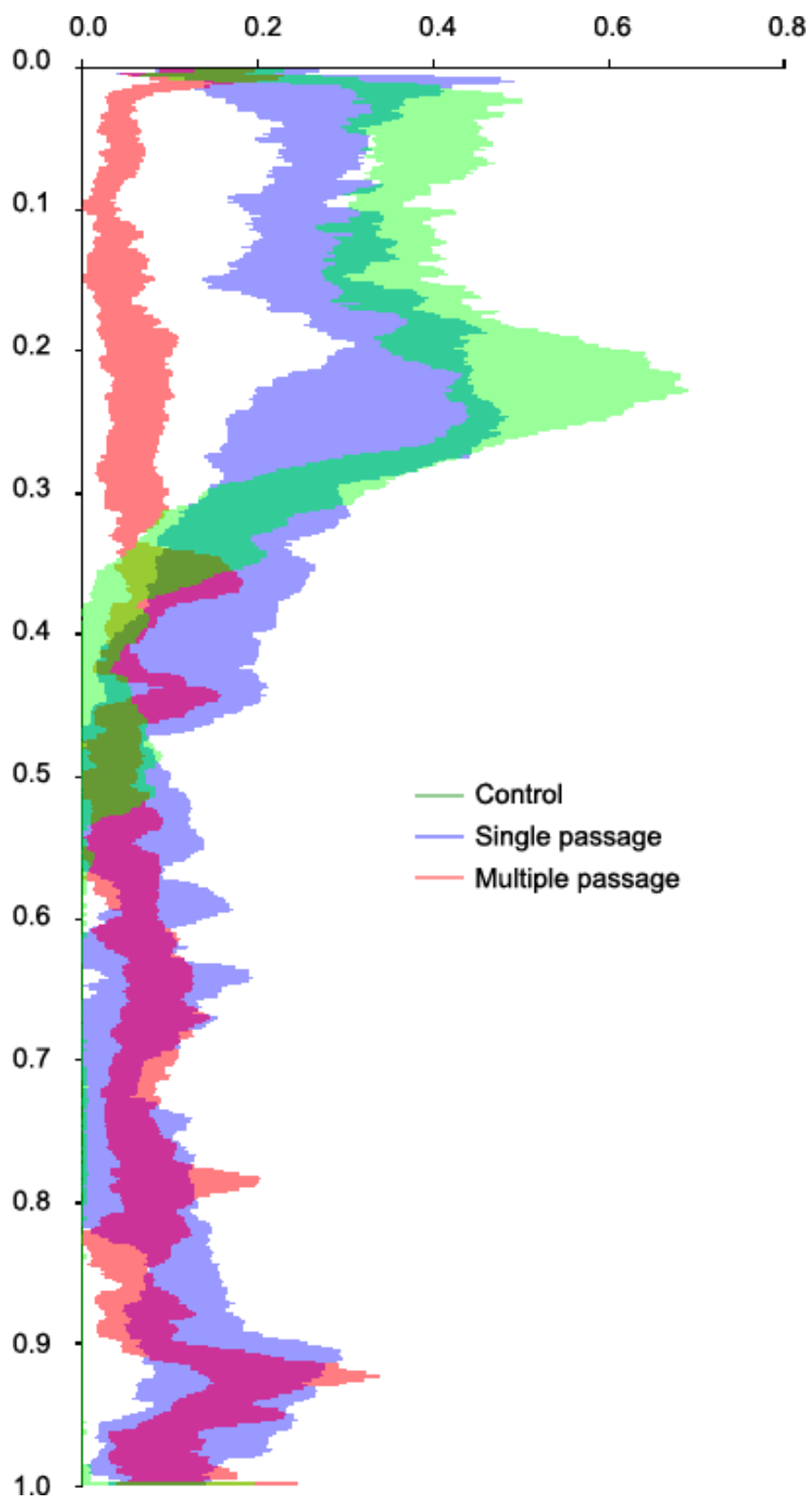


Figure 2.6 Variations of dye coverage (interquantile-range) vs. depth for the three treatments.

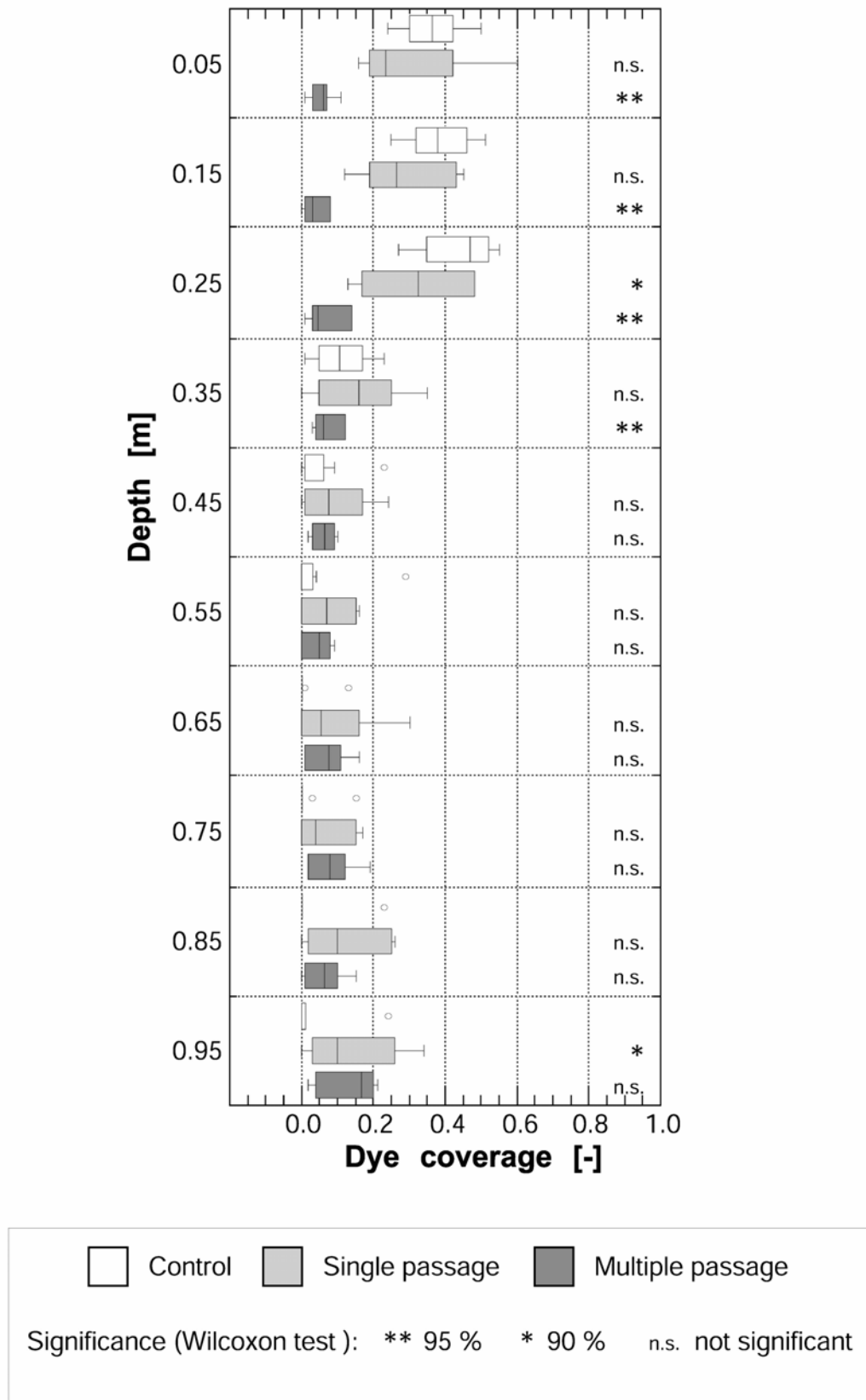


Figure 2.7 Dye coverage in depth increments of 0.1 m for the three treatments.

Discussion

The compaction detected by the laboratory measurements agree well with the results of the tracer infiltration measurements. The within treatment variability was significantly smaller than the variability between the treatments. This can be an expression of an a priori given larger scale variability in this particular field or, as hypothesised in our experiment, a compaction effect. The obvious difference between the flow patterns right underneath the wheel and just outside the wheel track observed in the multiple passage plot are very likely induced by compaction.

The analysis of the flow patterns showed that most of the homogeneously distributed network of flowpaths in the topsoil was no longer conductive in the trafficked plots. A significant decrease of macroporosity was measured at 15 cm depth for single passage plot and down to 35 cm depth for the multiple passage plot as compared to the control. During sprinkling, we observed water ponding on the surface of the two trafficked plots. Based on these measurements and observations we conclude that the permeability was drastically reduced by the vehicle traffic. In the control plot the water most likely infiltrated under unsaturated conditions. The top few centimeters of the soil in the two trafficked plots must have been closer to saturation or even saturated during sprinkling. We infer that the above postulated decrease in permeability caused by the vehicle traffic lead to local ponding, leading to enhanced preferential flow in the compacted plots. Several studies showed that preferential flow is more pronounced under high irrigation rates, especially under flooding conditions than under low irrigation rates (Flury et al., 1994; Gjetterman et al., 1997; McIntosh et al., 1999). Weiler and Naef (2000) found that macropore flow is initiated at the soil surface or at saturated or nearly saturated layers.

2.4 Conclusions

All measurements taken in this experiment indicate that the upper part of the soil profiles were compacted which apparently modified the flow regime. The laboratory measurements provide information about the depth dependence of compaction on infiltration, an information which cannot be drawn from the flow

patterns. On the other hand, the flow patterns provide not only information on possible compaction effects at all, but also clues about how compaction modifies water flow.

As discussed before, the change of permeability and the degree of water saturation during the infiltration play a major role with respect to the transport regime. The decreased macroporosity, which was measured in 15 cm depth of the two trafficked plots, as well as the reduction of the homogeneously distributed network of infiltration pathways shown by the flow patterns, and the observed water ponding on the soil surface of the two trafficked plots are evidence for a decrease of permeability caused by the vehicle traffic. The water saturation in the treated plots was most likely close to saturation, which lead to preferential flow (Weiler and Naef, 2000).

We therefore conclude that the influence of soil compaction on the flow patterns depends not only on the compaction and the soil type, but also on the sprinkling or rainfall intensity. Starting a hypothetical experiment at a very low infiltration rate, it is possible, that no or only small changes in the flow patterns become visible, indicating that the transport regime remains the same. If we imagine an increasing infiltration rate, the saturation near the surface would increase too and the preferential flow patterns would become obvious, as observed in our field experiment.

2.5 Acknowledgements

Financial support for this work was provided by the Research and Development fund of the Swiss Gas Industry (FOGA). We also thank the Swiss Federal Research Station for Agricultural Economics and Engineering (FAT), for supporting this collaboration at the Frauenfeld site. We acknowledge the help of J. Leuenberger in planning and conducting the field work and the contribution of M. Jaquillard in the field and his master thesis work on the flow path analysis.

2.6 References

- Alakukku, L., 1996. Persistence of soil compaction due to high axle load traffic. II. Long-term effects on properties of fine-textured and organic soils. *Soil & Tillage Research*. 37: 223-238.
- Allaire-Leung, S. E., S. C. Gupta, and J. F. Moncrief, 1999. Dye adsorption in a loam soil as influenced by potassium bromide. *Journal of Environmental Quality*. 28:1831-1837.
- Craul, P. J., 1994. Soil compaction on heavily used sites. *Journal of Arboriculture*. 20(2): 69-74.
- Ewing, R. P., and R. Horton, 1999. Discriminating dyes in soil with color image analysis. *Soil Science Society of America Journal*. 63: 18-24.
- Flury, M., and H. Flühler, 1994. Brilliant blue as a dye tracer for solute transport studies - A toxicological overview. *Journal of Environmental Quality*. 23: 1108-1112.
- Flury, M., H. Flühler, W. A. Jury, and J. Leuenberger, 1994. Susceptibility of soils to preferential flow of water: A field study. *Water Resources Research* 30(7):1945-1954.
- Flury, M., and H. Flühler, 1995. Tracer characteristics of Brilliant Blue FCF. *Soil Science Society of America Journal*. 59(1): 22-27.
- Forrer, I. N., and R. Kasteel, 1999. Longitudinal and lateral dispersion in an unsaturated field soil. *Water Resources Research*. 35(10): 3049-3060.
- Forrer, I. N., A. Papritz, R. Kasteel, H. Flühler, and D. Luca, 2000. Quantifying dye tracer in soil profiles by image processing. *European Journal of Soil Science*. 51: 313-322.
- Ghodrati M., and W. A. Jury, 1990. A field study using dyes to characterize preferential flow of water. *Soil Science Society of America Journal*. 54: 1558-1563

- Gjettermann B., K. L. Nielsen, C. T. Petersen, H. E. Jensen, S. Hansen, 1997. Preferential flow in sandy loam soils as affected by irrigation intensity. *Soil Technology*. 11: 139-152.
- Gysi M., G. Klubertanz, and L. Vulliet, 2000. Soil compaction due to heavy wheel traffic. Field data and modelling. *Soil and Tillage Research*. 56(3-4):117-129.
- Horton, R., M. D. Ankeny, and R. R. Allmaras, 1994. Effects of compaction on soil hydraulic properties. In: B. D. Soane, and C. van Ouwerkerk (Editors), *Soil Compaction in Crop Production*. Elsevier Science B. V. pp. 141-165.
- Ketelsen, H., and S. Meyer-Windel, 1999. Adsorption of brilliant blue FCF by soils. *Geoderma*. 90:131-145.
- McIntosh, J., J. J. McDonnell, and N. E. Peters, 1999. Tracer and hydrometric study of preferential flow in large undisturbed soil cores from the Georgia Piedmont, USA. *Hydrolic Processes*. 13:139-155.
- Soil Science Society of America, SSSA, 1997. Glossary of soil science terms. *Am. Soc. Agron. Madison, WI, USA*, pp.83.
- Using PCI Software, Version 5.3 Easi/Pace, 1994. pp. 216-224. PCI Inc. Ontario. Canada.
- Von Albertini, N., J. Leuenberger, H. P. Läser, and H. Flühler, 1995. Regeneration der Bodenstruktur eines verdichteten Ackerbodens unter Kunstwiese. *Bodenkundliche Gesellschaft der Schweiz Dokument* 7: 10-16. Juris Druck und Verlag Dietikon.
- Weiler M., and F. Naef, 2001. Effects of macropore flow on runoff generation. *Journal of Hydrological Processes* (in press).
- Zehe E., and H. Flühler, 2001. Slope scale variation of flow patterns in soil profiles. *Journal of Hydrology* 247:116-132.

Chapter 3

A multi-tracing method for detecting soil compaction impacts

Beatrice Kulli, Hannes Wydler, Markus Berli, Markus Jauslin, Jörg Leuenberger, Hannes Flühler und Rainer Schulin

Abstract

Soil compaction affects the structure and continuity of the pore network and often modifies the soil water regime. A previous study has shown differences in flow patterns under trafficked and non trafficked plots at the same site. However, spatial variability of the soil structure masks possible differences and weakens the conclusiveness of comparisons between flow patterns of 'treatment' and 'control' in neighbouring plots. The idea of this study is to compare flow patterns stained immediately before and after compaction at the same plot in order to overcome this basic problem of comparability between 'treatment' and 'control'. Therefore two fluorescent tracers were applied onto the same plot, a less mobile tracer before and a more mobile tracer after the soil was trafficked with a heavy tracked construction vehicle. The spatial distributions of the two tracers in the soil were recorded separately on profile walls using a digital camera equipped with tracer specific filters and light source: the superposition of the two concentration maps of the flow patterns yields direct measures of compaction-induced changes in the flow path network. We found systematic differences between the flow patterns of the two tracers on plots, where the tracers were applied onto the soil surface, as well as on plots where the topsoil was removed before sprinkling. The effect perceived based on visual inspection of the superimposed flow patterns of the two tracers were affirmed by a quantitative evaluation of the flow patterns. The mean distances of the pixels belonging to the flow pattern of the first tracer to the skeleton (medial axes) of

the flow pattern of the second tracer was larger at trafficked plots than at control plots, indicating that the vehicle traffic significantly changed the infiltration patterns.

3.1 Introduction

Heavy machinery used in modern agriculture and in off-road construction work can lead to soil compaction, usually a reduction of the pore volume, and to shearing that disrupts continuous macropores (Horton et al., 1994; Craul, 1994; Alakukku, 1996). A change in pore geometry affects water flow and solute transport as well as the availability of water and air to plants and micro organisms.

Soil water flow paths infiltration can be visualized by means of dye tracers added to infiltrating water (Ghodrati and Jury, 1990; Flury et al., 1994; Gjetterman et al., 1997; Zehe and Flühler 2001; Weiler and Naef, 2001). This technique can be used to identify structural changes in soil due to compaction, like for instance after the passage of a heavy vehicle. Experiments with the dye tracer Brilliant Blue for example revealed significant effects on the infiltration pattern due to single and multiple passages by a sugarbeet harvester (Chapter 2). Most of the fine infiltration pathways in the topsoil disappeared, while some vertically oriented worm burrows stayed open in the compacted plots, enhancing preferential flow bypassing the main root zone.

When a single dye tracer is applied, e.g., Brilliant Blue, the compaction effect can only be identified by comparing the stained infiltration patterns in trafficked plots with patterns in untreated control plots, because the method is destructive to the soil. Comparing the profiles of different plots entails major difficulties. The spatial heterogeneity of the soil causes variations between the flow patterns which have nothing to do with the treatment. Effects can be detected in front of this “background noise”, if they are quite strong and if a large number of replicate experiments can be made to ensure statistical significance. Besides, the quantitative comparison of flow patterns causes problems. When flow patterns of two plots have to be compared they cannot be overlaid directly. Parameters

have to be determined which characterize the general properties of the pattern in a statistical sense.

The application of two tracers, one before and one after compaction by vehicle traffic could solve some of these problems. The flow patterns of the two tracers found in one and the same plot could be overlaid and directly compared. It would be immediately visible when parts of the infiltration network had been inactivated after compaction. Even small compaction effects could be more reliably detected.

In the present study we tested this approach using two fluorescent tracers that can be distinguished by means of suitable optical filters. A field experiment was carried out, where the effect of a 30 t excavator moving on caterpillar tracks on the flow patterns of the tracers was studied. One tracer was applied before compaction and the other afterwards. In one experiment we investigated topsoil compaction and in the second experiment subsoil compaction. In the first case we applied the tracers onto the soil surface and in the second onto the subsoil after having the topsoil removed. One plot per treatment served as an uncompacted control to show the differences between the subsequent infiltrations of these tracers in absence of compaction. The 2-dimensional distribution of each tracer concentration was mapped independently of that of the other.

3.2 Materials and methods

Test site

The experiments were conducted on an agricultural soil near the village of Buttisholz (Switzerland). The soil type was a Gleyic Cambisol. This test site was selected for our experiment because of its low pre-consolidation load of less than 50 kPa down to a depth of 0.6 m (Hug und Krähenmann, 1999; Qasem et al., 2000) so that compaction effects were expected with the machine used in the experiment (see below).

The plots were situated in the vicinity of a brook. Texture, organic matter content and pH of the soil were measured at several locations in the experimental area (Table 3.1). These measurements show the rather large variability of the parameters on a relatively small scale of 1.2 – 8 m.

Table 3.1 Soil properties measured at the test site (minimum and maximum value of 4 profiles).

Depth [m]	Sand [kg kg ⁻¹]	Silt [kg kg ⁻¹]	Clay [kg kg ⁻¹]	Org. matter [kg kg ⁻¹]	pH [-]
0.07-0.17	0.35-0.42	0.35-0.40	0.23-0.25	0.030- 0.032	5.4-5.7
0.27-0.37	0.31-0.38	0.39-0.42	0.21-0.27	0.019- 0.025	5.6-6.6
0.47-0.57	0.29-0.37	0.37-0.45	0.25-0.30	0.020- 0.028	5.7-6.3
0.67-0.77	0.29-0.48	0.35-0.46	0.16-0.25	0.004- 0.006	5.9-6.8

Field experiment

The compaction experiment was conducted with a construction machine ‘Liebherr 942’ (Fig. 3.1). The vehicle was moving on caterpillar tracks with a mean contact pressure of 60 kPa (60 cm track width, 410 cm track length and 30 t net machine weight).

The construction machine passed on the plots four times (two times forward, two times backward) at a speed of 0.5 m s⁻¹. During the third passage, the vehicle stopped for half an hour on each plot in order to allow water displacement and complete consolidation of saturated subsoil horizons.



Figure 3.1 Tracked excavator used for the compaction experiment.

Dye tracer infiltration

For the infiltration experiments, the experimental area was divided into four plots with a size of 2 m² each. On two plots, the topsoil (about 0.2 m) was removed and replaced by 5 cm of sand. On the other two plots the topsoil was left undisturbed. Plots with and without topsoil were chosen in order to distinguish between the effect of topsoil and subsoil compaction.

The first tracer applied was a solution of Sulforhodamin B (SB), which is less mobile than the second tracer, Acid Yellow 7 (AY). On 13 consecutive days 10 to 14 mm of SB solution were applied with a mean concentration of 0.2 g l⁻¹. An exception was one of the two plots without topsoil, which was flooded by surface runoff after a strong rainfall event. Since the topsoil had been removed and replaced by 5 cm of sand, the surface of the plot was about 15 cm below the level of the surrounding field and we had to wait 6 days, until the water was

infiltrated, before we could continue with the application of the tracer. The total amount of water infiltrated in the respective plot was about the same as in the other plots, but only 7 of 13 tracer applications were sprinkled.

The tracer solution was applied by means of a watering can with a perforated horizontal tube (Fig. 3.2), allowing homogeneous sprinkling. The tracer was applied on the plot central area of 100×50 cm (Fig. 3.2). On the rest of each plot an equivalent amount of water was applied. Boxes were used to check the spatial distribution of the water and tracer application (Fig. 3.2).



Figure 3.2 Plot without topsoil. The area of the tracer application is the darker region in the middle of the plot. The boxes were used to check the spatial homogeneity of the application of water and tracer.

One plot with and one without topsoil were trafficked by an excavator one day after the last tracer application as described above. The profile from which the topsoil had been removed was refilled with sand and topsoil material prior to the passage of the heavy vehicle to level the top surface. After the passage of the construction vehicle, these repacked layers were removed before the second tracer was applied, in order to create the same upper boundary condition for the application of the second tracer as for the application of the first tracer.

Four days after trafficking, the second tracer was applied. On the two following days, 10 mm of tracer solution were applied at a concentration of 20 g l⁻¹ onto each plot at each day. Another 10 mm of tap water was applied at the last day onto the plots without topsoil and for two additional days on the plots with topsoil

Vertical profiles (1 × 1 m) were then excavated perpendicular to the driving direction of the vehicle and pictures of the stained vertical infiltration patterns were taken using the technique described below. In each plot, 2 to 3 vertical soil profiles were prepared and imaged at a separation distance of 10 cm. The imaged profile area marked by a frame was 70 cm × 60 cm. The profile was 10 cm wider than the wheel track.

Fluorescent tracers

Fluorescent dyes absorb light at specific wavelengths (excitation) and emit at other wavelengths of the spectrum (emission). When two dyes have clearly separated maxima in their emission spectra they can be independently visualized using tracer specific filters for illumination and detection (Aeby et al., 2001).

Sulforhodamin B (SB) adsorbs stronger to soil particles than Acid Yellow 7 (AY). This choice and sequence prevent the first tracer from being leached to greater depths by the second tracer solution. The chemical properties of SB are also described by Aeby et al. (2001) whereas AY is chemically comparable to BF, which unfortunately is no longer commercially available.

Detection of the tracer distribution

Figure 3.3 shows an illustration of the apparatus used for illuminating the profiles and for detecting the flow patterns. In order to avoid the interference of straylight, the pictures were taken under an opaque tent.

We took three pictures for each tracer: (i) Fluorescent image: excitation filter at the liquid light guide (Fig. 3.4) and emission filters at the camera. (ii) Reflection image: same as (i), but no filter at the camera. (iii) Flatfield image: same as (ii), but with a cardboard covering the profile. The flatfield image measures variations of illumination. It is used for correcting of inhomogeneous lighting.

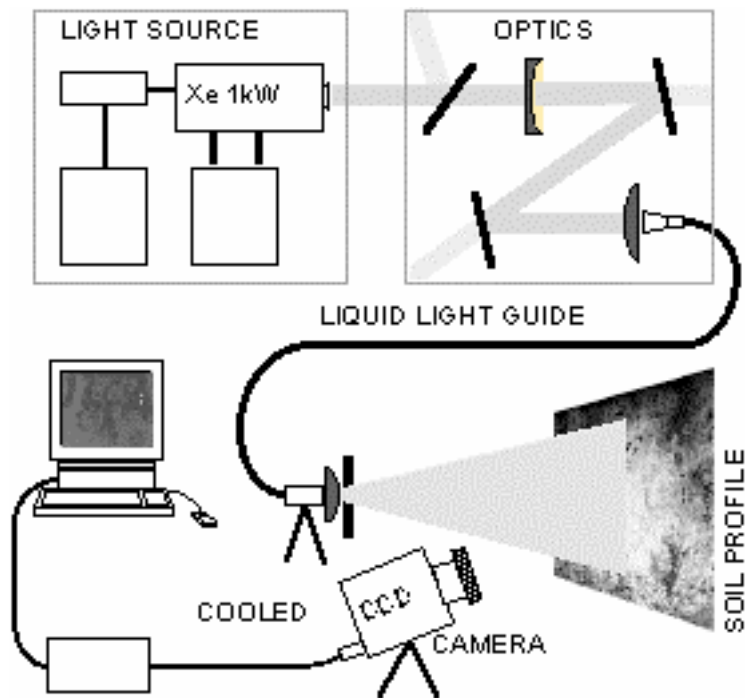


Figure 3.3 Illumination and digital detection device used for measuring the distributions of the two tracers in vertical soil profiles.

Digital image processing

The following image correction steps were carried out in order to obtain the concentration distribution of the fluorescent tracers in the 2-dimensional profiles.

- Geometrical correction: adjusting image to rectangular coordinates. After the geometrical correction the profile area of 70×60 cm is represented by 1050×900 pixels. One pixel corresponds with 0.67×0.67 mm at the profile.
- *Correction of inhomogeneous lighting: the lighting from a point source gives an illumination maximum of the centre of the profiles, decreasing towards the border area (Fig. 3.4). This inhomogeneity was corrected by means of the flatfield image.*
- Background correction: the influence of the variability of hue and reflection of the soil were corrected by means of the reflection image (Fig. 3.4).

- Calibration: in order to calibrate the tracer concentrations, samples of known tracer concentrations were attached to the frame and photographed with the profiles. By means of the grey values of these samples on the digital images it was possible to assign tracer concentrations to all pixels of the flow pattern image (Fig. 3.4).

In order to assess the influence of the traffic on the tracer infiltration, the concentration map of the two tracers were overlaid and compared. The images of the control plots may show differences between the concentration maps caused by differences in the infiltration conditions or by the chemical properties of the tracers.

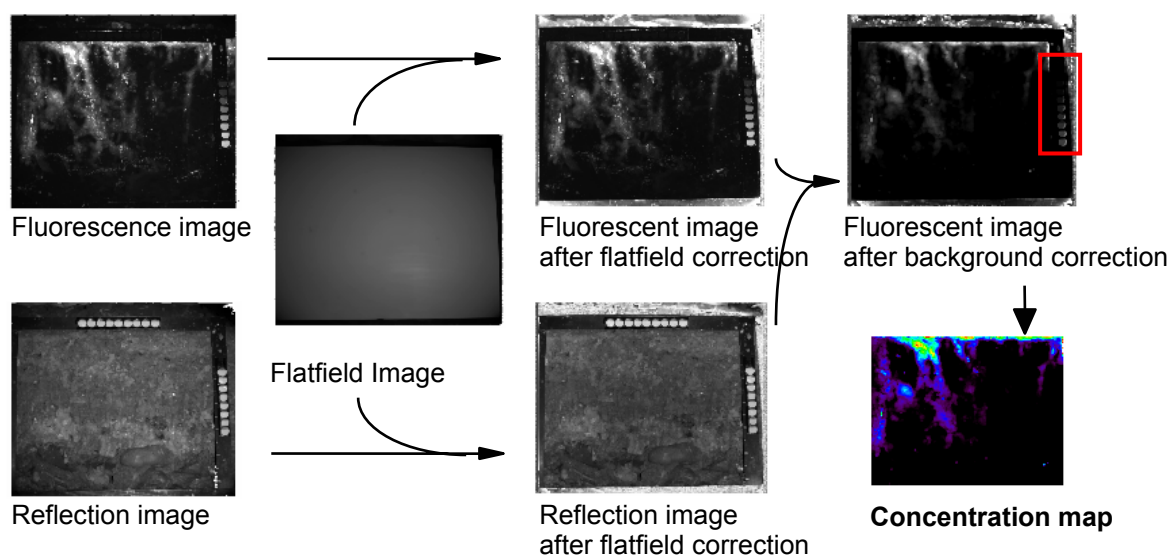


Figure 3.4 Correction steps leading from the original images to the concentration map. The red rectangle indicates the position of the calibration samples.

Qualitative and quantitative analysis of the results

In order to qualitatively visualize the differences of the concentration maps, the tracer distributions of SB and AY were overlaid using different colours for the two tracers.

To quantify effects, the distances between the pixels 'stained' by AY and the pixels stained by SB were determined for each profile. Figure 3.5 shows the image analysis steps carried out in order to calculate these distances.

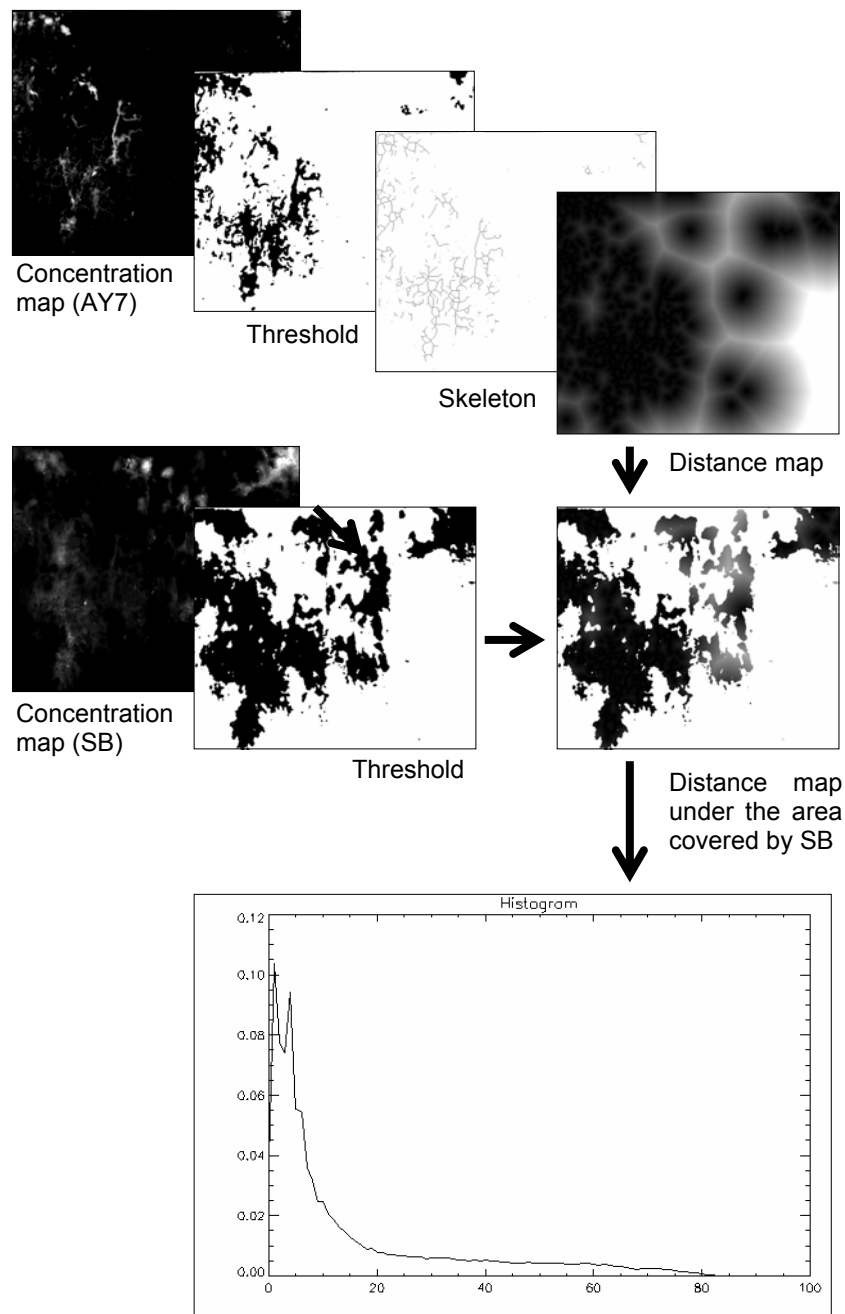


Figure 3.5 Steps carried out to obtain the distance between pixels belonging to the flow patterns of SB and AY.

By means of a threshold value, concentration maps were transformed into maps of dye-covered area. After this step each pixel of the binary image only contains the information whether it belongs to the stained flow pattern or not. In order to obtain the branches of the infiltration network of AY, the flow pattern of AY was skeletonized. Then a distance map was calculated showing by grey values

the distance of every white pixel of the skeleton image to the nearest black pixel (dark: small distance, bright: large distance).

The intersection of the flow pattern of SB and the distance map gives the distribution of distances of the pixels belonging to the flow pattern of the first tracer to the skeleton of the flow pattern of the second tracer. Means and histograms of these distributions give quantitative information about compaction effects on the flow patterns.

If the patterns remain approximately the same when the tracer is applied before or after the traffic, then the distances between stained areas of SB and AY are small. If the infiltration patterns change dramatically and some branches of the infiltration network of the first tracer are not stained by the second tracer, then the distances between the pixels stained by the first tracer to the nearest pixel stained by the second tracer is larger.

3.3 Results

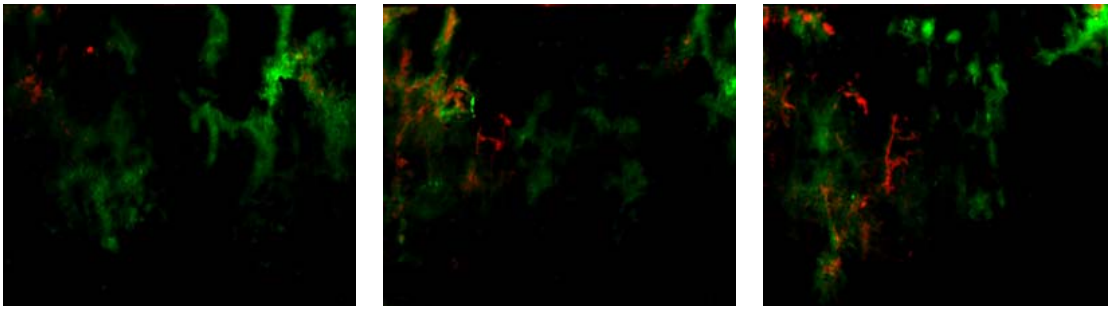
Qualitative results

Figure 3.6 shows overlay images of the tracer concentration maps for all the profiles recorded in this experiment. SB stained the flow paths active for transport before the compaction event, AY the flow paths still active afterwards.

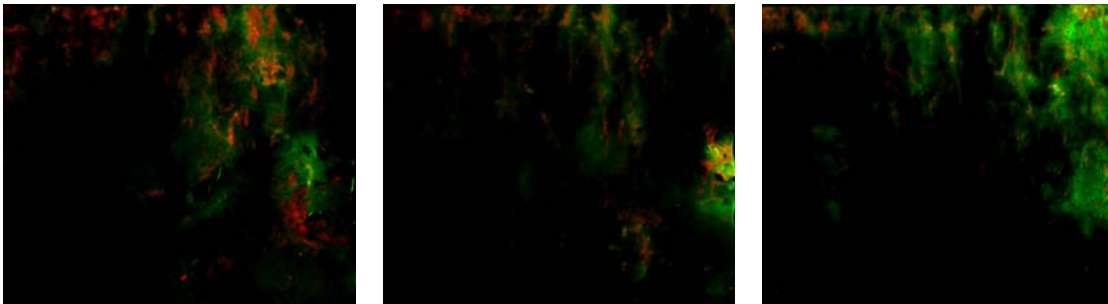
The overlay images show obvious differences between the flow patterns of the two tracers in the control profiles. The patterns do not match exactly. The areas stained by AY are smaller and look sharper than the areas stained by SB. In some cases, AY did not reach the same depth as SB. But it is clearly visible, that both tracers infiltrated through the same structures. The differences found in the patterns can be attributed to the difference of residence time of the two tracers in the soil.

The first SB application was sprinkled 14 days before the first application of AY. SB had much more time to propagate into the matrix by diffusion. Different sorption characteristics and the 100 times larger concentration of AY may also have affected the differences of the patterns in the control profiles.

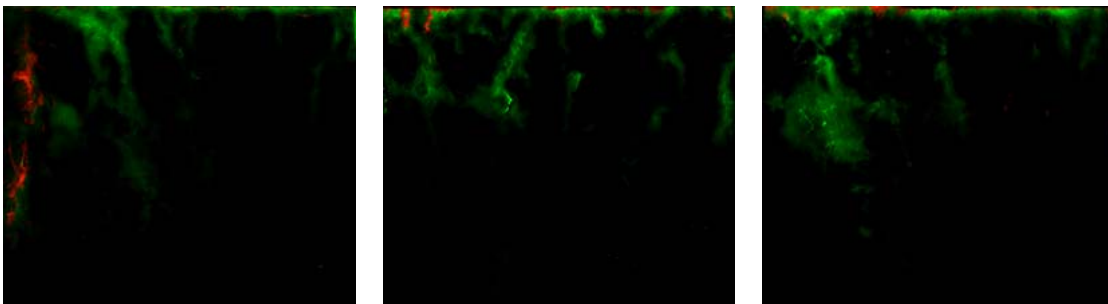
With topsoil, trafficked



With topsoil, control



Without topsoil, trafficked



Without topsoil, control

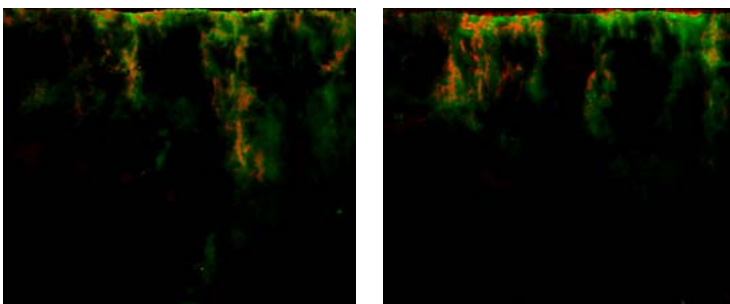


Figure 3.6 Overlay images of the concentration maps of the two fluorescent tracers. Green: SB (applied before compaction) Red: AY (applied after compaction)

The flow patterns of the trafficked plot sprinkled without topsoil, which was flooded by surface runoff after a strong rainfall event; do not show obviously different infiltration patterns of SB as compared to the other plots.

In the trafficked plots differences between the SB infiltration and the infiltration of AY go much beyond the differences found in the control plots. AY stained less flow paths than SB. Differences are more pronounced in the centre of the images and less pronounced or lacking near the left and right border. This observation agrees well with the area covered by the track, which was located in the centre of the profile, while 5 cm on each side of the profile were outside the wheel covered area.

Compaction effects are clearly visible in both the plot where the tracers were applied on the topsoil as well as the plot where the tracers were applied onto the subsoil. The difference between the flow patterns of trafficked and non-trafficked soil was smaller for the plots where the tracer was applied on the topsoil.

Quantitative results

Figure 3.7 shows the frequency distribution of the distances between every pixel belonging to the flow pattern of SB to the nearest pixel belonging to the skeleton of the flow pattern of AY.

The merged frequency distributions per plot show highly significant differences (Wilcoxon Rank sum Test) between the trafficked plot and the control plot for both, the plots with tracer application onto the topsoil as well as the plots with tracer application directly onto the subsoil. In all treatments the maximum occurs at small distances, but the distribution of the trafficked plots show smaller maxima and more tailing towards bigger differences. This behaviour can be observed in both the plot where the tracer was applied onto the topsoil as well as the plot where the tracer was applied directly onto the subsoil.

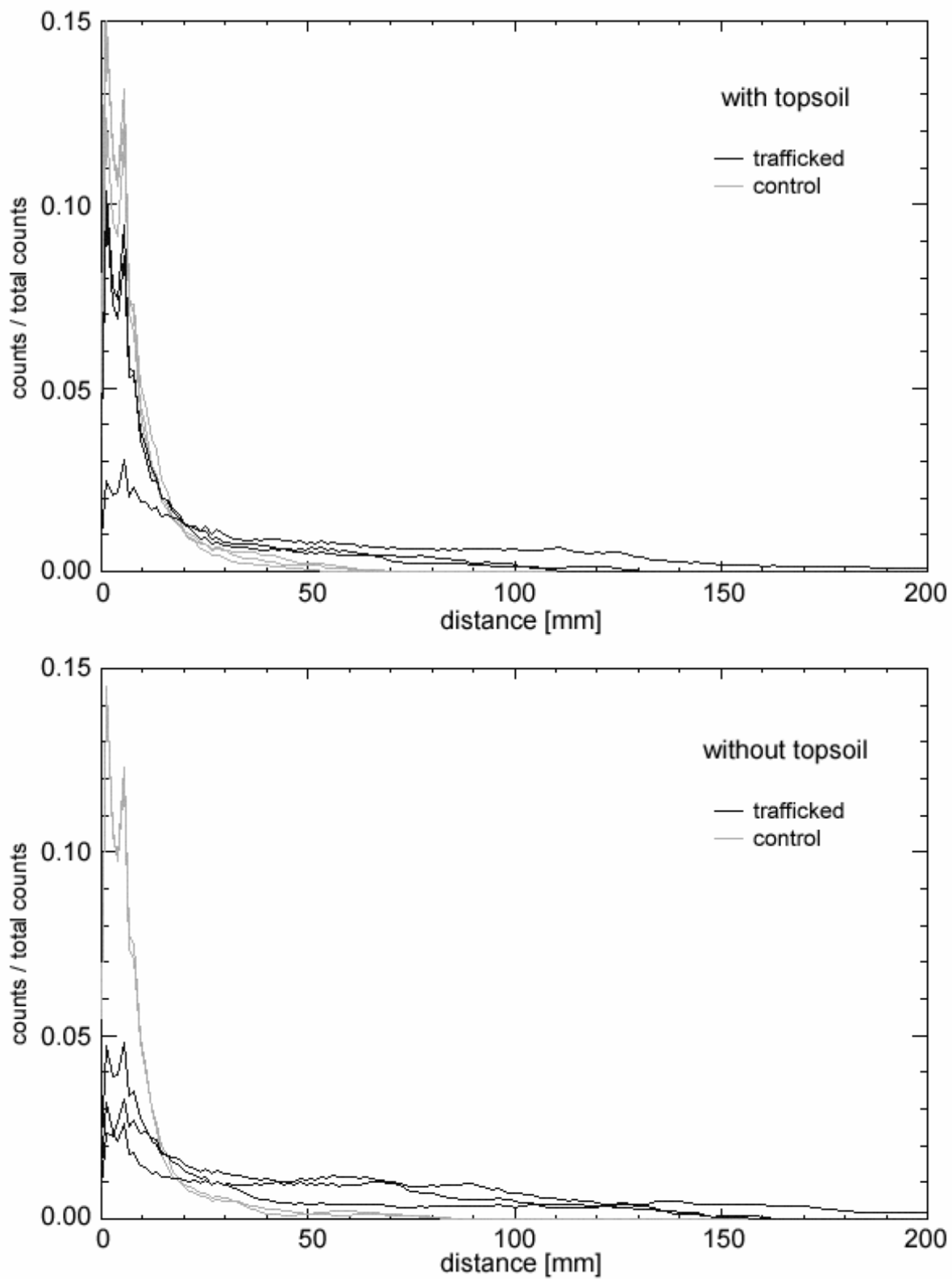


Figure 3.7 Distribution of the nearest distances of all pixels belonging to flow patterns of SB to the skeleton of the flow patterns of AY.

Figure 3.8 shows the mean distance between the pixels of the flow pattern of SB and the skeleton of the flow pattern of AY for the profiles of each treatment. The mean distances of the control plots are small and very close together, while the mean distances for the trafficked plots are significantly larger and have a larger variation.

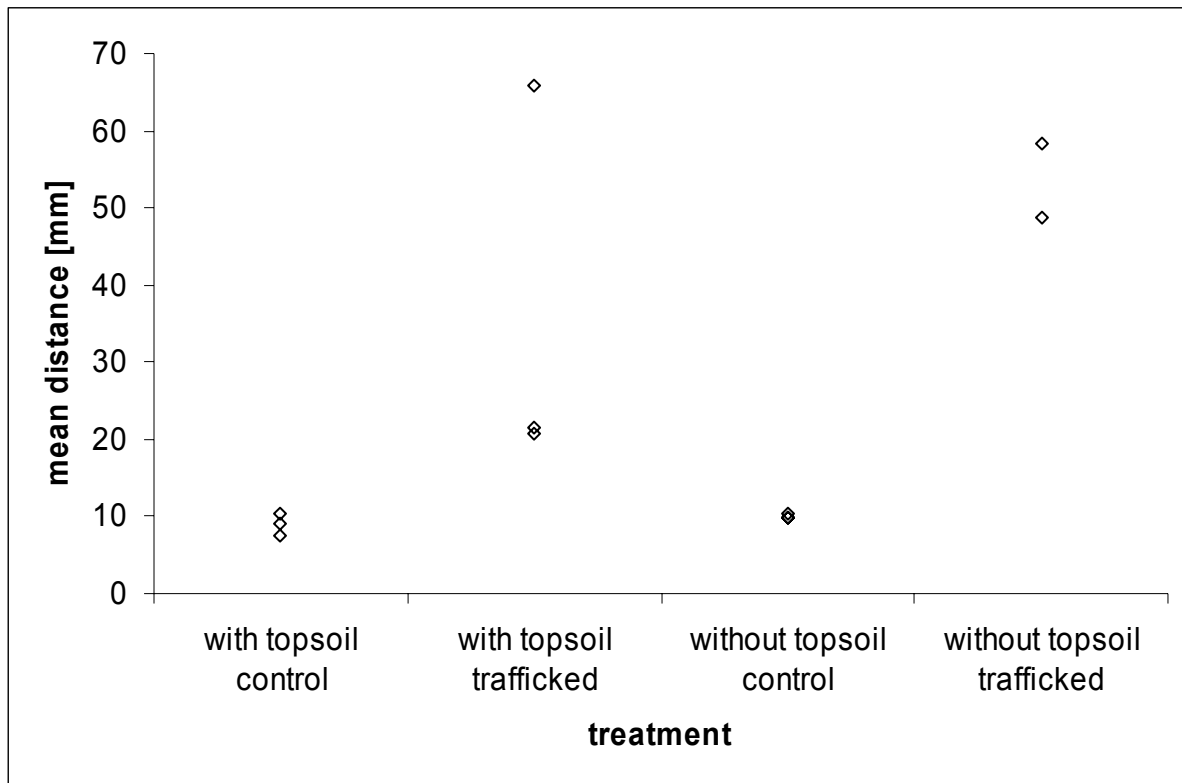


Figure 3.8 Mean distance between the pixels of the flow pattern of SB and the skeleton of the flow pattern of AY for the profiles of each treatment.

3.4 Discussion and conclusions

The tracer concentration maps of the plot, where the tracers were applied onto the topsoil, show that there was a compaction effect in the topsoil caused by the vehicle traffic. From the infiltration images of the plot where the tracers were applied directly onto the subsoil we conclude that there was also a compaction effect below 20 cm.

The overlay images of the concentration maps indicate that there is a stronger effect of compaction on the plot, where the tracer was applied directly onto the subsoil. This observation is confirmed by the quantitative results. However,

without knowing more about the mechanical properties (e.g. stability, elasticity and pressure propagation) of the refilled soil of the respective plot as compared to the original top soil layer, it is difficult to evaluate such small differences.

An exact assessment of the compaction effect with depth is still not possible based on the tracer distribution. Because every soil layer affects the flow pattern underneath, patterns found at a certain depth cannot be compared independently from the patterns above.

The study shows, that fluorescent tracers allow a direct comparison of the infiltration patterns before and after a compaction event at exactly the same position. This method is more sensitive than tracer experiments, where the infiltration pattern at a control plot is compared with the infiltration patterns at a trafficked plot, because the influence of pre-existing spatial variability of soil structure is excluded. Therefore fewer profiles have to be examined to determine effects. Experiments with fluorescent tracers, on the other hand, are more time consuming, because a complicated detection system is required consisting of a CCD camera, several filter sets, a light source and an opaque tent

3.5 Acknowledgements

Many thanks to M. Berli, M. Jauslin, J. Leuenberger for planning and conducting the field experiments and to H. Wydler for taking the pictures of the fluorescent tracer distribution and for evaluating the concentration maps of the tracers. Financial support for this work was provided by the Research and Development fund of the Swiss Gas Industry (FOGA).

3.6 References

- Aeby, P., U. Schultze, D. Braichotte, M. Bundt, F. Moser-Boroumand, H. Wydler and H. Flühler (2001). "Fluorescence Imaging of Tacer Distributions in Soil Profiles." *Environmental Science and Technology*. 35(4): 753-760.
- Alakukku, L., 1996. Persistence of soil compaction due to high axle load traffic. II. Long-term effects on properties of fine-textured and organic soils. *Soil & Tillage Research*. 37: 223-238.
- Craul, P. J., 1994. Soil compaction on heavily used sites. *Journal of Arboriculture*. 20(2): 69-74.
- FAO (1990). *FAO-Unesco Soil Map of the World*. Rome, Food and Agriculture Organisation of the United Nations (FAO), Revised Legend.
- Flury, M., H. Flühler, W. A. Jury, and J. Leuenberger, 1994. Susceptibility of soils to preferential flow of water: A field study. *Water Resources Research* 30(7):1945-1954.
- Ghodrati M., and W. A. Jury, 1990. A field study using dyes to characterize preferential flow of water. *Soil Science Society of America Journal*. 54: 1558-1563
- Gjettermann B., K. L. Nielsen, C. T. Petersen, H. E. Jensen, S. Hansen, 1997. Preferential flow in sandy loam soils as affected by irrigation intensity. *Soil Technology*. 11: 139-152.
- Horton, R., M. D. Ankeny, and R. R. Allmaras, 1994. Effects of compaction on soil hydraulic properties. In: B. D. Soane, and C. van Ouwerkerk (Editors), *Soil Compaction in Crop Production*. Elsevier Science B. V. pp. 141-165.
- Hug, E. and Krähenmann, K., 1999. Verdichtungsempfindlichkeit unterschiedlicher Bodentypen entlang der geplanten Erdgas-Transportleitung Däniken-Griespass. Diploma Thesis, Institut für terrestrische Oekologie, Eidgenössische Technische Hochschule Zürich, Schlieren, 65 pp.
- Qasem, H., Attinger, W., Berli, M. and Schulin, R., 2000. Zusammenhänge zwischen ödometrischer Verdichtungsempfindlichkeit und morphologischer

Merkmale von Böden, untersucht an ausgewählten Standorten auf dem Trasse der Transitgasleitungen Däniken-Grimsel (TRG2) und Rodersdorf-Lostorf (TRG3), Institut für terrestrische Ökologie der ETH Zürich, Schlieren.

Weiler M., and F. Naef, 2001. Effects of macropore flow on runoff generation. *Journal of Hydrological Processes* (in press).

Zehe E., and H. Flühler, 2001. Slope scale variation of flow patterns in soil profiles. *Journal of Hydrology* 247:116-132.

Chapter 4

Compaction of agricultural and forest subsoils by tracked heavy construction machinery

M. Berli, B. Kulli, W. Attinger, M. Keller, J. Leuenberger, H. Flühler, S.M. Springman and R. Schulin

Submitted for publication in 'Soil & Tillage Research'

Abstract

Precompression stress has been proposed as a criterion for subsoil compression sensitivity in regulations, limiting mechanical loads by vehicles, trafficking on agricultural and forest soils. In this study we investigated the applicability of this criterion to the field situation in the case of tracked heavy construction machinery. ‘Wet’ and ‘dry’ test plots at three different test sites along an overland gas pipeline construction site were experimentally trafficked with heavy tracked machines used for the construction work. The comparison of samples taken from beneath the tracks with samples taken from non-trafficked areas beside the tracks showed that no significant increase in precompression stress occurred in the subsoil. Comparing calculated vertical stress with precompression stress in the subsoil, only little compaction effects could have been expected. Precompression stress was determined by the Casagrande procedure from confined uniaxial compression tests carried out in the laboratory on undisturbed samples at -6 kPa initial soil water potential. Dye tracer experiments showed little differences between water flow patterns of trafficked and non-trafficked subsoils, in agreement with the results of the precompression stress, bulk density and macroporosity measurements. The results indicate that the existing precompression stress may be a suitable criterion to define the

maximum allowable stress in the contact area of a rigid track in order to protect agricultural and forest subsoils against compaction.

4.1 Introduction

Compaction has been recognised as a major threat to soil fertility of large areas of cultivated land. It is estimated to be responsible for the degradation of an area of 6.8×10^4 km² world-wide, of which 3.3×10^4 km² is located in Europe (Oldeman et al., 1991), adversely affecting crop production as well as environmental quality (Soane and Van Ouwerkerk, 1995). Compaction of subsoils is regarded as particularly problematic because of its persistence and the difficulty to remediate it. Natural regeneration can result from activity of soil fauna and flora (von Albertini et al., 1995) as well as from abiotic processes such as drought and frost induced shrinkage. Research reviewed by Håkansson and Reeder (1994) showed that the effectiveness of these processes, however, decrease rapidly with depth beneath the main root zone of the topsoil. Artificial loosening by deep ploughing, on the other hand, may aggravate rather than solve problems. For example Kooistra et al. (1984) reported that secondary soil compaction was even worse than the first compaction because subsoil structure had been disrupted and weakened by the loosening operation. Neilsen et al. (1990) found that reduced crop yields due to subsoil compaction were only partially compensated by fertiliser treatment.

The review by Håkansson and Reeder (1994) shows that the risk of subsoil compaction may be considerable for soils with high moisture content under vehicles with high axle loads. Other important factors, apart from axle load and moisture content, are tyre dimensions, contact stresses, number of passes, soil strength and stress history (Hadas, 1994). While many studies investigated soil compaction caused by wheeled traffic, only a few publications deal with the extent of (sub-)soil compaction in agricultural land due to tracked heavy construction machinery. McKyes (1980) found an increase in bulk density down to 0.3 m depth and a slight decrease in crop yield one year after construction of high voltage transmission lines in Canada. Culley et al. (1982) found that porosity and hydraulic conductivity were reduced and bulk density and penetration resistance were increased down to 0.3 m depth in a medium-to-fine

grained soil, affected by oil pipeline construction in Ontario, Canada. Moreover, yields of corn, soybeans and cereals were depressed for up to 10 years after the installation of the oil pipeline (Culley and Dow, 1988). Dumbleck (1984) carried out traffic experiments on arable land in Germany with heavy excavators (weighing up to 4.7×10^4 kg, mean stress in the contact area up to 100 kPa) under 'dry' (-30 to -100 kPa soil water potential) and 'wet' (\gg -6 kPa soil water potential) soil conditions. He found a decrease in the amount of macropores down to 0.65 m in the 'dry' and 1 m in the 'wet' soil. Håkansson (personal communication) found a decrease in crop yield of about 35% in the first year and about 5 % from the third to the fifth year on agricultural land trafficked by machines in the course of gas pipeline construction in Sweden.

In Switzerland, subsoil compaction has raised particular concern because of the use of agricultural land as temporary access way for heavy machinery required in construction work. Apart from road and railway line construction, the construction of overland gas pipelines has become a topical issue in this respect. Tracked vehicles weighing more than 3×10^4 kg are routinely used in this construction work. Even machines weighing more than 6×10^4 kg have been used. In a first study, von Rohr (1996) found changes in bulk density, porosity and pore size distribution down to 0.65 m depth of a soil trafficked with tracked pipeline construction machines weighing up to 3.3×10^4 kg (mean normal stress in the contact area: 73 kPa). While due to the relatively large contact area, the mean normal stress in the contact area is smaller than of some agricultural machines, however the stress reaches deeper into the soil. This was already reported by Söhne (1953; 1958) applying the theory of Boussinesq (1885) and Fröhlich (1934) on traffic induced stress propagation in agricultural soils.

The limited reversibility of subsoil compaction calls for measures to prevent it. That is to avoid stresses exceeding the soil's range of elastic behaviour and thus leading to plastic deformation. Horn (1981; 1988), Horn and Lebert (1994) and Kirby (1991b) proposed to use the precompression stress as a limiting criterion. According to this concept, reloading a soil at a given moisture status up to a stress which it had previously experienced will cause only elastic (i.e. reversible) and no plastic (i.e. non-reversible) compression (e.g. Terzaghi and Peck, 1948 p. 106f). This concept appears to be particularly appropriate for application in setting tolerance limits for the use of tracked construction

machinery on agricultural land. These machines drive slowly and exert compression stresses primarily through their weight, which is supported by a rather large contact area compared to wheeled machines. Consequently, precompression stresses determined under static stress conditions, as they occur in confined uniaxial compression tests, were assumed to represent critical stresses under the tracks of such construction machines adequately enough for practical purposes.

While the precompression stress concept is theoretically very appealing, only few investigations have been performed to test its suitability to assess soil compaction sensitivity under field conditions (Culley and Larson, 1987; Hammel, 1993; Blunden et al., 1994; Gysi et al., 1999). For example, differences in drainage conditions between field and laboratory experiments were considered as potentially limiting to the validity of laboratory determined precompression stresses. Furthermore, laboratory tests on intact samples cannot reproduce stress conditions of the undisturbed soil under field conditions exactly as it is not possible to reproduce the field boundary conditions in any detail. Oedometer tests e.g. subjecting a sample to uniaxial compression with lateral extension confined by a steel cylinder, offers different boundary conditions of strain to those experienced by undisturbed soil in the field, which is loaded by a tracked vehicle. Also precompression stress is usually not evident as a sharp bend in the stress-volumetric strain curve but rather an operationally defined point in an often rather gradual transition between recompression curve and virgin compression line, indicating that there is no abrupt change from purely elastic to plastic compression. In addition, precompression stress has to be as sensitive to changes of compactness as bulk density and pore size distribution, and additionally easy to determine under practical conditions.

While the mechanics of water saturated ‘engineering’ soils (Atkinson and Bransby, 1978 p. 2) has been extensively investigated, much less is known about the more complicated mechanical behaviour of unsaturated agricultural soils, in which structure is predominantly influenced by biological factors, i.e. the activity of organisms and their organic residues. Given these uncertainties about the feasibility of precompression stresses, the validity of this criterion in predicting subsoil compressibility under tracked heavy construction machinery and field conditions has to be demonstrated unequivocally.

To test the applicability of precompression stress as a criterion for susceptibility to compaction under ‘real world’ conditions, field traffic experiments were performed with tracked machinery in the course of pipeline construction work. For this purpose, wetted and non-wetted test plots of three different soils along the construction site were trafficked under controlled conditions. Precompression stress, bulk density, coarse- and coarse-to-intermediate porosity of samples taken from trafficked soil beneath tracks were compared to reference measurements of non-trafficked soil. In addition, dye tracer experiments were carried out in order to compare the flow patterns of water in the trafficked and non-trafficked subsoils. We expected precompression stress, bulk density and coarse-to-intermediate porosity to increase, coarse porosity to decrease and flow pathways to disappear if the predicted stress in the soil below the tracks exceeded the precompression stress.

4.2 Material and methods

The traffic experiments were performed in autumn 1996 and spring 1997 on the three different sites ‘Freienstein’, ‘Güllenhau’ and ‘Ruckfeld’, which were situated along the gas pipeline TRAWO, running from Zuzgen to Winterthur/Ohringen in northern Switzerland. Soil properties at the three test sites are given in Table 4.1.

Soil types according to FAO (1990) were an Eutric Cambisol at Freienstein, a Dystric Cambisol at Güllenhau and a Haplic Luvisol at Ruckfeld. The Freienstein and Ruckfeld site were under crop rotation and used as grassland in the year of the experiment. The Güllenhau site was situated in a pine forest.

The situation of the experiments at the three sites is depicted in Figure 4.1. The experimental trafficking was part of the pipeline construction process, i.e. under ‘real-world’ conditions.

At Freienstein and Ruckfeld, test plots were wetted prior to trafficking by sprinkling for one day at a rate of 0.1 m d^{-1} at Freienstein and five days at a precipitation rate of 0.1 m d^{-1} at Ruckfeld. Thereafter, the soil was left to redistribute the infiltrated water for one more day. At the forest site of Güllenhau, space allowed only for one trafficked plot. Due to the weather

conditions during the experiment, this site was relatively wet. In order to assess compaction effects from all test plots, samples were taken from non-trafficked areas beside the tracks.

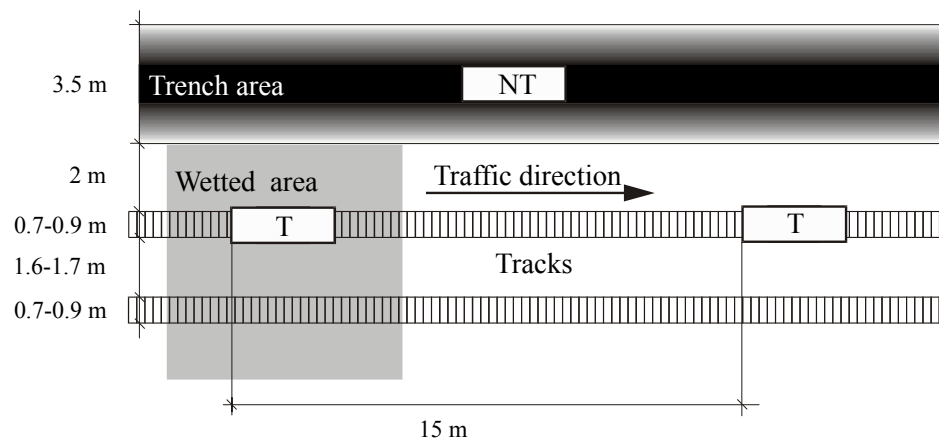
Table 4.1 Soil parameters at the three test sites Freienstein, Güllenhau and Ruckfeld

Site	Depth [m]	Silt [†] [kg kg ⁻¹]	Clay [†] [kg kg ⁻¹]	Gravel [m ³ m ⁻³]	Organic matter [‡] [kg kg ⁻¹]	Bulk density [kg m ⁻³]
Freienstein	0.07–0.17	0.31	0.25	2	0.028	1510
	0.27–0.37	0.34	0.24	< 1	0.012	1620
	0.47–0.57	0.34	0.25	< 1	0.011	1590
	0.67–0.77	0.43	0.32	< 1	0.013	1510
Güllenhau	0.07–0.17	0.52	0.17	8	0.044	1130
	0.27–0.37	0.51	0.20	8	0.010	1330
	0.47–0.57	0.48	0.19	12	0.007	1530
Ruckfeld 'wet' plot	0.07–0.17	0.55	0.14	< 0.01	0.033	1310
	0.27–0.37	0.60	0.12	< 0.01	0.011	1570
	0.47–0.57	0.57	0.17	< 0.01	0.011	1510
	0.67–0.77	0.57	0.18	< 0.01	0.010	1520
Ruckfeld 'dry' plot	0.07–0.17	0.57	0.16	< 0.01	0.031	1360
	0.27–0.37	0.55	0.16	< 0.01	0.025	1530
	0.47–0.57	0.58	0.16	< 0.01	0.015	1540
	0.67–0.77	0.56	0.17	< 0.01	0.012	1610

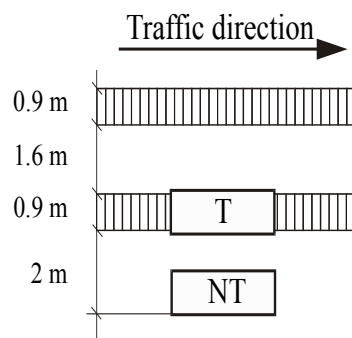
[†] Determined with the pipette method

[‡] Measured as weight loss after oxidation by H₂O₂.

Freienstein



Güllenhau



Ruckfeld

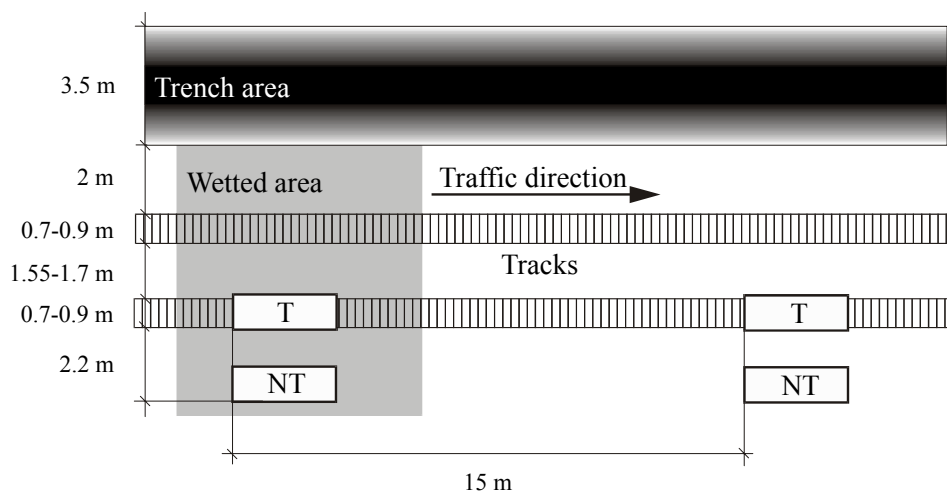


Figure 4.1 Situation of the test plots at the three experimental sites with sampling and sprinkling areas: NT non-trafficked, T trafficked.

For the traffic experiment, three different types of construction machines were used, as given in Table 4.2. The machinery used in the experiments were Fiat FH 300 excavators and Fiat Allis PL 40 C as well as Cat 583 sidebooms, specially constructed for placing large diameter pipes into trenches. The machines were driving directly on the soil surface without a protecting layer put on top of it. Table 4.3 gives the sequence, duration and mean normal stress in the contact area performed by these machines in the three experiments.

Table 4.2 Characteristics of the machinery used in the experiments

Machine type	Net machine weight [kg]	Length of the contact area [m]	Width of the contact area (twice track width) [m]	Net mean normal stress in the contact area [kPa]
Fiat FH 300	3.02×10^4	4.0	1.8	42
Fiat Allis PL 40 C	2.56×10^4	3.5	1.4	51
Cat 583	3.8×10^4	3.2	1.5	78

Table 4.3 Test sequence for the three test sites

Machinery used	'Wet' plot		'Dry' plot	
	Load duration [s]	Mean normal stress in the contact area [kPa]	Load duration [s]	Mean normal stress in the contact area [kPa]
Freienstein				
1st Fiat FH 300	20	42	20	42
1st Fiat Allis PL 40C	20	51	20	51
2nd Fiat Allis PL 40C	20	51	20	51
3rd Fiat Allis PL 40C	20	51	920	86 [†]
2nd Fiat FH 300	920	72 [†]	920	72 [†]
Güllenhau				
Fiat FH 300	40	42	-	-
Ruckfeld				
1st Fiat FH 300	140	42	140	42
Fiat Allis PL 40C	140	51	140	51
Cat 583	140	78	140	78
2nd Fiat FH 300	140	42	140	42

[†] Normal stress under the trench closest track during the placement of pipe.

At the Freienstein site, a Fiat FH 300 followed by three Fiat Allis PL 40 C and a second Fiat FH 300 trafficked slowly over the two plots at a velocity of 0.1-0.2 m s⁻¹. The second Fiat FH 300 stayed for 900 s on each plot while placing the pipe in the trench. The third Fiat Allis PL 40 C stayed for 900 s on the ‘dry’ plot holding up the pipe. Holding up and placing the pipe leads to an additional load of 4×10³ kg per excavator or sideboom and increases the mean normal stress in the contact area of the trench closest track up to 72 kPa for the Fiat FH 300 and to 86 kPa for the Fiat Allis PL 40 C.

At Güllenhau, only a Fiat FH 300 was available which trafficked the plot once forward and backward with a velocity of 0.1-0.2 m s⁻¹. The machine did not perform any other working action and also did not carry any additional load during the experiment.

In the experiment at Ruckfeld a Fiat FH 300 was followed by a Fiat Allis PL 40 C, a Cat 583 and a second Fiat FH 300. These machines drove at a velocity of 0.1-0.2 m s⁻¹, stopping on each of the plots for 120 s. Again the machines did not perform any working action and also carried no additional load during the experimental passages.

Table 4.4 Soil water potential of the three test sites at different depths immediately before the passage of the machines

Site	Test plot	Soil water potential [kPa]			
		0.1-0.15 m depth	0.3-0.35 m depth	0.5-0.55 m depth	0.7-0.75 m depth
Freienstein	‘dry’	-70.1	-48.3	-14.7	-5.7
	‘wet’	-17.3	-6.7	-5.5	-7.2
Güllenhau	‘wet’	-3.9	-4.2	-1.7	-0.7
Ruckfeld	‘dry’	<-85.0	-85.0	-33.4	-16.3
	‘wet’	-5.2	-2.7	-0.7	-0.2

‘Wet’ and ‘dry’ conditions varied considerably between the three sites and between depths as shown by the tensiometer readings taken immediately before

the passage of the machines (Table 4.4). In the subsoil of Güllenhau and the wetted plots at the other two sites, water potential was around -7 kPa or higher, while in the subsoils of the non-wetted plots of Freienstein and Ruckfeld they were around -15 kPa or lower down to 0.55 m depth. Below that depth, the subsoils showed the same water potential of around -6 to

-7 kPa in both plots at Freienstein, whereas the same difference as in the upper subsoil was also found at 0.7-0.75 m depth at Ruckfeld.

Table 4.5 Size (D/H: diameter/height) and number of samples of the three test sites

Site	Precom- pression stress		Bulk density		Coarse porosity		Coarse-to- intermediate porosity	
	D/H [m/m]	No.	D/H [m/m]	No.	D/H [m/m]	No.	D/H [m/m]	No.
Freienstein								
topsoil	0.1/ 0.06	16	0.1/ 0.06	16	0.1/ 0.06	16	-	-
subsoil	0.108/ 0.11	4-6	0.108/ 0.11	4-6	0.05/ 0.02	8	0.05/ 0.02	8
Güllenhau								
topsoil	0.108/ 0.11	8	0.108/ 0.11	8	0.108/ 0.11	3	-	-
subsoil	0.108/ 0.11	8	0.108/ 0.11	8	0.108/ 0.11	3	-	-
Ruckfeld								
topsoil	0.108/ 0.11	6	0.108/ 0.11	6	-	-	-	-
subsoil	0.108/ 0.11	6	0.108/ 0.11	6	0.05/ 0.02	8	0.05/ 0.02	8

To measure the stress distribution under the vehicle tracks, four Bolling probes (Bolling, 1987) were placed in the centreline of the track at a depth of 0.32 m in the 'wet' test plot at Ruckfeld. Pressure readings were taken electronically every 2 s. In order to compare measurements of different Bolling probes, pressure

values were expressed as relative pressure i.e. pressure readings, taken as a function of time, divided by the mean of the pressure readings over the measured time interval.

After trafficking, soil profiles were opened across the plots at right angles to the direction of the passage and soil cores were sampled using sharpened thin-walled metal cylinders. Size and number of the samples used for the determination of precompression stress, bulk density, coarse- and coarse-to-intermediate porosity are given in Table 4.5.

Given the asymmetric loading situation at the Freienstein site, trafficked soil was sampled only beneath the track adjacent to the trench. Non-trafficked soil samples were also taken from the trench area between the 'wet' and 'dry' trafficked plot before the traffic experiment took place. At Güllenhau and Ruckfeld trafficked soil beneath the track most removed (distant) from the trench was sampled. Non-trafficked soil samples were taken 2 m at right angles from the centreline of the track farthest the trench, in order to avoid influence of the load but also to be as close as possible to minimise the influence of spatial heterogeneity (Fig. 4.1). It was not possible to take undisturbed soil cores at Güllenhau beneath 0.4 m depth due to the high gravel content.

For the dye tracer experiment, test plots of 'wet' and 'dry' trafficked and non-trafficked soil were chosen adjacent to the sampling areas of the three test sites. The dye 'Brilliant Blue FCF' (Flury and Flühler, 1995) was dissolved in water (4 kg m^{-3}) and sprinkled by a constant rate of 5 mm h^{-1} during 8 h on an area of 1.5 by 1.5 m using the apparatus described by Flury et al. (1994). The sprinkling rate was kept so low in order to avoid dye ponding on the soil surface. For the Freienstein and Güllenhau soil 0.09 m^3 and for the Ruckfeld soil 0.225 m^3 of dye tracer were applied on each test plot. At Freienstein, the topsoil was removed first and then the dye was applied directly on the subsoil surface in 0.2 m depth. At Güllenhau, the dye was applied on the undisturbed topsoil. At Ruckfeld, the topsoil was loosened manually down to 0.3 m depth in order to create similar surface conditions for the application of the tracer on trafficked and non-trafficked soil. One day after sprinkling, a 1.5 m deep trench was dug with the face perpendicular to the border of the sprinkled area. For the trafficked plots, the trench centreline was aligned with the centreline of the track. Between 3 and 10 vertical profiles of 1 by 1 m (0.1 m horizontal distance between the

profiles) were prepared at the trench face, exposing the infiltrated dye. Each profile was photographed with a 35-mm camera. The pictures were digitalised, their geometrical distortion and illumination were corrected and the colours adjusted in order to distinguish the dye in the flow paths from the surrounding soil (Forrer et al., 2000). In order to obtain the flow pattern of the whole test plot we laid the resulting 'maps' of the flow paths of each profile on top of each other.

Precompression stress was determined from confined uniaxial compression tests. Prior to the compression test, the samples were conditioned to an initial soil water potential of -6 kPa (values with respect to the sample's centre) by applying a hanging water column. Samples were kept within the coring cylinders which were built into the compression cell and subsequently subjected to stepwise increased stress. Stresses from a range of 8 to 2000 kPa were applied through a piston, which fitted the inner diameter of the cylinders. Each compression step lasted for 1800 s after which the stress was increased to the next level. This stress duration was assumed to represent the duration a machine stays at the same place during normal construction work. Precompression stress was determined from the resulting stress-strain curves using the graphical procedure of Casagrande (1936). After the oedometer test, the samples were dried at 105 °C for at least 24 hours and weighed to determine the dry bulk density.

For the subsoil from Freienstein and Ruckfeld, coarse- (equivalent pore diameter $> 5 \times 10^{-5}$ m) and coarse-to-intermediate (equivalent pore diameter 5×10^{-5} – 5×10^{-6} m) porosity was determined using 4×10^{-5} m³ core samples with a pressure cell apparatus (Richards, 1941; Richards and Fireman, 1941). Because of the higher gravel content, samples to determine coarse porosity taken from Freienstein topsoil and Güllenhau top- and subsoil were larger i.e. of 4.73×10^{-4} m³ and 10^{-3} m³ volume, respectively. After saturation, the samples were drained by applying a 0.6 m hanging water column. The drained volume fraction was interpreted as representing the coarse porosity of the sample at -6 kPa soil water potential.

4.3 Results

The comparison of the samples from trafficked and non-trafficked parts of the plots (Fig. 4.2, 4.5 and 4.8) indicates that precompression stress was significantly ($P < 0.05$) increased by trafficking only in the wetted topsoil of the Ruckfeld site.

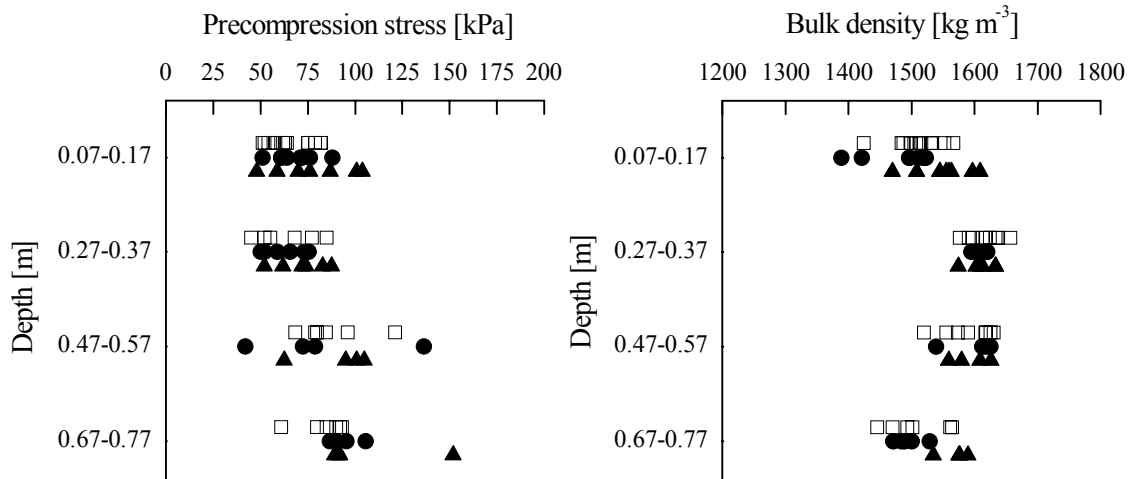


Figure 4.2 Precompression stress (left) and bulk density (right) of the non-trafficked (\square), 'wet'-trafficked (\bullet) and 'dry'-trafficked (\blacktriangle) Freienstein soil.

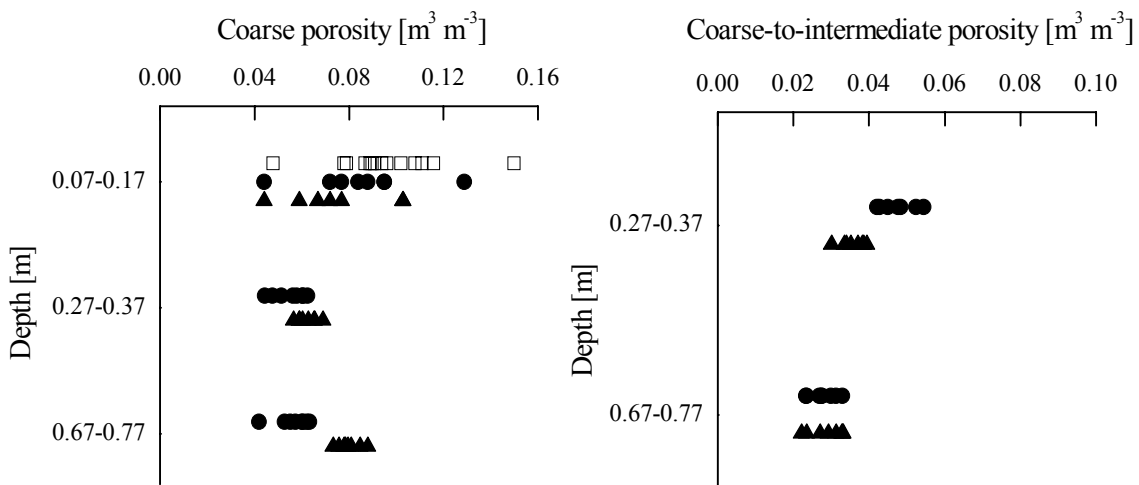


Figure 4.3 Coarse porosity (left) and coarse-to-intermediate porosity (right) of the non-trafficked (\square), 'wet'-trafficked (\bullet) and the 'dry'-trafficked (\blacktriangle) Freienstein soil.

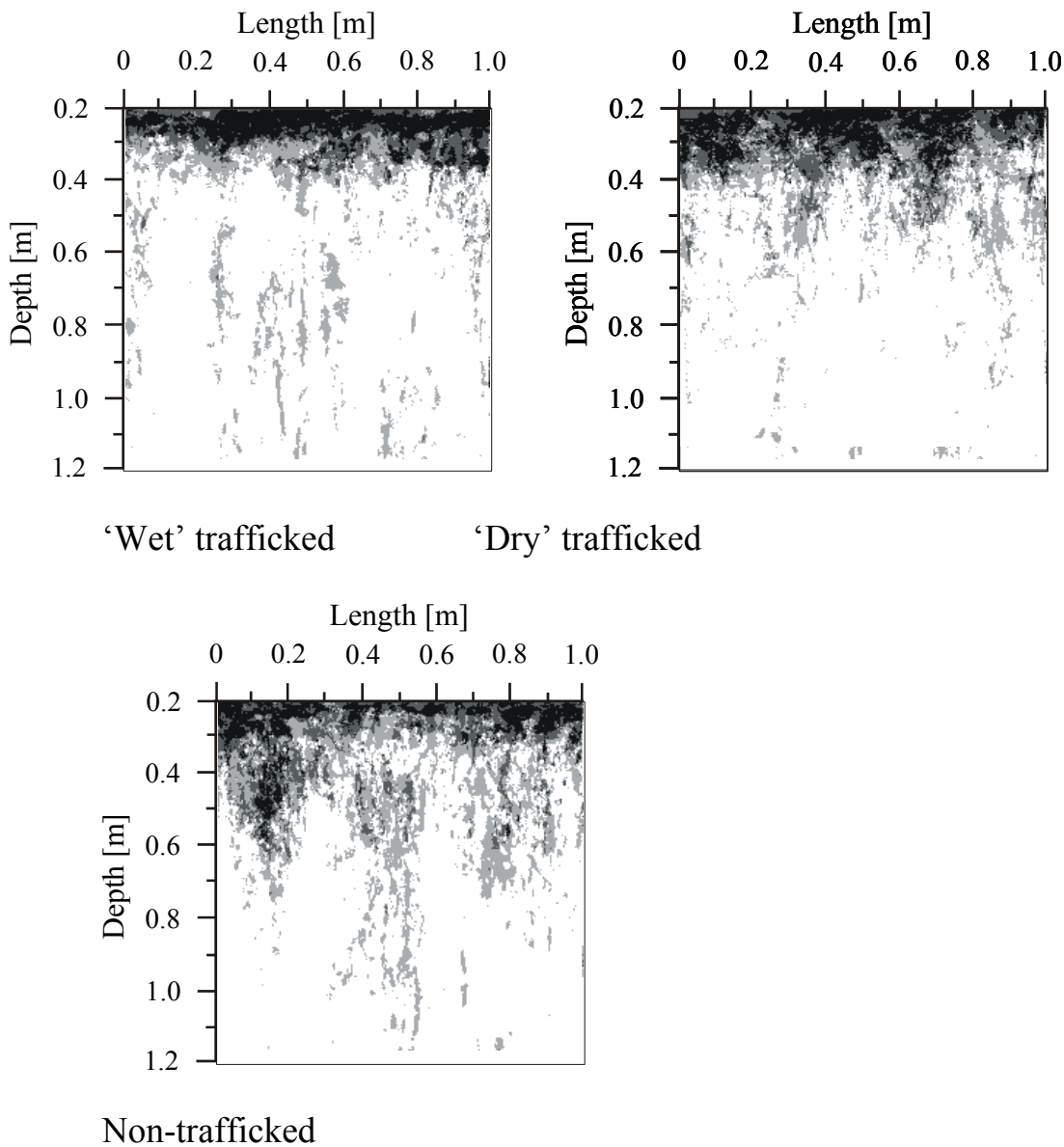


Figure 4.4 Flow pattern of dye tracer in the 'wet', 'dry' and non-trafficked Freienstein soil.

At Freienstein the subsoil samples of 0.67-0.77 m depth, at Güllenhau the topsoil and subsoil samples (0.07-0.17 m and 0.27-0.37 m depth) and at Ruckfeld the samples of the 'dry' subsoil (0.47-0.57 m depth) from the trafficked plot tended to have higher precompression stresses than the samples from the non-trafficked plot. However, these differences were not significant ($P < 0.05$).

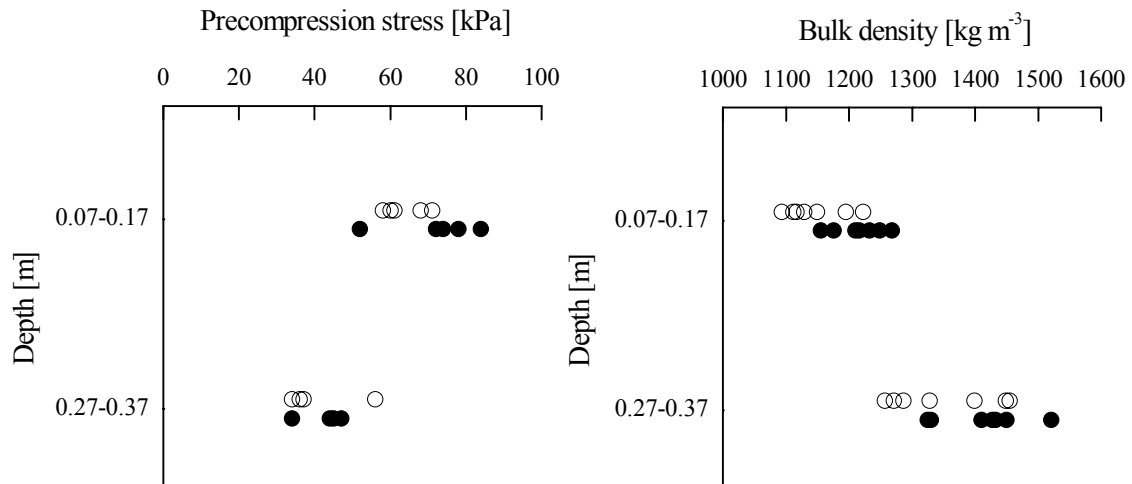


Figure 4.5 Precompression stress (left) and bulk density (right) of the trafficked (●) and the non-trafficked (○) Güllenhau soil.

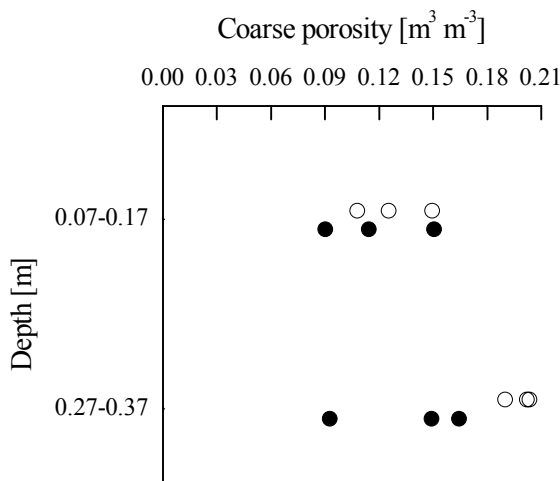


Figure 4.6 Coarse porosity of the trafficked (●) and non-trafficked (○) Güllenhau soil.

Statistically significant differences in bulk density between trafficked and non-trafficked soil were found at Freienstein in 0.07-0.17 m and 0.67-0.77 m depth of the ‘dry’ plot, in the topsoil of Güllenhau and in the wetted plot of Ruckfeld in 0.07-0.17 and 0.47-0.57 m depth. In 0.27-0.37 m depth at Güllenhau, bulk densities tended to be higher in the trafficked than in the non-trafficked plot. The increased bulk density in the topsoil of the ‘wet’ Ruckfeld plot and the absence of a similar increase in the ‘dry’ plot agree with the corresponding effects on precompression stress.

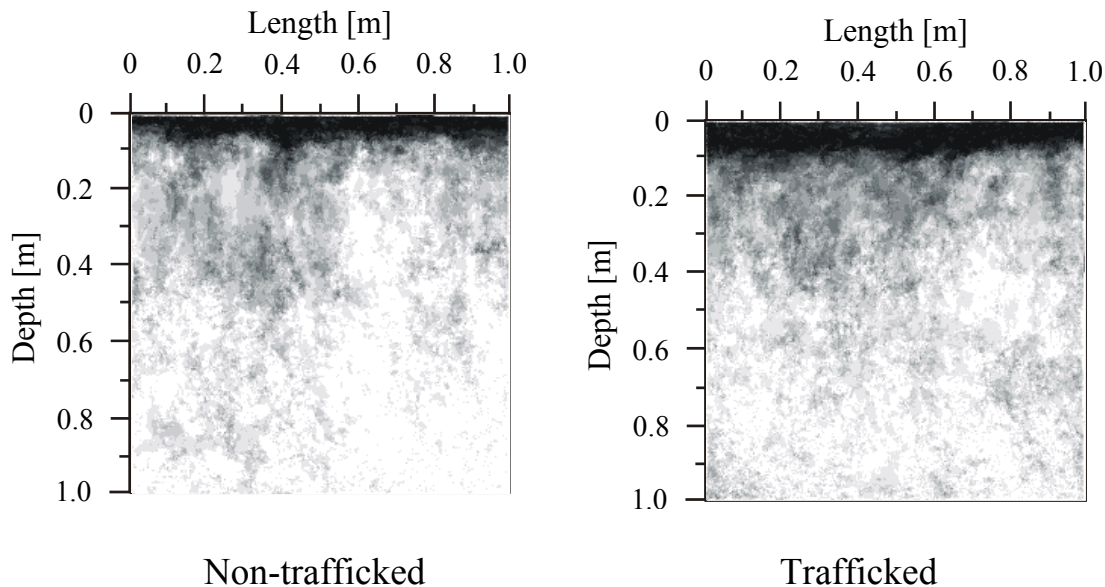


Figure 4.7 Flow pattern of dye tracer in the trafficked and non-trafficked Güllenhau soil.

At Freienstein, we found significantly ($P < 0.05$) decreased coarse porosity in the ‘dry’ trafficked compared with the non-trafficked topsoil (0.07-0.17 m) and higher coarse porosity values in the ‘dry’ compared with the ‘wet’ trafficked subsoil (0.27-0.37 and 0.67-0.77 m depth). Also at Güllenhau, coarse porosity was significantly lower in the trafficked than the non-trafficked subsoil (0.27-0.37 m). In contrast, coarse-to-intermediate porosity was significantly higher ($P < 0.05$) in the ‘wet’ than in the ‘dry’ trafficked subsoil (0.27-0.37 m) at Freienstein and higher in the ‘dry’ trafficked than in the non-trafficked subsoil (0.27-0.37 m) at Ruckfeld. No significant effects on coarse porosity were found, however, in the topsoil at Güllenhau and in the ‘wet’ plot at Freienstein. It may therefore be questioned whether the before mentioned differences in the subsoil of Güllenhau and the ‘dry’ plot of Freienstein were caused by trafficking or rather represented pre-existing differences between the plots. A comparison between the non-trafficked reference plots at Ruckfeld shows that such differences must be taken into account (Fig. 4.8). The absence of effects on the precompression stress in these cases also suggests such an interpretation of the apparent inconsistency of porosity and density effects in this pattern.

Further support derives from the analysis of the flow patterns. We found less flow paths in 0.4-0.6 m depth of the ‘wet’ trafficked and below 0.6 m of the ‘dry’ trafficked Freienstein subsoil compared with the flow pattern of the non-

trafficked soil. Neither in the Güllenhau nor in the Ruckfeld subsoil did we observe differences in flow patterns between trafficked and non-trafficked plots. The pattern in the ‘wet’ trafficked was slightly more distinct than in the ‘dry’ and the non-trafficked subsoil at Ruckfeld, due to the higher moisture content which allowed more dye to flow from coarser into finer pores. The absence of significant effects on flow pattern and precompression stress agrees well.

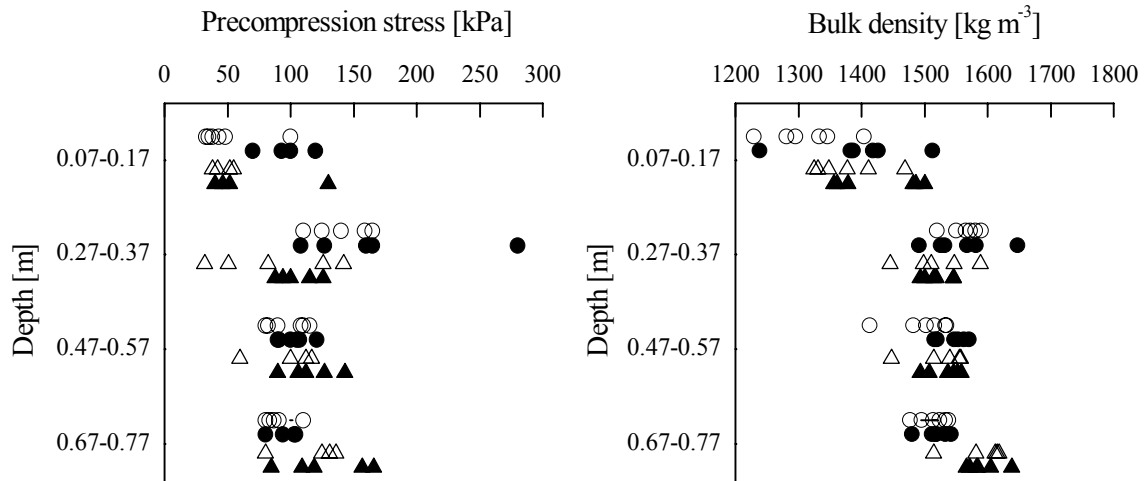


Figure 4.8 Precompression stress (left) and bulk density (right) of the ‘wet’ trafficked (●), ‘dry’ trafficked (▲), ‘wet’ non-trafficked (○) and ‘dry’ non-trafficked (△) Ruckfeld soil.

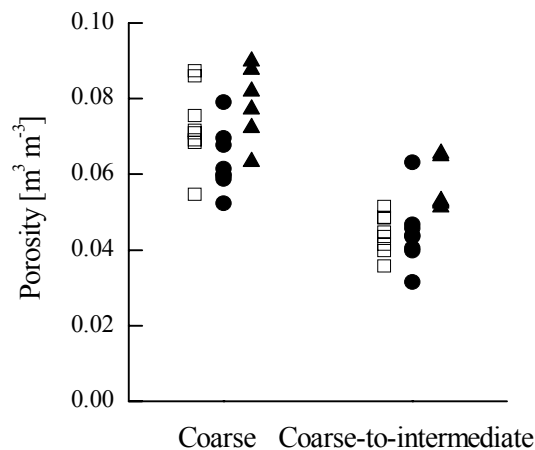


Figure 4.9 Porosity of the non-trafficked (□), ‘wet’ trafficked (●) and ‘dry’ trafficked (▲) Ruckfeld subsoil at 0.27-0.37 m depth.

Lack of statistical significance does not mean that compaction effects can be entirely excluded. Minor effects may have been concealed by the rather large scatter of the measured values, which was primarily due to a high degree of short-range spatial variability of these parameters.

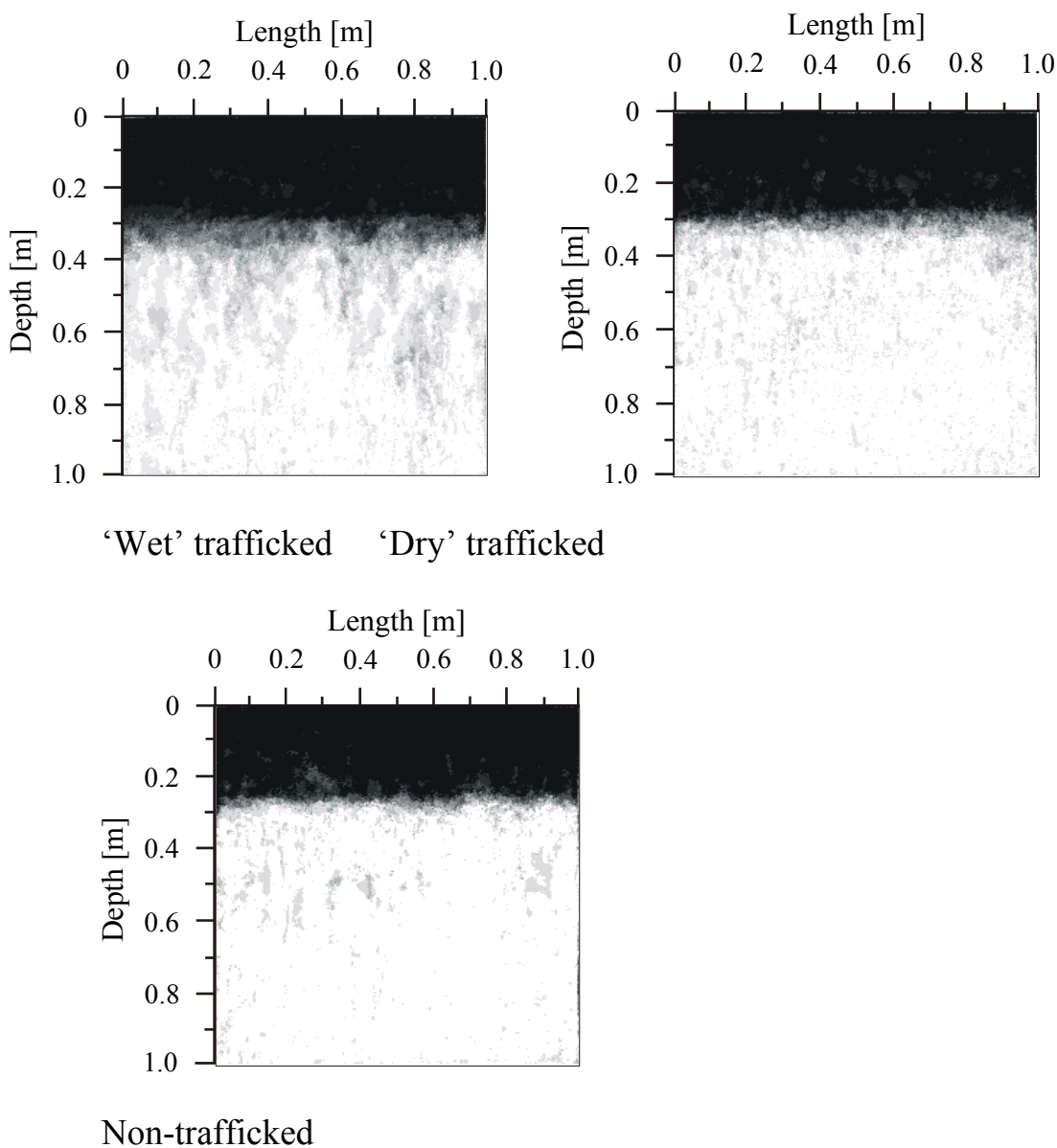
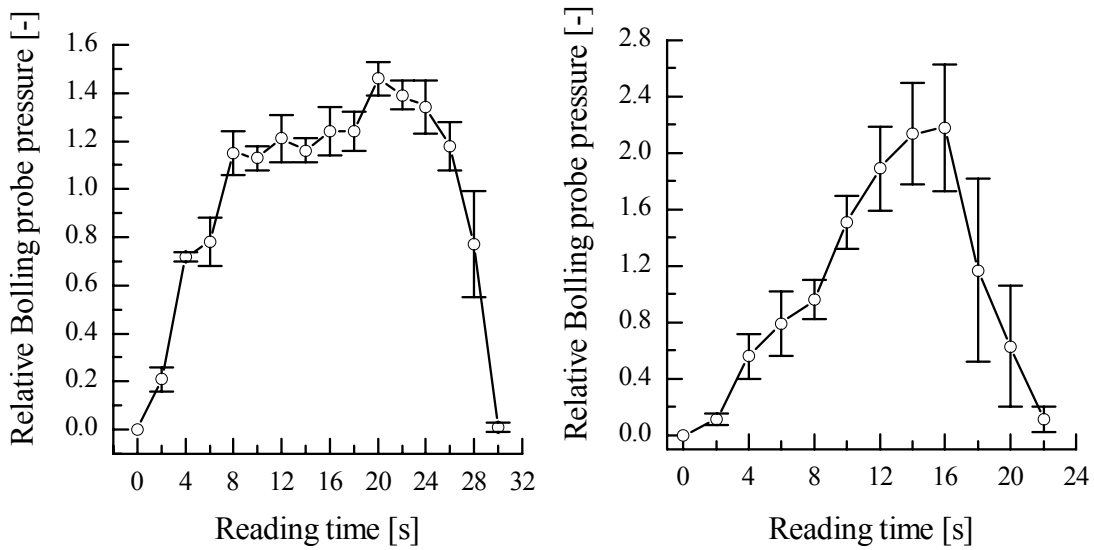
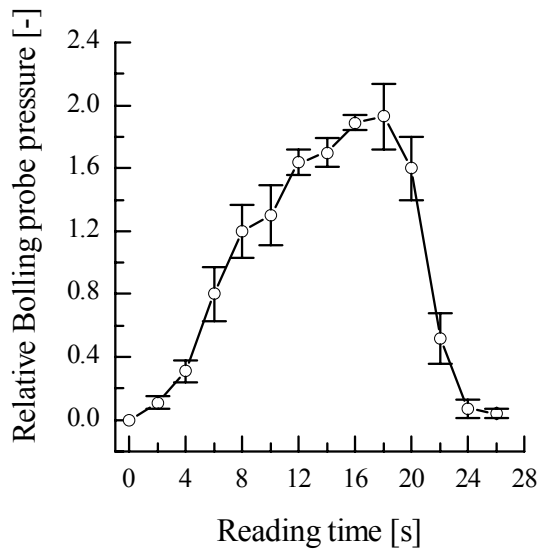


Figure 4.10 Flow pattern of dye tracer in the 'wet', 'dry' and non-trafficked Ruckfeld soil.



Fiat FH 300 Fiat Allis PL 40C



Cat 583

Figure 4.11 Relative Bolling probe pressure (pressure readings as a function of time divided by the mean of the pressure readings over the measured time interval) determined at 0.32 m depth of the 'wet' plot at Ruckfeld under the tracks of the machinery used for the traffic experiment. The error bars indicate standard errors.

The total variation between samples from the same horizon and site was much larger than the analytical error e.g. in respect of the determination of bulk

density. The variation coefficient of bulk density measurements in this study was larger than 1.3% while the analytical error was smaller than 0.7%. Likewise the differences in bulk density and porosity of the subsoils described above may simply represent spatial variability at longer range. For example at 0.67-0.77 m depth of the Ruckfeld site, the difference between bulk density of the 'wet' and 'dry' plot is larger than between the values of trafficked and non-trafficked plot. From a strictly objective point of view, however, it also cannot be excluded that spatial variability instead of traffic influence is the reason for the significant effects in precompression stress and bulk density in the 'wet'-trafficked topsoil at Ruckfeld.

Relative Bolling probe pressure showed that stress at 0.32 m depth along the track centreline was rather 'triangularly' than 'rectangularly' distributed over time (Fig. 4.11). The relative pressures of the Fiat Allis PL 40 C and the Cat 583 showed a distinct maximum. This maximum was under the Fiat FH 300 1.5, under the Fiat Allis PL 40 C 2.2 and under the Cat 583 1.9 times the measured mean relative pressure. Koolen and Kuipers (1983) stated that for tracked machinery under practical conditions the maximum stress in the contact area is 1.4 to 3.0 times the mean normal pressure.

4.4 Discussion and conclusions

The results show that no consistent compaction effects were observed in the subsoil (Table 4.6). The only clear compaction, which was likely due to the trafficking, occurred in the wetted topsoil at Ruckfeld. At Güllenhau, a similar topsoil effect was likely but the evidence was less constant.

While these scarcity of significant and consistent compaction effects may partially be due to the large spatial variability of soil properties within and between plots, it also does not contradict expectations, if we compared the measured precompression stresses with estimates of the normal stresses exerted by the trafficking machines. Since stress is not homogeneously distributed beneath the track centreline (Fig. 4.11), peak rather than mean stress in the contact area could govern compaction.

Table 4.6. Effects found at the three test sites for ‘wet’ and ‘dry’ trafficked plots compared with non-trafficked plots
(-: no effect, (+): trend, +: significant effect, n.d.: not determined)

Site	Depth [m]	Precompression stress		Bulk density		Coarse porosity		Coarse-to-intermediate porosity		Flow pattern	
		‘wet’	‘dry’	‘wet’	‘dry’	‘wet’	‘dry’	‘wet’	‘dry’	‘wet’	‘dry’
Freienstein	0.07-0.17	-	-	-	+	(+)	+	n.d.	n.d.	n.d.	n.d.
	0.27-0.37	-	-	-	-	n.d.	n.d.	n.d.	n.d.	-	-
	0.47-0.57	-	-	-	-	n.d.	n.d.	n.d.	n.d.	(+)	-
	0.67-0.77	(+)	(+)	-	+	n.d.	n.d.	n.d.	n.d.	-	(+)
Güllenhaus	0.07-0.17	(+)	n.d.	+	n.d.	-	n.d.	n.d.	n.d.	-	n.d.
	0.27-0.37	(+)	n.d.	(+)	n.d.	+	n.d.	n.d.	n.d.	-	n.d.
Ruckfeld	0.07-0.17	+	-	+	-	n.d.	n.d.	n.d.	n.d.	n.d.	n.d.
	0.27-0.37	-	-	-	-	-	-	-	+	-	-
	0.47-0.57	-	(+)	+	-	n.d.	n.d.	n.d.	n.d.	-	-
	0.67-0.77	-	-	-	-	n.d.	n.d.	n.d.	n.d.	-	-

To check for this, we compared two contact stress scenarios. In the ‘best case’ scenario, the normal stress in the contact area was taken to be the mean normal stress, i.e. the weight of machine and load divided by the total contact area (Table 4.3). In the ‘worst case’ scenario the normal stress in the contact area was assumed to be 2.2 times the mean normal stress for the Fiat Allis PL 40 C, 1.5 times for the Fiat FH 300 and 1.9 times for the Cat 583. We assumed that the Fiat FH 300 for the ‘wet’ and the Fiat Allis PL 40 C for the ‘dry’ Freienstein plot, the Fiat FH 300 for Güllenhau and the Cat 583 vehicle for the Ruckfeld site was likely to govern compaction. In both scenarios, soil-vehicle interaction was simplified as a plane strain problem. Stress propagation in the soil was modelled according to Fröhlich (1934) with the track idealised as an infinite strip load with homogeneous contact stress distribution on ‘dry’ (concentration factor $n = 4$) and ‘wet’ (concentration factor $n = 5$) soil. In addition to traffic induced stress, vertical stress due to the weight of the overlying soil at each depth was considered.

The calculated total vertical stresses in the soil below the track centreline were compared with the precompression stresses in the respective depths of 0.12, 0.32, 0.52 and 0.72 m. The median of precompression stress values depicted in Figure 4.2, 4.5, and 4.8 were chosen in order to calculate the vertical stress/precompression stress ratio. Since precompression stress depends on soil moisture conditions (e.g. Culley and Larson, 1987; Horn, 1988; Kirby, 1991a), its values in the field were assumed to be higher or lower than the measured values at -6 kPa initial water potential if water potentials in the field were lower or higher than -6 kPa, respectively. Compaction effects were expected if the total vertical stress/precompression stress ratio exceeded 1 and the soil water potential in the field experiment was above -6 kPa and vice versa. In all other cases compaction effects were considered as ‘possible’. The results are given separately for the three sites in Table 4.7, 4.8 and 4.9.

Comparing expected (according to the scenario analysis, Table 4.7-4.9) with observed effects (Table 4.6), it emerges that the ‘worst case’ expectations did not agree better with observed effects in the subsoil than the ‘best case’ scenario. The ‘worst case’ scenario predicted compaction in the subsoil of the ‘wet’ plot in 0.27-0.37 and 0.67-0.77 m depth at Ruckfeld, although no effect was found. For the ‘best case’ scenario, the increased bulk density in the ‘dry’ Freienstein

plot at 0.67-0.77 m depth and the ‘wet’ Ruckfeld plot at 0.47-0.57 m depth (Table 4.6) disagreed with expectations. The increased bulk density in the ‘wet’ Ruckfeld plot at 0.47-0.57 m depth, however, was inconsistent with the lack of an increase in precompression stress or an effect on the flow pattern. As pointed out already in the results, this inconsistency may have been due to natural variability.

Table 4.7. Effects expected at the Freienstein sites for ‘wet’ and ‘dry’ trafficked compared with non-trafficked plots under the assumption of a minimum (‘best case’) and maximum (‘worst case’) normal stress at the soil surface

Scenario	Depth [m]	Total vertical stress [kPa]		Total vertical stress/pre-compression stress [-]		Compaction effect expected	
		‘wet’	‘dry’	‘wet’	‘dry’	‘wet’	‘dry’
Best case [†]	0.12	74	88	1.18	1.39	possible	possible
	0.32	76	84	1.22	1.35	possible	possible
	0.52	73	74	0.89	0.90	possible	no
	0.72	69	66	0.79	0.75	no	possible
Worst case [‡]	0.12	107	185	1.7	2.94	possible	possible
	0.32	108	172	1.74	2.78	possible	possible
	0.52	102	147	1.25	1.80	yes	possible
	0.72	95	126	1.08	1.43	possible	yes

[†] ‘best case’: Normal stress = net mean stress + stress due to pipe weight under the trench closer track of Fiat FH 300 for the ‘wet’ and Fiat Allis PL 40 C for the ‘dry’ plot.

[‡] ‘worst case’: Normal stress = (net mean stress + stress due to pipe weight under the trench closer track of Fiat FH 300 for the ‘wet’ and Fiat Allis PL 40 C for the ‘dry’ plot) × 1.5 (Fiat FH 300), 1.9 (Cat 583) or 2.2 (Fiat Allis PL 40 C) for maximum stress along the track.

Table 4.8. Effects expected at Güllenhau for the trafficked compared with the non-trafficked plot for a minimum ('best case') and maximum ('worst case') normal stress at the soil surface

Scenario	Depth [m]	Total vertical stress [kPa]	Total vertical stress/pre-compression stress [-]	Compaction effect expected
Best case [†]	0.12	44	0.72	possible
	0.32	46	1.25	yes
Worst case [‡]	0.12	63	1.04	yes
	0.32	65	1.75	yes

[†] 'best case': Normal stress = net mean stress in the contact area of Fiat FH 300.

[‡] 'worst case': Normal stress = net mean stress \times 1.5 (Fiat FH 300) for the maximum stress along the track.

Table 4.9. Effects expected at Ruckfeld for 'wet' and 'dry' trafficked compared with non-trafficked plots for a minimum ('best case') and maximum ('worst case') normal stress at the soil surface

Scenario	Depth [m]	Total vertical stress [kPa]		Total vertical stress/pre-compression stress [-]		Compaction effect expected	
		'wet'	'dry'	'wet'	'dry'	'wet'	'dry'
Best case [†]	0.12	80	80	1.95	1.70	yes	possible
	0.32	79	77	0.53	0.70	possible	no
	0.52	74	70	0.75	0.74	possible	no
	0.72	68	62	0.80	0.49	possible	no
Worst case [‡]	0.12	153	152	3.72	3.24	yes	possible
	0.32	148	144	0.99	1.39	possible	possible
	0.52	135	126	1.36	1.26	yes	possible
	0.72	119	109	1.40	0.85	yes	no

[†] 'best case': Normal stress = net mean stress in the contact area of Cat 583.

[‡] 'worst case': Normal stress = net mean stress \times 1.9 (Cat 583) for the maximum stress along the track.

In summary, the 'best case' scenario tended to underestimate while the 'worst case' scenario overestimated subsoil compaction. Under the investigated experimental conditions, it appears to be adequate to estimate the effective

normal stress in the contact area under the tracks as about 1.5-times the mean normal stress. For the prediction of topsoil compaction, however, the inhomogeneity of the load distribution may not be negligible. An indication for this are the results observed at Güllenhau where only the ‘worst case’ scenario clearly predicted such compaction whereas it could not necessarily have been expected according to the ‘best case’ scenario.

As discussed before, such interpretations should be taken with caution. Inconsistency may also have arisen from factors such as the natural heterogeneity between the plots and sites which is not captured by replicate measurements within plots. Differences in the experimental conditions between field and laboratory are other factors of uncertainty and possible inconsistency within the results. Taking these limitations into account as well as reservations concerning the exact physical meaning of the precompression stress as determined by the procedure of Casagrande (1936), the agreement between expectations and measurements is surprisingly good. Therefore, we conclude that the precompression stress may provide a useful and practical criterion for assessing the compaction sensitivity of soils under field conditions.

4.5 Acknowledgement

We thank the Research and Development Fund of the Swiss Gas Industry (FOGA) for supporting this project. We are especially grateful to David Schönbächler, Monika Weber and Stephanie Zimmermann providing data from their diploma theses and semester work respectively as well as to Anna Grünwald and Hassan Qasem for their technical support in the field and laboratory.

4.6 References

- Atkinson, J.H. and Bransby, P.L., 1978. The Mechanics of Soils: An Introduction to Critical State Soil Mechanics. McGraw-Hill University Series in Civil Engineering. McGraw-Hill Book Company, 375 pp.
- Blunden, B.G., McBride, R.A., Daniel, H. and Blackwell, P.S., 1994. Compaction of an earthy sand by rubber tracked and tyred vehicles. Australian Journal of Soil Research, 32: 1095-1108.
- Bolling, I., 1987. Bodenverdichtung und Triebkraftverhalten bei Reifen - Neue Mess- und Rechenmethoden. PhD Thesis, Forschungsbericht Agrartechnik des Arbeitskreises Forschung und Lehre der Max-Eyth-Gesellschaft (MEG), Technische Universität München, München, 274 pp.
- Boussinesq, M.J., 1885. Applications des potentiels à l'étude de l'équilibre et du mouvement des solides élastiques. Gauthier-Villars, Paris, 721 pp.
- Casagrande, A., 1936. The determination of pre-consolidation load and its practical significance. 1st International Conference on Soil Mechanics and Foundation Engineering, Harvard University, Cambridge, Massachusetts. pp. 60-64.
- Culley, J.L.B. and Dow, B.K., 1988. Long-term effects of an oil pipeline installation on soil productivity. Canadian Journal of Soil Science, 68(Feb.): 177-181.
- Culley, J.L.B., Dow, B.K., Presant, E.W. and MacLean, A.J., 1982. Recovery of productivity of Ontario soils disturbed by an oil pipeline intallation. Canadian Journal of Soil Science, 62(May): 267-279.
- Culley, J.L.B. and Larson, W.E., 1987. Susceptibility to compression of a clay loam Haplaquoll. Soil Science Society of American Journal, 51: 562-567.
- Dumbeck, G., 1984. Einfluss aussergewöhnlicher Druckbelastung auf das Bodengefüge und die Durchwurzelung. Mitteilungen der Deutschen Bodenkundlichen Gesellschaft, 40: 61-62.

- FAO, 1990. FAO-Unesco Soil Map of the World, Food and Agriculture Organisation of the United Nations (FAO), Revised Legend, Rome.
- Flury, M. and Flühler, H., 1995. Tracer characteristics of Brilliant Blue FCF. Soil Science Society of America Journal, 59(1): 22-27.
- Flury, M., Flühler, H., Jury, W.A. and Leuenberger, J., 1994. Susceptibility of soils to preferential flow of water: A field study. Water resources research, 30(7): 1945-1954.
- Forrer, I., A., P., Kasteel, R., Flühler, H. and Luca, D., 2000. Quantifying dye tracers in soil profiles by image processing. European Journal of Soil Science, 51(June): 313-322.
- Fröhlich, O.K., 1934. Druckverteilung im Baugrunde mit besonderer Berücksichtigung der plastischen Erscheinungen. Verlag von Julius Springer, Wien, 185 pp.
- Gysi, M., Ott, A. and Flühler, H., 1999. Influence of single passes with high wheel load on a structured , unploughed sandy loam soil. Soil & Tillage Research, 52: 141-151.
- Hadas, A., 1994. Soil compaction caused by high axle loads - review of concepts and experimental data. Soil & Tillage Research, 29: 253-276.
- Håkansson, I. and Reeder, R.C., 1994. Subsoil compaction by vehicles with high axial load - extend, persistence and crop response. Soil & Tillage Research, 29: 277-304.
- Hammel, K., 1993. Spannungsverteilung und Bodenverdichtung unter profilierten Reifen am Beispiel zweier Böden unter Grünland. PhD Thesis, Institut für Bodenkunde und Standortlehre, Universität Hohenheim, Stuttgart, 141 pp.
- Horn, R., 1981. Eine Methode zur Ermittlung der Druckbelastung von Böden anhand von Drucksetzungsversuchen. Zeitschrift für Kulturtechnik und Flurbereinigung, 22(1): 20-26.

- Horn, R., 1988. Compressibility of arable land. In: J. Drescher, R. Horn and M. De Boodt (Editors). *Impact of Water and External Forces on Soil Structure*, Catena Supplement 11. Catena-Verlag, Cremlingen-Destedt, pp. 53-71.
- Horn, R. and Lebert, M., 1994. Soil compactibility and compressibility. In: B.D. Soane and C. van Ouwerkerk (Editors). *Soil Compaction in Crop Production*. Elsevier, Amsterdam, pp. 45-69.
- Kirby, J.M., 1991a. Critical-state soil mechanics parameters and their variation for Vertisols in eastern Australia. *Journal of Soil Science*, 42: 487-499.
- Kirby, J.M., 1991b. Strength and deformation of agricultural soil: measurement and practical significance. *Soil Use and Management*, 7: 223-229.
- Kooistra, M.J., Bouma, J., Boersma, O.H. and Jager, A., 1984. Physical and morphological characterisation of undisturbed and disturbed ploughpans in a sandy loam soil. *Soil & Tillage Research*, 4: 405-417.
- Koolen, A.J. and Kuipers, H., 1983. *Agricultural Soil Mechanics*. Advanced Series in Agricultural Sciences 13. Springer-Verlag, Berlin, 241 pp.
- McKyes, E., Stemshorn, E. and Bousquet, R., 1980. Damage to agricultural fields by construction traffic. *Transactions of the American Society of Agricultural Engineers*, 23(6): 1388-1391.
- Neilsen, D., MacKenzie, A.F. and Stewart, A., 1990. The effect of buried pipeline installation on fertilizer treatments on corn productivity on three eastern Canadian soils. *Canadian Journal of Soil Science*, 70(May): 169-179.
- Oldeman, L.R., Hakkeling, R.T.A. and Sombroek, W.G., 1991. *World Map of the Status of Human-Induced Soil Degradation: An Explanatory Note*, International Soil Reference and Information Centre (ISRIC), Wageningen.
- Richards, L.A., 1941. A pressure-membrane extraction apparatus for soil solution. *Soil Science*, 51: 377-386.
- Richards, L.A. and Fireman, M., 1941. A pressure-plate apparatus for measuring moisture sorption and transmission by soils. *Soil Science*, 56: 395-404.

- Soane, B.D. and Van Ouwerkerk, C., 1995. Implications of soil compaction in crop production for the quality of the environment. *Soil & Tillage Research*, 35: 5-22.
- Söhne, W., 1953. Druckverteilung im Boden und Bodenverformung unter Schlepperreifen. *Grundlagen der Landtechnik*, 5: 49-63.
- Söhne, W., 1958. Fundamentals of pressure distribution and soil compaction under tractor tires. *Agricultural Engineering*, May: 276-291.
- Terzaghi, K. and Peck, R.B., 1948. *Soil Mechanics in Engineering Practice*. John Wiley and Sons, New York, 566 pp.
- von Albertini, N., Leuenberger, J., Läser, H.P. and Flühler, H., 1995. Regeneration der Bodenstruktur eines verdichteten Ackerbodens unter Kunstwiese. *Aktuelle Bodenforschung in der Schweiz*. Bodenkundliche Gesellschaft der Schweiz, St. Gallen. pp. 10-16.
- von Rohr, G., 1996. Auswirkungen des Rohrleitungsbaus auf bodenphysikalische Kenngrößen. Diploma Thesis, Geographisches Institut der Universität Bern, Bern, pp.108

Chapter 5

Comparing infiltration patterns in soils

Beatrice Kulli, Christian Stamm, Andreas Papritz, and Hannes Flühler*

Submitted for publication in the 'Vadose Zone Journal'

Abstract

Dye tracer experiments have often been used to study the prevailing flow regime, e.g. the role and extent of preferential flow of water. Flow patterns in 2-dimensional profiles provide qualitative information but are difficult to analyze and compare quantitatively. The scope of this study is to develop a quantitative method to analyze the spatial distribution of the stained areas in vertical profiles and to compare the properties of the pattern with soil properties and structure.

Dye tracer infiltration experiments were carried out on 25 plots at 8 sites. The spatial distribution of the stained areas in vertical profiles was analyzed and compared using digital image processing. Since soil layering strongly affects infiltration patterns, we first split the flow patterns into homogeneous layers based on the width distribution of the stained areas. All layers found for the flow patterns of the 25 plots were then partitioned into groups of similar patterns by hierarchical clustering. The sequence of layers found in the pattern was finally compared qualitatively with the sequence of morphological layers observed on the soil profiles.

The obtained classification reliably distinguished between homogeneous infiltration and preferential flow, but also between zones of pronounced preferential flow and zones of lateral spreading, e.g., sand or gravel lenses. Dye coverage and mean width of stained structures were the most indicative factors for the different clusters. We found a good agreement of the sequences of layers found in the flow patterns and the soil horizons.

5.1 Introduction

Dye tracer infiltration experiments are widely used to study water flow and transport of solutes in soils. They have often been used to examine the prevailing flow regime, as for instance the role and extent of preferential flow of water (Ghodrati and Jury, 1990; Flury et al., 1994; Gjetterman et al., 1997; Zehe and Flühler 2001; Weiler and Naef, 2001) or to guide selective sampling of flow paths and by-passed soil matrix. (Bundt et al., 2000; Sinaj et al. 2002).

In order to compare stained flow patterns in a quantitative and objective way or to distinguish site specific variation from that occurring at different sites or under differing boundary conditions, we need to capture the geometric and distributional features of the pattern. Forrer et al. (2000) quantified the 2-dimensional concentration distributions of dye tracer plumes, which infiltrated from line sources applied at the soil surface. They calculated horizontal and vertical distributions of the tracer mass and thereby reduced the data to 1-dimensional quantities. This procedure provides information about mass balance but misses the spatial characteristics of the flow pattern. Pattern features have been characterized with different methods. Flury and Flühler (1995) modeled the patterns and their development in time using a diffusion-limited aggregation algorithm; Baveye et al. (1998) used fractal geometry to describe flow patterns quantitatively.

One of the important factors affecting infiltration patterns are soil texture and soil structure. We often find layers in flow patterns that correspond to differently textured soil horizons e.g. a sandy layer at about 0.6 m depth in the soil profile shown in Figure 5.1, which lead to lateral spreading of the tracer. Therefore we detect and compare layers in the flow patterns instead of comparing the entire flow patterns of vertical profile walls. The flow patterns of two layers observed in a given soil (e.g., a loamy layer above a sandy layer) may exhibit considerable differences, while on the other hand different soils may have similarly stained horizons, as for instance the plough layer.

In this study we develop a method for the detection of layer boundaries in flow patterns. The layers found in the patterns are then classified and the sequence of layers is qualitatively compared with the sequence of morphological layers observed in the soil profile of the respective plot.



Figure 5.1 Layering in flow patterns reflect layers of hydraulically different materials.

5.2 Material and methods

Figure 5.2 summarizes the steps of the method described in this chapter.

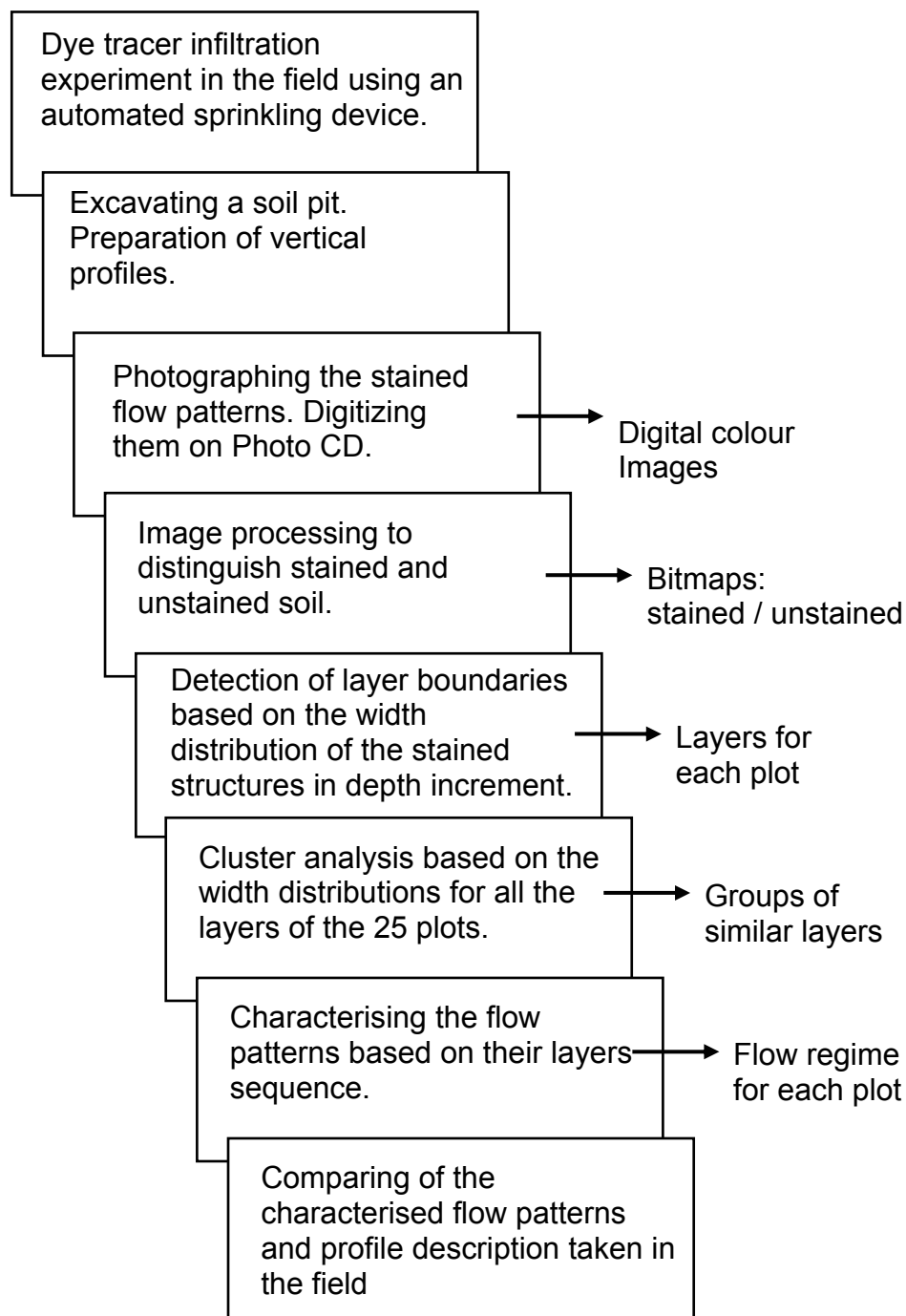


Figure 5.2 Methodological steps presented in this chapter.

Field experiments

A solution of the dye Brilliant Blue FCF at a concentration of 4 g lt^{-1} was used to stain the flow paths (Flury and Flühler, 1994; Ketelsen and Mayer-Windel, 1997; Allaire-Leung et al., 1999). The tracer was applied at a constant rate of 5 mm h^{-1} for 8 h, using the sprinkling apparatus described by Flury et al. (1994).

One day after sprinkling, a soil pit was excavated and vertical profiles were prepared. Using the method by Forrer et al. (2000), a Kodak colour- and greyscale as well as a $1 \times 1 \text{ m}$ frame were attached to the profile and photographed with the pattern to allow corrections by digital image analysis. The stained flow patterns were photographed on 4 to 10 profiles per plot. The distance between adjacent profiles was 0.1 m.

The field experiments were conducted at 8 sites where 25 plots were investigated, resulting in 171 single images of flow patterns available for further analysis.

Image processing

The color slides were developed and digitized onto a photo CD by a commercial laboratory. Image analysis included (i) geometrical correction, (ii) correcting inhomogeneous illumination, (iii) correcting variations in color between the pictures and (iv) classifying each pixel as 'stained' or 'unstained' based on its red, green and blue value. This procedure is described in detail by Forrer et al. (2000). The resulting binary images show the flow paths of the tracer solution in the soil. Each picture consists of 1000×1000 pixels, each pixel representing 1 mm^2 of the original soil profile. Figure 5.3 illustrates the sequential image processing.

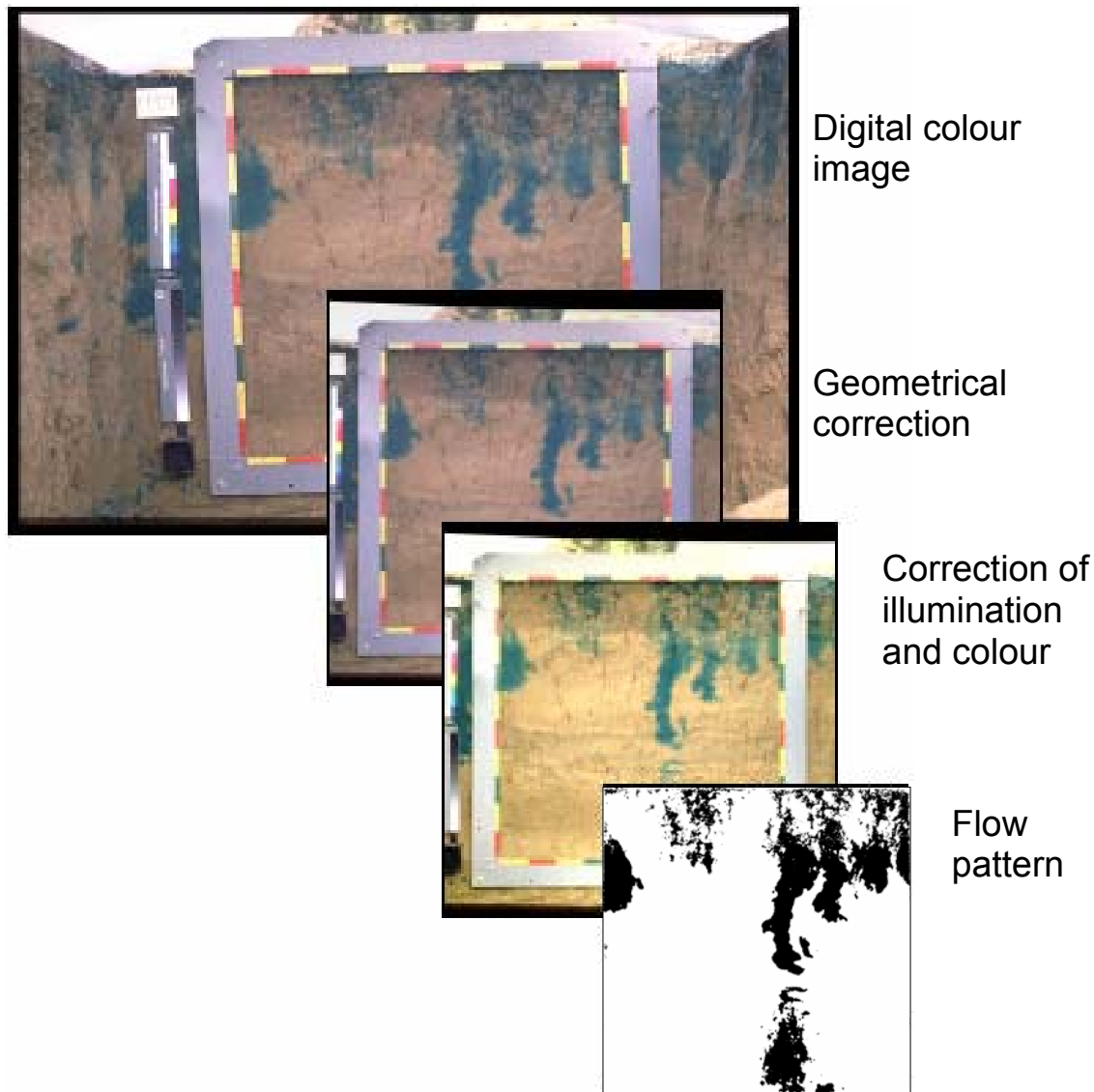


Figure 5.3 Sequence of the image processing.

Defining and discriminating of layers

The purpose of the following step is to objectively discriminate homogeneous layers in the flow patterns of every plot. Different layers can be identified by differences in the spatial distribution of the stained area. As input variable for our analysis we chose the width of the flow paths, which is an indicator for the fineness of the stained structures. We measured the widths of the stained areas in 1 mm depth increments (horizontal line of the flow patterns) and determined

their distribution for each depth. For that purpose, each line of the pattern was extracted and the lengths of the black pixel chains, indicating that the pixel belongs to the stained area, were measured as shown in the upper part of Figure 5.4. The flow patterns as well as the widths of the flow paths are considered to be horizontally translation invariant. Besides, the widths of the stained structures are oriented parallel to the horizontal layer boundaries we are looking for. In order to look for layer boundaries representative for an entire plot and not only for one single profile, we merged the width distributions for a given depth of all replicated profile images.

We now want to separate the profile into two layers by maximizing the variability of the width distributions of the stained areas between those layers. Therefore we divide the profile images into two layers at a certain depth z_L . We denote the upper part as X-layer and the lower as Y-layer. The cumulated width distributions of the stained flow paths of all lines of the X-layer are then compared with the cumulated width distributions of all lines of the Y-layer by the Wilcoxon Rank-Sum Test (Fig. 5.4, below).

The null hypothesis is that the width distributions of the layers X and Y have the same median. This it is tested against the hypothesis that they differ. The test value Z is:

$$Z = \frac{|W_X - N_X(N_X + N_Y + 1)|}{\sqrt{\frac{N_X N_Y (N_X + N_Y + 1)}{12}}} \quad (1)$$

The pooled width distributions of all depth increments of the layers X and Y are ranked and the ranks of the X-layer are summed up to W_X . N_X and N_Y are the number of line segments of the two distributions. The module RS_TEST (IDL Reference Guide, 1997) was used to carry out the rank sum test. An increasing Z indicates an increase of the difference between the two distributions.

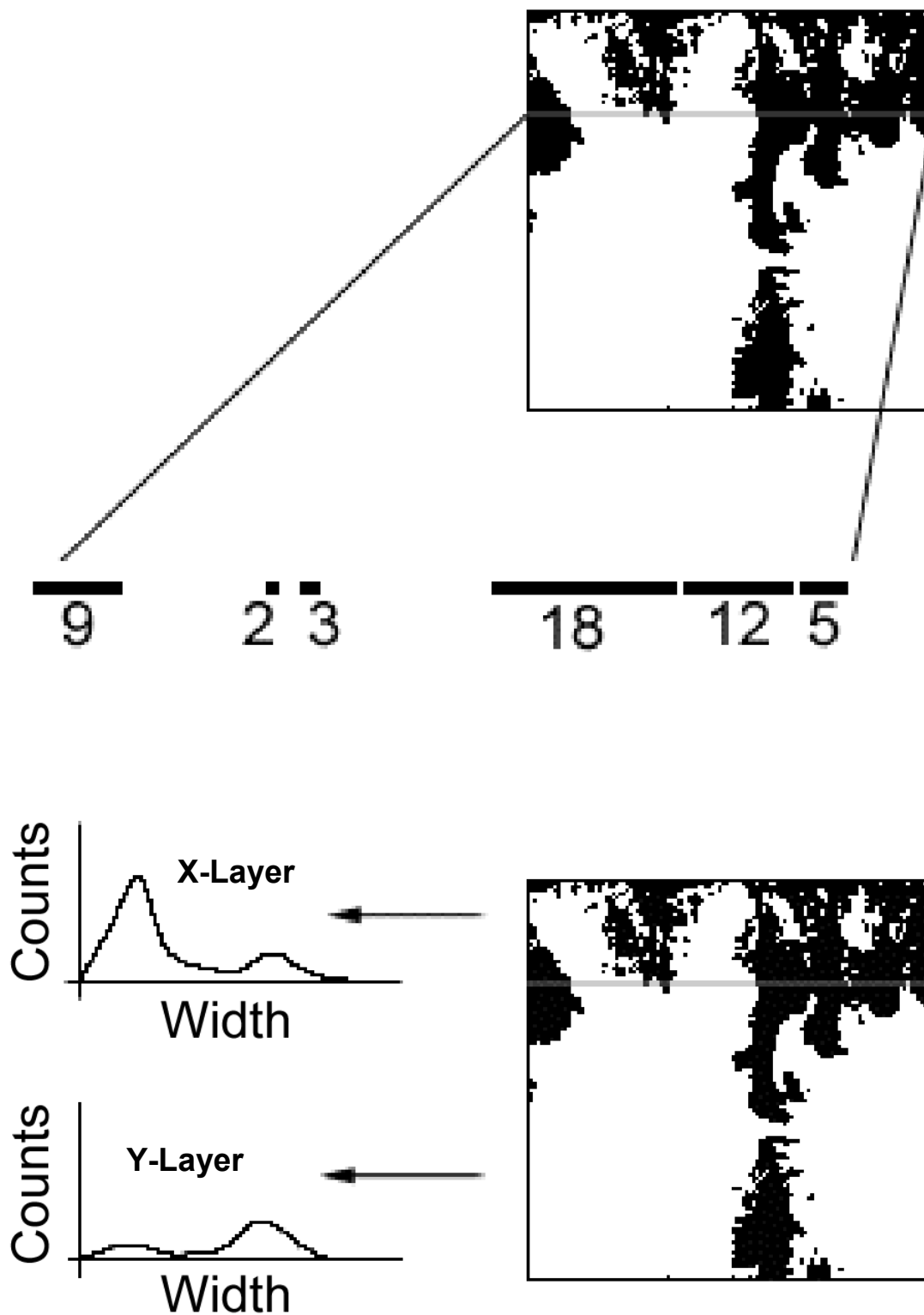


Figure 5.4 Analysis of the width distributions of the stained areas. Top: Width distributions are determined for every horizontal line (1 mm depth increment). Bottom: For each depth z_L the width distributions below and above the respective depth are pooled and compared.

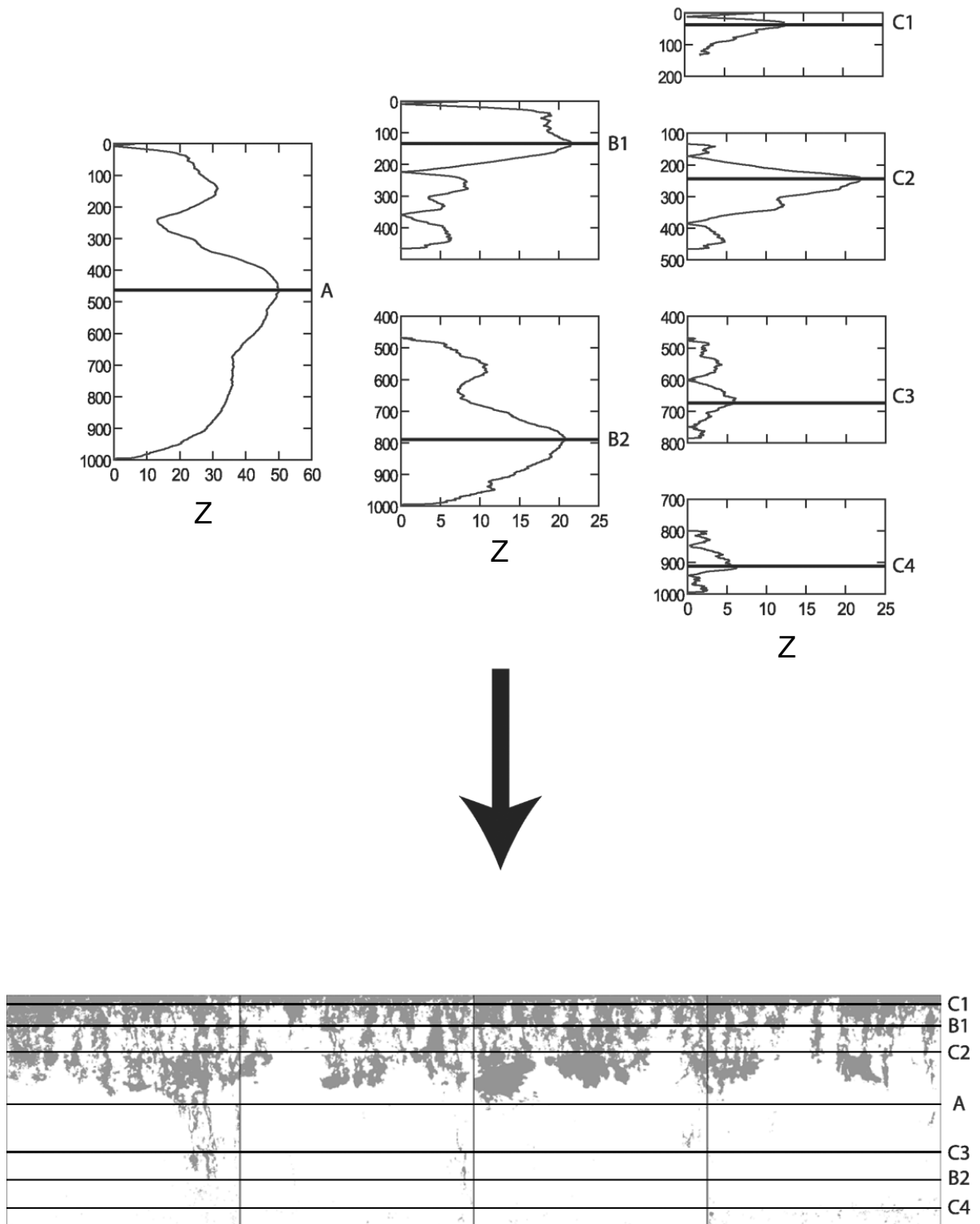


Figure 5.5 Maximizing Z to detect layer boundaries. Top: Iterative discrimination of dissimilar layers. Bottom: all images of a given plot lined up

Z was calculated for each position z_L (separation depth of layer X and Y) of the flow patterns, resulting in Z as a function of depth. The position z_L of the largest value of Z was taken to insert a first layer boundary. The two parts above and below this new boundary were then analyzed separately following the same procedure, which yields two new boundaries (Fig. 5.5). This procedure was iteratively repeated. The Z -value of the first iteration is at the boundary that coincides with the most characteristic change of the pattern. The maximum of the Z -values decreases with each iteration, resulting in many boundaries with small Z -values. In a first analysis, we stopped the iterations when no more $Z > 1$ were found. The number of boundaries found depending on Z was then analyzed in order to find a suitable Z -value for every plot to eliminate the least significant boundaries.

Z could be used to calculate the probability by which two distributions differ. But in our case the probabilities of the Wilcoxon-Test are not a suitable criterion to stop iteration, because Z is not calculated independently for each depth and cannot be used to judge the statistical significance. In order to find a suitable cut-off value for Z to discriminate the least meaningful boundaries, the number of boundaries was analyzed depending on their Z -value. Threshold values between 1 and 50 were tested and the boundaries with Z -values larger than that particular threshold were counted. The resulting monotonously decreasing function has a highly negative slope for small thresholds. The slope changes to very small negative values after a certain threshold. We consider this threshold as a suitable point to cut off unnecessary boundaries. The curve can be approximated by two straight line segments of different slopes (Fig. 5.6). The first line was fitted to the first part of the function and the second line segment to the second part. The best fit of the two lines was calculated by minimizing the chi-square error statistic depending on the threshold value, where the discontinuity between the two lines was located. Figure 5.6 shows the number of boundaries as a function of the threshold value as well as the best fit of the two lines. The Figure also shows the chi-square error depending on the location of the discontinuity. Only the boundaries with Z -values larger than the threshold value of the discontinuity were taken into account for further analysis. This evaluation was carried out independently for every plot.

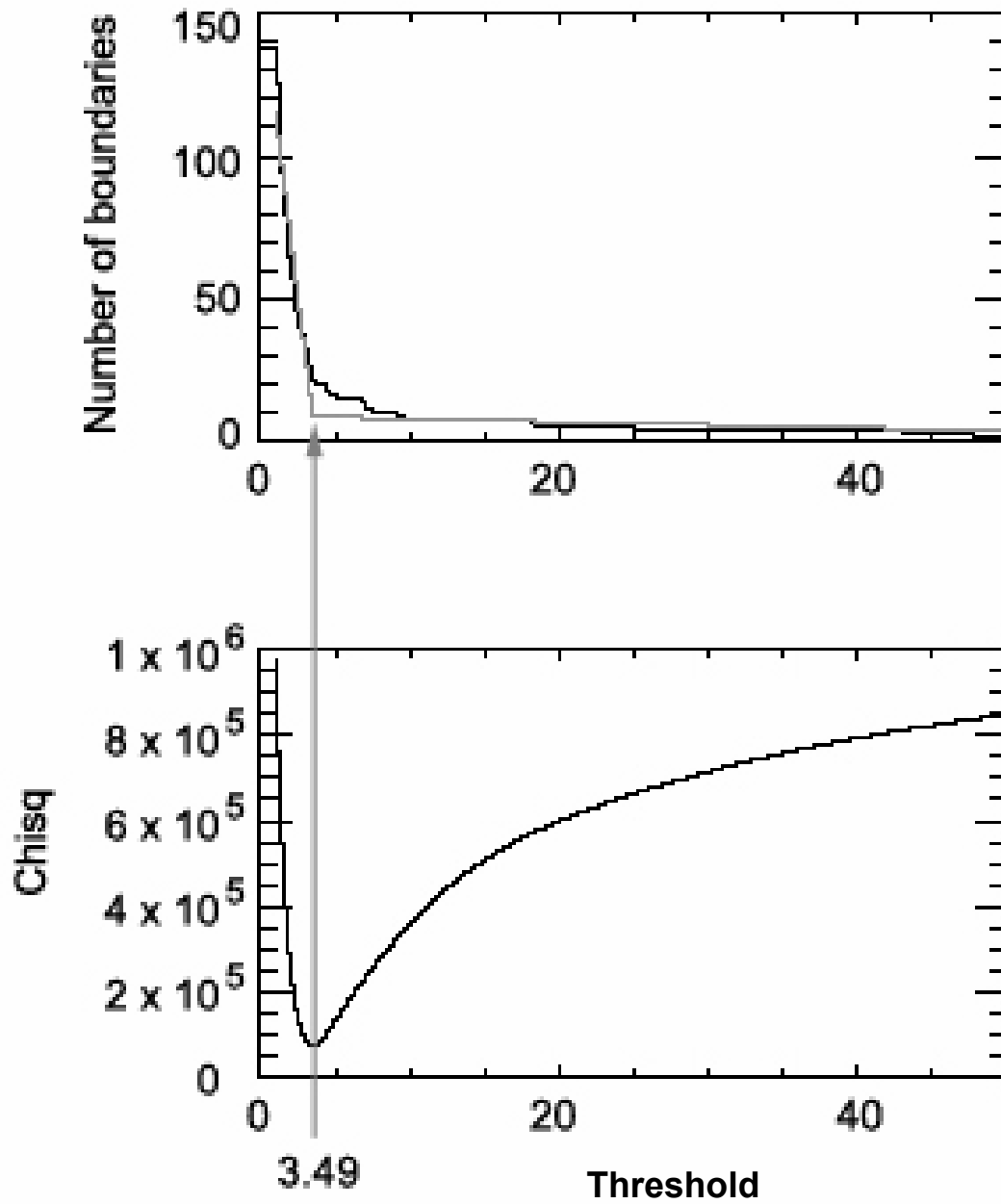


Figure 5.6 Top: Number of boundaries depending on the threshold (black) and best fit of the two straight line segments with the least chi-square error (grey). Bottom: Sum of squared errors for the fit of the line segments depending of the threshold.

Cluster analysis

A hierarchical cluster analysis was performed in order to group the identified layers according to pattern similarity. This analysis was carried out based on the width distributions of the individual layers. The input variables for the cluster analysis were minimum, maximum, mean, standard deviation, and median of the width distribution of the stained structures per layer and the dye coverage (fraction of stained area in a layer). The clustering of the data was carried out by the Ward's minimum variance method (Ward, 1963). The routines 'dist', 'hclust' and 'cutree' of the programming environment R were used (Ihaka and Gentleman, 1996). Cluster numbers between 2 and 20 were tested in order to find a suitable number of groups.

The method of Xu et al. (1993) was used to find the optimal number of clusters. Based on the minimum of "between cluster distances" (MBCD) and the sum of squared errors (SSE) within the clusters, we calculated the parameter E indicating the number of clusters most suitable for grouping of the data. E is calculated as follows:

$$E(i) = \frac{M(i) - M(i+1)}{\sqrt{J(i)} - \sqrt{J(i+1)}}, \quad i = 2, 3, 4, \dots \quad (2)$$

$$M(i) = \min[d_{jk}], \quad j < k, \quad j, k = 1, 2, \dots, i \quad (3)$$

$$d_{jk} = \sqrt{\frac{n_j \times n_k}{n_j + n_k}} \times |m_j - m_k|, \quad j, k = 1, 2, \dots, i \quad (4)$$

$$J(i) = \sum_{k=1}^i J_k \quad (5)$$

$$J_k = \sum_{x \in X_k} \|x - m_k\|^2 \quad (6)$$

Where i is the total number of clusters; d_{jk} is the distance between the j^{th} and the k^{th} cluster (Ward, 1963); $M(i)$ is the minimum of d_{jk} when i clusters are distinguished; J is the SSE for i clusters; n_j and n_k are the number of samples in cluster j and k respectively; m_j and m_k are the mean values of the clusters. High

values (or a global maximum of $E(i)$) indicate cluster numbers for suitable partitioning of the data.

5.3 Results and interpretation

Figure 5.7 summarises the results for six plots. Each row shows the results of one plot. The first column shows the background images of one of the replicated profile images per plot. These background images contain only the image information of the blue channel. At the respective wavelengths the reflection (and light absorption) by the tracer is eliminated, but structural information is retained. The second column illustrates the pattern variability found in the experiments, by showing one example flow pattern per plot. The third column shows the superimposed 4 to 10 flow patterns of each plot. The dark pixels in the resulting overlay-image indicate many profiles having a stained flow path at that location, whereas light pixels indicate no or only few profiles being stained at this point. The fourth column shows the results of the cluster analysis for a total number of 3, 7 and 20 clusters. The cluster memberships of a layer are indicated by the color in the respective depth. The cluster numbers are identified by the large color scale on the right-hand side of Figure 5.7. The results of the layer boundary detection are shown in the fifth column, where the layer boundaries are visualized as red horizontal lines.

Layer detection

In total 535 layers have been identified in the flow patterns of the 25 plots. Examples are shown in the fifth row of Figure 5.7. For most of the plots, many narrow layers have been detected by our method. However, some of the boundaries turn out to be irrelevant after the classification, because consecutive layers may belong to the same group.

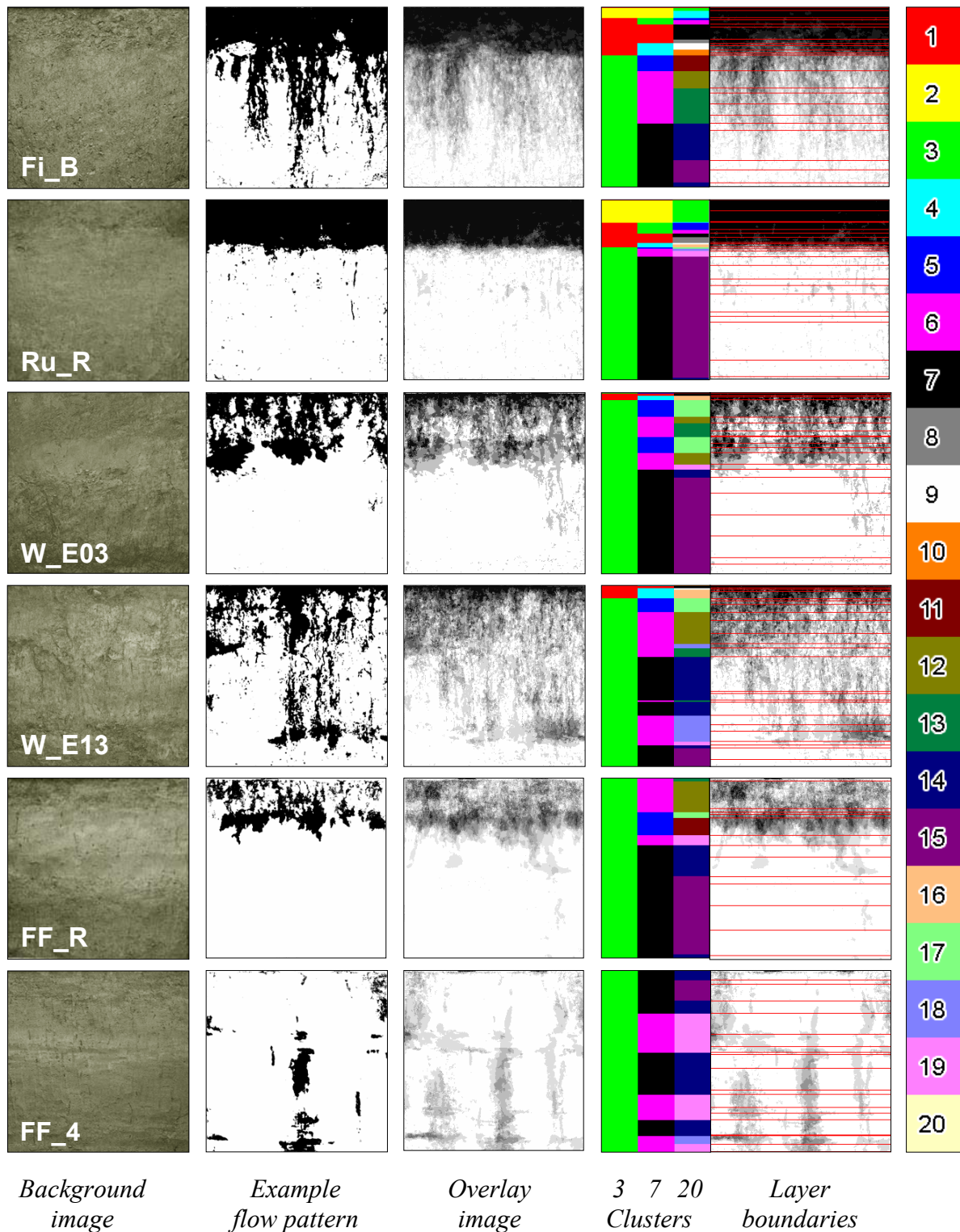


Figure 5.7 Overview of the results for six sites (rows). The background image on the left is followed by an example flow pattern of each plot and an overlay image of all flow patterns of the plot. The results of the cluster analysis for a total of 3, 7 and 20 clusters are given by the color bars next to another overlay image with the layer boundaries. The color scale on the right identifies the cluster numbers by the colors.

Cluster analysis

Figure 5.8 shows the dependence of the parameter E on cluster number obtained by the method of Xu et al. (1993). The curve exhibits three peaks. The global maximum occurs at a cluster number of 20. Two local maxima can be found at cluster numbers of 3 and 7, whereas the peak at a cluster number of 7 is almost as high the global maximum at a cluster number of 20. In order to investigate the effect of the cluster number on the resulting layer classification, all three numbers of clusters indicated by the maxima of the parameter E were taken into account for the further analysis.

The results of the cluster analysis are shown in the fourth row of Figure 5.7. The three color-scales indicate the membership of each layer for a total number of clusters of 3, 7, and 20. On the right-hand side of Figure 5.7 the cluster numbers are identified by the colors. Within a certain total number of clusters, layers identified by the same color belong to the same group. For different total numbers of clusters the colors can not be compared directly.

The total number of clusters affects the degree of detail of layer discrimination. Three clusters seem to be sufficient to capture the main characteristics of the infiltration patterns at the plot Fi_B and Ru_R, where zones of homogeneous infiltration and zones of preferential flow are nicely distinguished. At the other four plots (W_E03, W_E13, FF_R and FF_4) the classification is definitely not sensitive enough to capture the main characteristics of the pattern. A total of 7 clusters results in a more detailed sequence of layers, which captures the changes in the flow patterns better than a total number of 3 clusters, especially for the latter four sites, where the sequence of preferential-flow layers and tracer-spreading layers is detected appropriately. In case of Ru_R and Fi_B, additional layers are detected showing the transition of the homogeneous infiltration zone to the zone where almost no tracer was found. At Ru_R these gradual changes are much closer together than at Fi_B, but both plots show a sequence of layers with the same clusters memberships in their flow patterns. Dividing the layers into a total of 20 clusters increases the complexity of the layer sequence for all sites revealing the existence of several very small layers of enhanced or suppressed spreading (e.g. clusters 18 and 19 at the plots W_E13 and FF_4). Generally the complexity of the sequence of layers for a total of 20 clusters goes beyond the accuracy of layer differentiation in the field. In our

case, a total number of seven clusters provides sufficiently detailed information to characterize these flow patterns and compare them with the sequence of soil horizons found in the field.

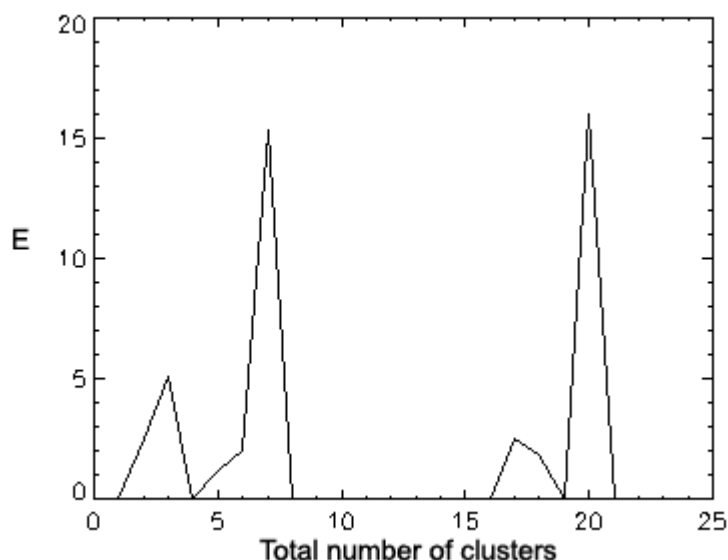


Figure 5.8 Cluster number optimized by the method of Xu et al. (1993).

Comparison of the layers found in the patterns and the soil horizons

The next step is a qualitative comparison between the layer sequence found in the flow patterns and the soil horizons found in the field. Table 5.1 shows some information about the soils of the example plots shown in Figure 5.7. The first column of Figure 5.7 shows the background images of one of the replicated profile images per plot. These background images contain only the image information of the blue channel. At the respective wavelengths the reflection (and light absorption) by the tracer is eliminated, but structural information is retained.

Based on the flow patterns, the sites can be roughly divided into two groups. Ru_R and Fi_B exhibit a transition from intensive staining to tracer absence at a depth of 1 meter. At both sites the top layer with a low bulk density shows a homogeneous infiltration pattern and no indication of preferential flow. In order to mimic the effect of ploughing, the topsoil was homogenized on both plots

before sprinkling. These top layers are followed by a well-structured horizon with higher density. In case of Fi_B this layer was a clayey loam with a high density of earthworm burrows and cracks. At Ru_R the ploughlayer was followed by a very homogeneous silt loam with definitely fewer worm burrows. In these subsoil layers, the flow became preferential. In case of Fi_B, worm burrows are the most important flow paths. Further down the profile, the soil density gradually increases and the stained flow paths (root channels/worm burrows) gradually disappeared. In case of Ru_R, preferential flow is less pronounced, probably due to a smaller number of worm burrows and cracks.

The other four plots stand for another type of flow pattern. The dye coverage is overall decreasing with depth, but also increases in some layers indicating enhanced lateral spreading.

Table 5.1 Some information about the soils and the experimental conditions at the example sites.

site	soil type	skeleton	comments
Fi_B	alluviale cambisol, clayey loam	(-/+)	homogeneous; ploughing simulated before sprinkling many worm burrows
Ru_R	deep, at >60 cm partially pseudo gleyic loamy luvisol, loess.	(-)	homogeneous, ploughing simulated before sprinkling
W_E03	layerd alluvial gley, loam to silty loam with sandy-gravel horizons.	(+)	highly variable
W_E13	layerd alluvial gley, loam to silty loam with sandy-gravel horizons.	(+)	highly variable
FF_R	deep alluvial calcaric cambisol, sandy loam to loam	(-)	highly variable, not compacted
FF_4	deep alluvial calcaric cambisol, sandy loam to loam	(-)	highly variable, compacted

The two plots W_E03 and W_E13 are located at the same site. The soil is strongly layered and very heterogeneous due to the alluvial deposition of the material. Similar to the plots Fi_B and Ru_R, a layer with a homogeneous infiltration pattern is followed by a layer where preferential flow is initiated. On both plots, the topsoil was not homogenized. Grass was growing at that site and the topsoil was densely rooted. The infiltrating water first followed the root network. As the root density decreases, the flow paths become thinner and dye coverage decreases. In case of W_E03, the loamy layer of the top soil is followed by a sandy layer, at a depth of about 25 cm. This can be seen by the texture of the background image as shown in the first column of Figure 5.7. In this sandy layer, the dye tracer spread laterally, the flow tongues widened and the dye coverage increased. The sandy layer is followed by a layer with clay loam at a depth of 40-50 cm. The front of the flow pattern stops across the entire profile at about the same depth. There are two explanations for this. The change in soil texture allowed only very few flow paths to be continuous to greater depth. On the other hand, infiltration may have been stopped at the time when the front reached the respective depth. Flow patterns are not only influenced by the soil structure, but also by the experimental conditions. The rate as well as the cumulated amount of infiltration and the initial conditions, especially the initial saturation, play an important role for the infiltration regime.

In case of plot W_E13, the water infiltrated to greater depth on the right hand side of the profile. As the background image shows (Fig. 5.7), the sandy layer at depth 25-40 cm was only present on the left hand side of the profile. The water storage capacity was probably greater in the sand lens on the left hand side than in the loamy soil on the right hand side. The dye tracer, which reached greater depth on the right hand side of the profile, spread laterally once again in the gravel layer at depth 70-85 cm.

The two plots FF_R and FF_4 show the same tendency of having zones with a decreasing dye coverage followed by zones with increasing dye coverage. However they do not show a homogeneous infiltration front near the soil surface, unlike most of the other sites. Both plots were located at the same site. The topsoil was a sandy loam. Layers of coarser material were found in the subsoil. Plot FF_4 was strongly compacted by multiple passages of a sugarbeet harvester, while plot FF_R plot was left as it was. Soil compaction decreased the

infiltration capacity of the fine pore network in the main root zone of the grass covering the site. Some vertical earthworm burrows remained open and acted as preferential flow paths. Due to this difference in the topsoil, the two flow patterns look entirely different. But sand and gravel layers affected the patterns in both cases, giving them a characteristic change between layers with higher and lower dye coverage.

Analysis of the characteristics of the flow patterns

Figure 5.9a and b) show box plots of the variables used for the cluster analysis (minimum, maximum, mean, standard deviation, and median of line sequence width per layer as well as the dye coverage), depending on the cluster membership, for a total number of clusters of 3 (Fig. 5.9a) and 7 (Fig 5.9b). Table 5.2 shows the main characteristics of the clusters for the same total numbers of groups. The division of all layers into 20 clusters is not discussed in this context, because the degree of detail exceeds the information needed for this purpose.

In case of a total number of clusters of 3, the layers belonging to the clusters 1 and 2 have high maxima of the width distribution of the stained area per layer and a large dye coverage. The layers of cluster 2 have a higher mean and median of the width distribution of the stained areas than those of cluster 1, and tend to higher dye coverage. The layers belonging to clusters 3 have low maximum, mean, median and dye coverage. Cluster 2 represents almost closed homogeneous infiltration fronts. Cluster 1 contains layers with homogeneous infiltration with some unstained areas. Cluster 3 contains layers of preferential flow, but also layers with almost no stained areas.

Since we conducted our cluster analysis by a hierarchical algorithm, an increase of the total number of clusters usually leads to a division of clusters into several new groups. Increasing to total number of clusters from 3 to 7 leads to a division of cluster 1 and 3 into three clusters each, while cluster 2 remains the same. Table 5.2 shows which clusters for a total of 7 clusters emerged from which cluster for a total of 3. For a total number of 7 clusters, the layers belonging to cluster 1, 2 and 3 have high maxima of the width distribution of stained areas and a high dye coverage. However, they differ in mean and median, whereas the

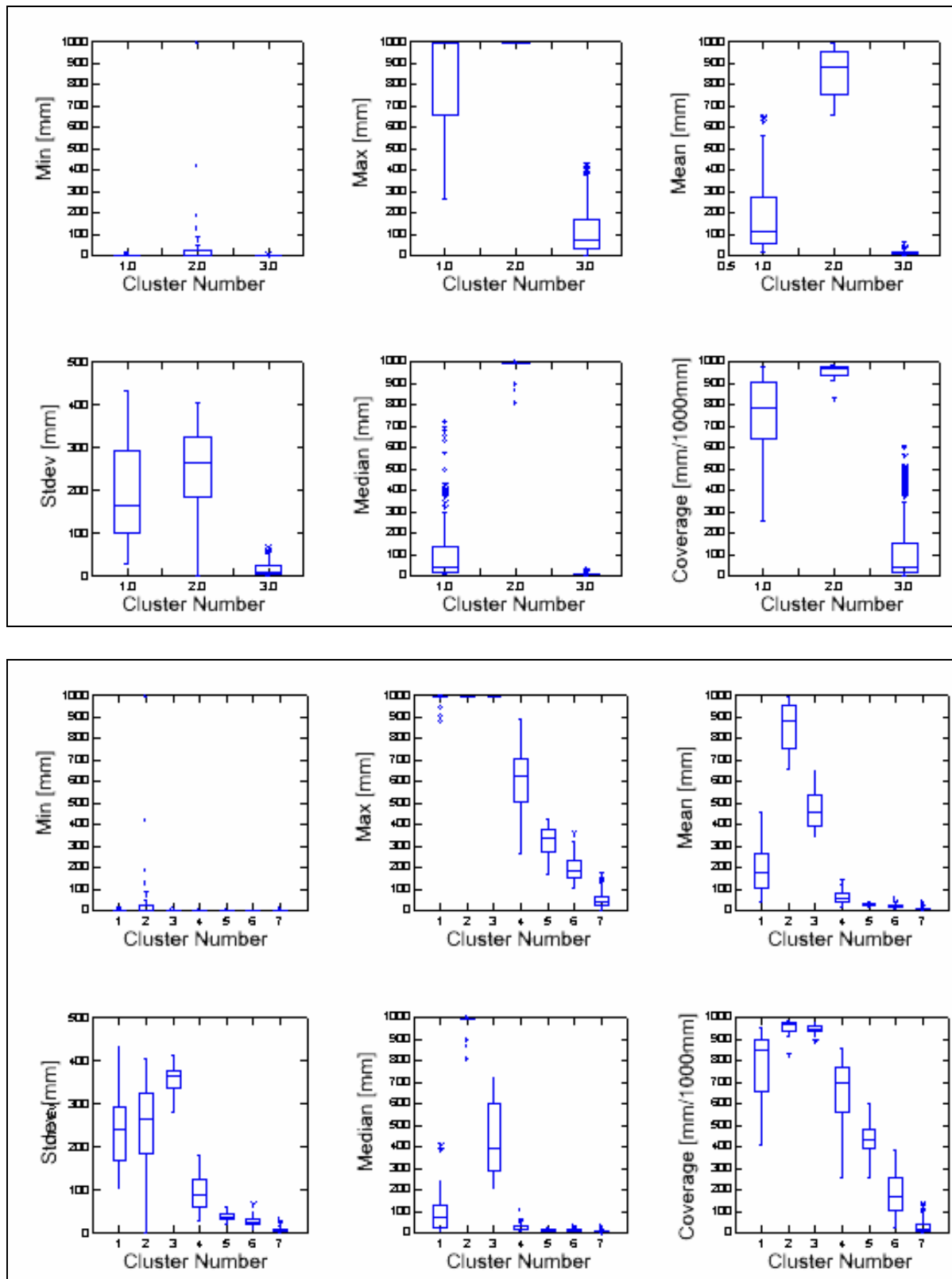


Figure 5.9 Box plots, showing the variability of the variables for every cluster for a total number of clusters of 3 (above) and 7 (below).

Table 5.2 Cluster protocol: Main characteristics of the clusters for a total number of clusters of 3 and 7.

Clst. No.	Total number of clusters: 3	Clst. No.	Total number of clusters: 7
2	min 3-997, max 999-999 mean 660-999, stdev 0-406 median 808-999, cov. 828-990	2	min 3-997, max 999-999 mean 660-999, stdev 0-406 median 808-999, cov. 828-990
1	min 1-7, max 267-999 mean 13-652, stdev 30-433 median 6-720, cov. 225-982	3	min 3-4, max 999-999 mean 343-652, stdev 283-412 median 209-720, cov. 895-982
		1	min 1-7, max 878-999 mean 40-462, stdev 105-433 median 8-411, cov. 410-955
		4	min 1-3, max 267-891 mean 13-142, stdev 30-179 median 6-106, cov. 255-858
3	min 1-7, max 2-429 mean 1-56, stdev 0-68 median 1-30, cov. 0-601	5	min 1-3, max 168-429 mean 16-41, stdev 22-60 median 8-23, cov. 258-601
		6	min 1-3, max 102-361 mean 7-56, stdev 10-68 median 5-29, cov. 21-388
		7	min 1-7, max 2-171 mean 1-36, stdev 0-32 median 1-30, cov. 0-136

layers belonging to cluster 2 have the highest mean and median of the width distribution of the stained areas, followed by cluster 3 and cluster 1. All three clusters contain layers of homogeneous infiltration. Cluster 4 contains layers where the flow changes from homogeneous infiltration to preferential flow. The three remaining clusters contain layers with preferential flow, reaching from layers with dye coverage around 0.5 to layers with almost no dye coverage. Layers with many flow paths, broader structures and higher dye coverage belong to cluster 5. The layers belonging to cluster 6 show fewer flow paths, finer structures and less dye coverage. Cluster 7 contains zones of very few on no flow paths and low dye coverage.

5.4 Discussion and conclusions

Flow patterns may be divided into three categories associated with different flow regimes (Flühler et al., 1996) (i) the 'attractor zone', where homogeneous flow is funnelled into preferential flow ports, (ii) the transmission zone where rapid and by-passing preferential flow is the main transport mechanism, and (iii) a 'dispersion zone', where the solute is spreading out laterally. Looking at the sequence of clusters, to which the individual layers were assigned to, the above categories of flow regimes were found in different combinations. Sites with strongly layered alluvial soils showed one or more dispersion zone, while soils without sharp textural layer boundaries had a typical sequence of layers of a homogeneous infiltration front followed by layers of preferential flow with gradually decreasing widths of stained areas and decreasing dye coverage.

The groups of layers found in the cluster analysis can easily be assigned to the two flow regimes 'homogeneous infiltration front' and 'preferential flow'. However, to find out whether a layer acts as a transmission or dispersion zone the entire sequence of layers has to be studied. For a total number of 7 clusters, the cluster-types 1, 2 and 3 contain layers belonging to homogeneous infiltration zones. While the maximum of the width distribution of the stained structures as well as the dye coverage do not allow to separate the three clusters, the mean and median of the width distribution allow a clear distinction between cluster 1, 2 and 3. The other clusters contain layers of preferential flow. In contrast to the clusters containing layers of homogeneous infiltration zones, the clusters

containing layers of preferential flow can better be distinguished by the dye coverage and maximum, than by the mean or median of the width distribution of the stained structures.

The method of Xu et al. (1993) to find of an optimum number of groups resulted in a global maximum and two local maxima for the cluster numbers we tested. We compared all three total numbers of clusters and found one of the local maxima to be best suited to group our layers. However, we think that for the data we processed, and probably for other environmental measurements as well, the optimal number of clusters is specific for the data. The distribution of the data in the variable space shows fractal characteristics. They are clustered on different scales. There may be several total numbers of clusters, dividing the data into reasonable groups, giving information with a different degree of detail. The degree of detail suitable for the specific question has to be found independently.

5.5 Acknowledgements

Financial support for this work was provided by the 'Research and Development Fund of the Swiss Gas Industry' (FOGA). We acknowledge the excellent collaboration of Dr. Michael Gysi and the staff of the 'Swiss Federal Research Station for Agricultural Economics and Engineering' (FAT), and the opportunity for collaboration at the experiments at the FAT site in Frauenfeld. The help of J. Leuenberger in planning and conducting the field work and the contribution of M. Jaquillard in the field and his work on the evaluation of the pictures from FF during his master thesis are gratefully acknowledged.

5.6 References

- Allaire-Leung S. E., S. C. Gupta, and J. F. Moncrief, 1999. Dye adsorption in a loam soil as influenced by potassium bromide. *Journal of Environmental Quality*. 28:1831-1837.
- Baveye P., C.W. Boast, S. Ogawa, J.Y. Parlange, and T. Steenhuis, 1998. Influence of image resolution and thresholding on the apparent mass fractal characteristics of preferential flow patterns in field soils. *Water Resources Research*, 34 (11): 2783-2796.
- Bundt M., Albrecht A., Froidevaux P., Blaser P., Flühler H., 2000. Impact of preferential flow on radionuclide distribution in soil. *Environmental Science & Technology* 34 (18): 3895-3899
- Flühler H., Durner W., Flury M., 1996. Lateral solute mixing processes - A key for understanding field-scale transport of water and solutes. *GEODERMA* 70 (2-4): 165-183.
- Flury, M., and H. Flühler, 1994. Brilliant blue as a dye tracer for solute transport studies - A toxicological overview. *Journal of Environmental Quality*. 23: 1108-1112.
- Flury, M., H. Flühler, W. A. Jury, and J. Leuenberger, 1994. Susceptibility of soils to preferential flow of water: A field study. *Water Resources Research* 30(7):1945-1954.
- Flury M., and H. Flühler, 1995. Modeling solute leaching in soils by diffusion-limited aggregation: Basic concepts and application to conservative solutes, *Water Resources Research*, 31, 2443-2452.
- Forrer I. N., A. Papritz, R. Kasteel, H. Flühler, and D. Luca, 2000. Quantifying dye tracer in soil profiles by image processing. *European Journal of Soil Science*. 51: 313-322.
- Ghodrati M., and W.A. Jury, 1990. A field study using dyes to characterize preferential flow of water. *Soil Science Society of America Journal*. 54: 1558-1563

- Gjettermann B., K.L. Nielsen, C.T. Petersen, H.E. Jensen, S. Hansen, 1997. Preferential flow in sandy loam soils as affected by irrigation intensity. *Soil Technology*. 11: 139-152.
- Ihaka R., and R. Gentleman, 1996. R: A Language for Data Analysis and Graphics. *Journal of Computational and Graphical Statistics*, 5(3): 299--314
- Ketelsen H., and S. Meyer-Windel, 1999. Adsorption of brilliant blue FCF by soils. *Geoderma*. 90:131-145.
- Sinaj S., Ch. Stamm, G.S. Toor, L.M. Condron, T. Hendry, H.J. Di. K.C. Cameron, and E. Frossard, 2002. Phosphorus exchangeability and leaching losses from two grassland soils. *J. Environ. Qual.*, 31: 319-330.
- Stamm et al. (in press)
- IDL, Reference Guide, Research Systems, Inc. 1997. Volume 2, 786-787.
- Ward J.H., 1963. Hierarchical grouping to optimize an objective function *J Am. Stat. Assoc.* 58 (301): p 236.
- Weiler M., and F. Naef, 2001. Effects of macropore flow on runoff generation. *Journal of Hydrological Processes* (in press).
- Xu S., M.V. Kamath, and D.W. Capson, 1993. Selection of partitions from a hierarchy. *Pattern Recognition Letters*, 14 (1): 7-15.
- Zehe E., and H. Flühler, 2001. Slope scale variation of flow patterns in soil profiles. *Journal of Hydrology* 247:116-132.

Chapter 6

Synthesis

Several compaction experiments carried out along construction sites of a new gas pipeline showed no clear effect of subsoil compaction. Most of these sites were under intensive agricultural use and therefore already compacted to a certain degree. The mean contact pressure of the tracked vehicles used for the gas pipeline project did not exceed the pre-consolidation load of the soil at the respective sites.

The traffic of the sugarbeet harvester, on the other hand, strongly affected the flow patterns as well as the soil mechanical parameters. Its contact pressure was twice the contact pressure of the caterpillars used for gas pipeline construction, and it exceeded the pre-consolidation load of the soil at the investigated site.

In most cases there was good agreement between the conclusions drawn from the soil mechanical measurements and those drawn from the flow pattern analysis. However, at the site of Güllenhau the results did not match (Table 4.6). The soil was a very loose forest soil, where a compaction effect was evident based on the soil mechanical and soil physical measurements at samples taken in a depth of 7-17 cm, but no obvious difference between the flow patterns was found. Although the soil was slightly compacted, the pore network was probably not damaged to a degree that limits water infiltration at the chosen rate. We found living and dead root material in all of the stained structures. This organic material may have stabilized the pore structures and kept them active for transport.

The field experiment with the sugarbeet harvester showed that soil mechanical measurements provide information about compaction at various depths, while the infiltration patterns show changes of water infiltration pathways caused by the soil compaction. At the compacted plots, the water was funneled into preferential flow ports, mainly worm burrows. Wetting of the main root zone

decreased because a significant fraction of the infiltrating solution bypassed the matrix.

Most of the tracer experiments were conducted using the dye tracer Brilliant Blue. In these experiments, we compared the flow patterns observed in the trafficked plots with those in the non-trafficked plots. Using a single tracer for visualising the flow patterns, the spatially variable soil structure hampers the comparability between flow patterns of neighbouring plots. Comparing flow patterns before and after compaction at one and the same plot overcomes this basic experimental difficulty.

One experiment was carried out using two fluorescent tracers at the same plot. The less mobile tracer was applied before and a mobile tracer after the compaction treatment with a heavy tracked excavator. The distributions of the two tracers visible on the excavated vertical profiles were then photographed using a digital camera and light source, both equipped with suitable tracer specific filters. The superposition of the flow patterns of the two tracers shows the effect of the compaction directly.

This method is more sensitive for detecting compaction induced changes than experiments using a single tracer, because the effect does not need to be more significant than the spatial variability within the field. Therefore fewer profiles have to be prepared in order to allow a reliable conclusion. Besides, a quantitative comparison of the fluorescent tracer images before and after compaction is easier because the images have the same coordinate system and the same underlying soil structure. This allows a one-to-one comparison of the patterns.

We intended to develop a quantitative method to analyze the spatial distribution of the stained areas in vertical profiles and to link flow pattern features with the soil properties and structure. Since soil layers strongly affect the infiltration patterns we first split the flow patterns into layers of similar patterns. All layers found in the multiple replications of flow patterns of 25 plots at 8 sites were then partitioned into groups of similar layers by hierarchical clustering. Next, the sequence of layers found for each plot was compared with the sequence of morphological layers observed on the soil profiles.

The groups of layers detected with this method reliably distinguish between homogeneous infiltration and preferential flow, but also between zones of strong preferential flow and zones of lateral spreading, e.g., sand or gravel lenses. The dye coverage and the mean width of the stained structures were the most indicative factors for the different clusters. We found a good agreement of the sequences of layers found in the flow patterns and the soil properties.

List of Figures

Figure 2.1	Sugar beet harvester used in the experiment.....	10
Figure 2.2	Bulk density, total porosity and macroporosity with depth in the three treatments.	13
Figure 2.3	Superimposed blue channels of the flow pattern pictures for each treatment. The blue channel shows the background of the soil profiles without the dye tracer. The little squares show the sampling depths at 0.15 m, 0.25 m, 0.35 m, 0.45 m, and 0.55 m.....	14
Figure 2.4	Superimposed images of all flow patterns observed in the individual treatments. The intensity of shading of a given areal unit (pixel) stands for the fraction of the pictures being stained at this particular coordinate.	15
Figure 2.5	Example plot for the multiple passage plot and the control showing the role of worm burrows for the transport of the dye tracer. Above: red channel showing the flow pattern. Below: blue channel showing the soil structure without the flow pattern.....	16
Figure 2.6	Variations of dye coverage (interquantile-range) vs. depth for the three treatments.	18
Figure 2.7	Dye coverage in depth increments of 0.1 m for the three treatments.	19
Figure 3.1	Tracked excavator used for the compaction experiment.	29
Figure 3.2	Plot without topsoil. The area of the tracer application is the darker region in the middle of the plot. The boxes were used to check the spatial homogeneity of the application of water and tracer.	30
Figure 3.3	Illumination and digital detection device used for measuring the distributions of the two tracers in vertical soil profiles.....	32

Figure 3.4	Correction steps leading from the original images to the concentration map. The red rectangle indicates the position of the calibration samples.....	33
Figure 3.5	Steps carried out to obtain the distance between pixels belonging to the flow patterns of SB and AY.....	34
Figure 3.6	Overlay images of the concentration maps of the two fluorescent tracers. Green: SB (applied before compaction) Red: AY (applied after compaction).....	36
Figure 3.7	Distribution of the nearest distances of all pixels belonging to flow patterns of SB to the skeleton of the flow patterns of AY.	38
Figure 3.8	Mean distance between the pixels of the flow pattern of SB and the skeleton of the flow pattern of AY for the profiles of each treatment...	39
Figure 4.1	Situation of the test plots at the three experimental sites with sampling and sprinkling areas: NT non-trafficked, T trafficked.	49
Figure 4.2	Precompression stress (left) and bulk density (right) of the non-trafficked (□), ‘wet’-trafficked (●) and ‘dry’-trafficked (▲) Freienstein soil.	55
Figure 4.3	Coarse porosity (left) and coarse-to-intermediate porosity (right) of the non-trafficked (□), ‘wet’-trafficked (●) and the ‘dry’-trafficked (▲) Freienstein soil.	55
Figure 4.4	Flow pattern of dye tracer in the ‘wet’, ‘dry’ and non-trafficked Freienstein soil.	56
Figure 4.5	Precompression stress (left) and bulk density (right) of the trafficked (●) and the non-trafficked (○) Güllenhau soil.....	57
Figure 4.6	Coarse porosity of the trafficked (●) and non-trafficked (○) Güllenhau soil.	57
Figure 4.7	Flow pattern of dye tracer in the trafficked and non-trafficked Güllenhau soil.	58

Figure 4.8	Precompression stress (left) and bulk density (right) of the ‘wet’ trafficked (●), ‘dry’ trafficked (▲), ‘wet’ non-trafficked (○) and ‘dry’ non-trafficked (△) Ruckfeld soil.	59
Figure 4.9	Porosity of the non-trafficked (□), ‘wet’ trafficked (●) and ‘dry’ trafficked (▲) Ruckfeld subsoil at 0.27-0.37 m depth.	59
Figure 4.10	Flow pattern of dye tracer in the ‘wet’, ‘dry’ and non-trafficked Ruckfeld soil.....	60
Figure 5.1	Layering in flow patterns reflect layers of hydraulically different materials.	75
Figure 5.2	Methodological steps presented in this chapter.	76
Figure 5.3	Sequence of the image processing.	78
Figure 5.4	Analysis of the width distributions of the stained areas. Top: Width distributions are determined for every horizontal line (1 mm depth increment). Bottom: For each depth z_L the width distributions below and above the respective depth are pooled and compared.	80
Figure 5.5	Maximizing Z to detect layer boundaries. Top: Iterative discrimination of dissimilar layers. Bottom: all images of a given plot lined up	81
Figure 5.6	Top: Number of boundaries depending on the threshold (black) and best fit of the two straight line segments with the least chi-square error (grey). Bottom: Sum of squared errors for the fit of the line segments depending of the threshold.	83
Figure 5.7	Overview of the results for six sites (rows). The background image on the left is followed by an example flow pattern of each plot and an overlay image of all flow patterns of the plot. The results of the cluster analysis for a total of 3, 7 and 20 clusters are given by the color bars next to another overlay image with the layer boundaries. The color scale on the right identifies the cluster numbers by the colors.	86
Figure 5.8	Cluster number optimized by the method of Xu et al. (1993).	88

Figure 5.9 Box plots, showing the variability of the variables for every cluster for a total number of clusters of 3 (above) and 7 (below).	92
--	----

List of Tables

Table 2.1	Detailed information about the tyres.....	10
Table 3.1	Soil properties measured at the test site (minimum and maximum value of 4 profiles).....	28
Table 4.1	Soil parameters at the three test sites Freienstein, Güllenhau and Ruckfeld.....	48
Table 4.2	Characteristics of the machinery used in the experiments.....	50
Table 4.3	Test sequence for the three test sites	50
Table 4.4	Soil water potential of the three test sites at different depths immediately before the passage of the machines	51
Table 4.5	Size (D/H: diameter/height) and number of samples of the three test sites	52
Table 4.6	Effects found at the three test sites for 'wet' and 'dry' trafficked plots compared with non-trafficked plots	77
Table 4.7.	Effects expected at the Freienstein sites for ‘wet’ and ‘dry’ trafficked compared with non-trafficked plots under the assumption of a minimum (‘best case’) and maximum (‘worst case’) normal stress at the soil surface	65
Table 4.8.	Effects expected at Güllenhau for the trafficked compared with the non-trafficked plot for a minimum (‘best case’) and maximum (‘worst case’) normal stress at the soil surface	66
Table 4.9.	Effects expected at Ruckfeld for ‘wet’ and ‘dry’ trafficked compared with non-trafficked plots for a minimum (‘best case’) and maximum (‘worst case’) normal stress at the soil surface	66
Table 5.1	Some information about the soils ant the experimental conditions at the example sites.....	89

Table 5.2	Cluster protocol: Main characteristics of the clusters for a total number of clusters of 3 and 7.....	109
-----------	---	-----

Curriculum vitae

1970	Born on April 2 in Zürich (Switzerland)
1977-1985	Primary and secondary school in Glattbrugg
1985-1989	Gymnasium Bülach
1989	Matura Typus C
1989-1995	Environmental sciences at the Swiss Federal Institute of Technology (ETHZ)
1995	Diploma in Natural Sciences
1994-1999	Education in teaching at the ETHZ
1999	Diploma for teaching environmental courses and physics
1995-1996	Research assistant at the Institute of Terrestrial Ecology (ITOe)
1997-2002	PhD student and research assistant at the ITOe
1999-2001	Administrator of the computer network of the Centro Stefano Franscini (CSF)